TECHNISCHE UNIVERSITÄT MÜNCHEN

Lehrstuhl für Nanoelektronik

Fabrication and Characterization of Carbon Nanotube Thin-Films for Gas Sensing Applications

Ahmed Abdelhalim

Vollständiger Abdruck der von der Fakultät für Elektrotechnik und Informationstechnik der Technischen Universität München zur Erlangungen des akademischen Grades eines

Doktor-Ingenieurs (Dr.-Ing.)

genehmigten Dissertation.

Vorsitzender: Univ.-Prof. Dr.-Ing. Wolfgang Kellerer

Prüfer der Dissertation:

1. Univ.-Prof. Paolo Lugli, Ph.D.
2. Univ.-Prof. Dr.rer.nat.habil. Bernhard Wolf

Die Dissertation wurde am 08.01.2015 bei der Technischen Universität München eingereicht und durch die Fakultät für Elektrotechnik und Informationstechnik am 29.07.2015 angenommen.

To my parents,

To Know, is to know that you know nothing. That is the meaning of true knowledge

SOCRATES

Abstract

In this work, we utilize random carbon nanotubes (CNTs) networks in gas sensing applications. In that context, we present two different processes for depositing high performance CNT thin-films on any substrate; spray deposition and transfer printing. Employing the former technique, we fabricate CNT-based gas sensor with high sensitivity as well as immediate response towards four different test gases; NH_3, ethanol CO and CO_2. We further enhance the sensitivity and alter the performance of the sensing elements by functionalizing them with metallic nanoparticles (NPs) such as Au, Ag and Pd. We study as well the interaction between Au NPs and the CNT layer in terms of the changes introduced in the optical properties, surface morphology and work function. Incorporating the insights gain by metallic NPs functionalization of the CNT layers, we realize CNT-based gas sensor array composed of four different sensing elements each is functionalized with different metal. This sensor array is capable to discriminate between the different test gases. Moreover, we fabricated the CNT-based gas sensor array on rigid (Silicon) and flexible (Kapton) substrates. Finally, we performed complex impedance characterization on CNT thin-films and CNT-based gas sensors, where we investigate the behavior of the CNT network and the response of the CNT-based gas sensor under different frequencies. We show that selectivity can be achieved by extracting the recovery time of the gas sensor towards different test gases at certain frequencies.

Contents

Chapter 1

Introduction

In the last few decades the technology of building electronic devices that can detect and sense different smells have experienced great advances. Such devices are commonly referred to as electronic nose or e-nose [1]. This technology was applied in wide range of applications such as: grading of coffee blends or beans [2] [3], roasting level of coffee [4] freshness of fish [2] [5]or meat [6], air-pollution monitoring [7] as well as industrial applications [8]. The basic principle of the e-nose is to mimic the remarkable ability of the human nose. The sense of smell has an important role in our daily live. In general, everything we smell consists of volatile molecules, which are generally light, so they can float through the nasal passage and attach to a patch of neurons (receptors). These neurons are unique and they have hair-like projections called cilia that increase their surface area. When an odor molecule attaches to these cilia, it triggers the neurons which results in perceiving the smell [1]. From an electrical point of view, such system is equivalent to a sensor array and pattern recognition system. Incorporating both in one device (e-nose) results in a system that has the functionality of the human nose.The recent advances in electronic sensing was able to outclass the human nose by detecting odorless and toxic vapors [9] [10]as well.

For instance, in the field of robotics, one of the greatest challenge is the capability of robots to navigate in natural environments autonomously [11] . Although an e-nose in robots has a reduced importance, they can take advantage from such a feature when it comes to perform chemical tasks such as follow odor tracks or find sources of odor like gas leaks, drugs, explosives, landmines, etc. [11]

Electronic noses can be manufactured based on inorganic or organic technology. The former is the conventional semiconductor technology which is used in fabricating electronic

[1] According to the book Molecular Biology of the cell, Humans can distinguish more than 10,000 different smell which are detected by specialized olfactory neurons lining the nose

devices since the beginning of the last century. The latter has paved the way to variety of applications [12] [13] [14] [15] [16] [17] since the discovery of conducting polymers in 1970s. By the discovery of carbon nanotubes CNTs in 1991, the field of organic electronics, in particular CNT-based devices, has gained an increasing importance, as organic materials can be used as an alternative for conventional inorganic semiconductors.

The main attractiveness of such technology is their promise to deliver low-cost devices that can be fabricated on large scale. This technology allows the manufacturing of the different electronic components on flexible substrates based on simple coating or printing techniques, which has several substantial ecological and economical advantages. Utilizing such technology in fabricating e-noses/gas sensors [2] opens new horizons in the field of flexible, cost-effective and scalable electronic device. Nevertheless, in order to commercialize gas sensors based on organic or/and CNT materials, several factors has to be targeted and optimized. In the following some of these important factors are summarized:

- Material life time
- Large area and high throughput manufacturing process
- High sensitivity and selectivity
- Fast response and recovery period

The main aim of this work is to show the potential of utilizing CNTs in delivering highly sensitive, selective and flexible gas sensors. In that context, we target two of the main obstacles that prevent CNT-based gas sensors from successful commercialization, high-throughput manufacturing process and high selectivity in detecting different gases. Plenty of research has been conducted proposing solutions for the drawbacks of organic materials in general. However, the processing technology enabling industrial-scale and large area manufacturing has been largely neglected in literature. In the past 15 years, CNTs have been reported as a highly sensitive material for detecting different organic and inorganic gases. It is commonly known as well that pristine CNTs lack the selectivity when it detects pure or mixture of gases. Hence, most research conducted has been driven to overcome this problem. Nevertheless, providing a solution that employ scalable manufacturing process and deliver highly sensitive and selective CNT-based gas sensors, was rarely achieved. It is only through targeting those two factors simultaneously, rapid product commercialization can be obtained.

[2] From this point on, we will use the technical term gas sensor instead of e-nose

In chapter 2 we give an overview on the different technologies employed to fabricate gas sensors. We highlight the three common gas sensor technologies based on electrical variation of the sensing element upon gas exposure, metal semiconducting, polymers and CNTs. Then, we focus on the different techniques utilized to deposit CNT thin-film, spin coating, dip coating, vacuum filtration and spray coating. we introduce as well different approaches to enhance the selectivity of the CNT-based gas sensors.

We demonstrate the fabrication of high quality CNT-thin films through a reliable, reproducible and scalable spray deposition techniques in chapter 3. We spray deposit CNT on glass as well as plastic substrate. The different preparation methods for the solution-based CNTs and their effect on the performance of the deposited film is investigated. Additionally, we introduce transfer printing process for depositing CNT thin-films on any substrate. We compare as well between CNT thin-films deposited on glass and on plastic substrates using both techniques, spray deposition and transfer printing.

After optimizing the spray deposition parameters to fabricate high performance CNT thin-films, in chapter 4 we employ this technique in fabricating CNT-based gas sensors with exceptional as well as immediate response towards different test gases. Moreover, we show that metallic nanoparticles (NPs) alter the performance of the gas sensor and some kind of metals enhance the sensitivity of the sensor towards all test gases. We investigated the change introduced on the surface of the CNT due to the deposition of Au and Ag NPs with different loads.

In chapter 5, we present the development of selective CNT-based gas sensor array on rigid and flexible substrates. We utilize different metal NPs at different loads to alter the performance of the different sensing elements on the array. Based on the knowledge obtained by functionalizing single CNT-based gas sensors in chapter 4, we developed strategy framework for finding the optimized combination of metallic loads that can discriminate between various test gases. In this chapter as well, we present the fabrication of CNT-based gas sensor array on Kapton. Such sensor array is able to discriminate NH_3 from the other test gases.

The possibility of obtaining selective CNT-based gas sensor by performing advanced characterization techniques is presented in chapter 6. In this chapter we present the complex impedance characterization technique, where we characterize CNT thin-films and CNT based gas sensors in a frequency 20 Hz-2MHz. We show that the frequency response is highly dependent on the resistance of the CNT layer. By extracting the recovery time for CNT-based gas sensors towards different test gases at different frequencies, we are able to categorize the different gases into pre-defined classes.

We present in chapter 7 conclusion and outlook on future work, where the important findings of this work are highlighted. We introduce as well some novel ideas relevant to the continuation of this work. Figure 1.1 shows a simplified chart for the outline of the thesis and the sequence of the topics discussed.

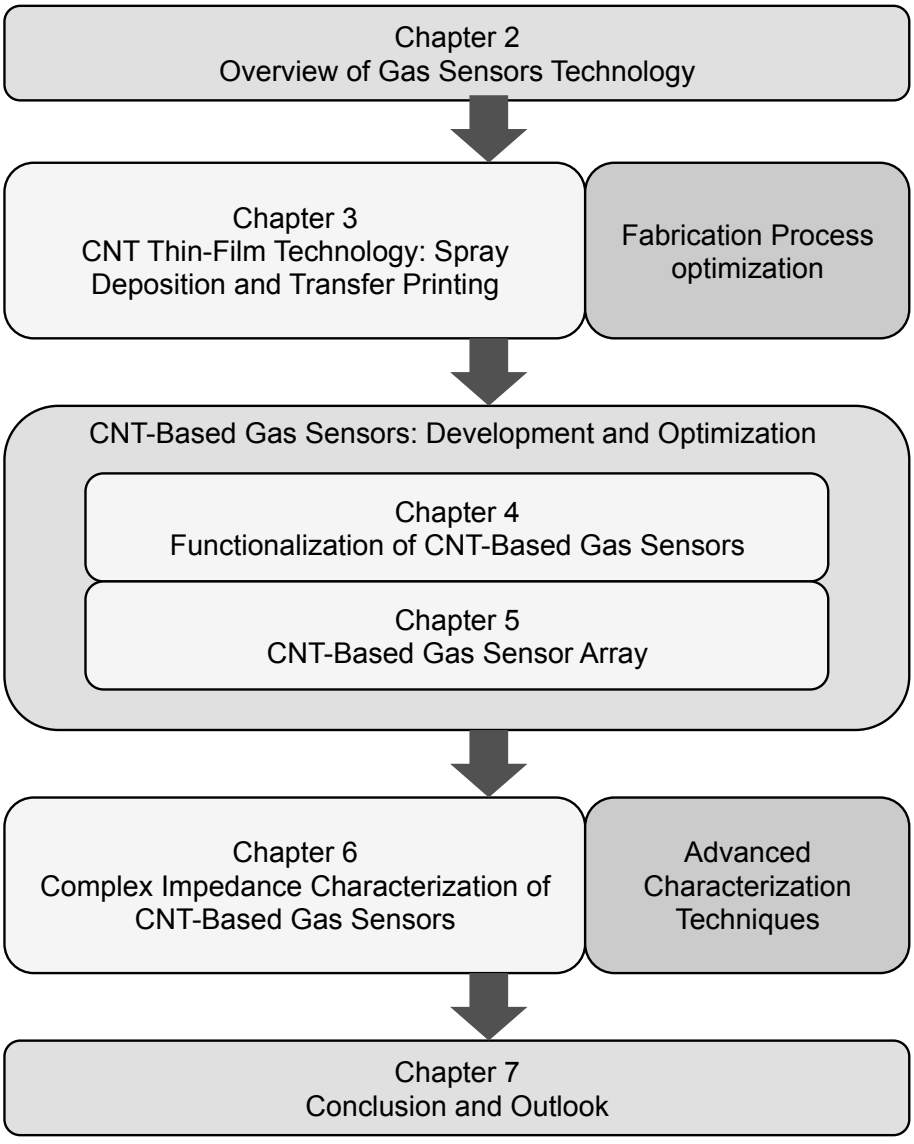

Figure 1.1: Chart shows the outline of the work presented here.

Chapter 2

Gas Sensors Technology and Development

In this chapter, we give an overview on the development in manufacturing gas sensor devices. In this context, we present briefly three main gas sensor technologies based on electrical variation of the sensing element upon gas exposure, while highlighting the technology developed and utilized in this work, CNTs. An evaluation scheme is proposed to compare between the different approaches available to overcome the problems facing the development of CNT based gas sensors. We discuss as well the different techniques used to prepare CNTs thin-films based on processable solution onto different substrates, spin-coating, dip-coating, vacuum filtration and spray deposition. By comparing between the different techniques, we show that spray deposition is most promising technique to be utilized in fabricating CNT based gas sensors. Due to the fact that spray deposition is capable of fulfilling the requirement of low-cost, flexible, reproducible and scalable CNT-based gas sensors. Finally, we present the process development framework utilized to fabricate and characterize devices presented in this work.

2.1 Gas Sensing Technologies

The development in gas monitoring becomes an essential aspect with the progressive industrialization of the society. Gas detection is highly required in the domestic as well as the industrial life. These kinds of sensors can be applied in wide range of applications such as combustion process, environmental monitoring and medical application. Incorporating features like, low weight and flexibility enables gas sensors to be applied in smart packaging application as well.

In principle gas sensors are devices, which are capable of detecting the presence of a certain gas in a certain area. Several technologies have been employed to fabricate high performance and reproducible gas sensors. The common detection procedure usually depends on the variation of the electrical or the optical properties of the sensing

material upon gas exposure. Other methods for gas detection have been reported as well such as: acoustic method [18] [19] , gas chromatography [20] [21] and colorimetric methods [22] [23]. Here, we focus on the gas detection based on the electrical variation of the sensing material. Three main technologies are used to fabricate gas sensors based on such a method, metal oxide semiconductors, polymers and CNTs. In order to evaluate the advantages and disadvantage of each technology, we identified an evaluation scheme, which is based on seven criteria, sensitivity, selectivity, response time, energy consumption, recovery time, adsorptive capacity and fabrication cost.

2.1.1 Metal Oxide Semiconductor Gas Sensors

Metal oxide semiconductors (MOS) are the most commonly used sensing materials [24] [25] [26]. It was firstly demsontrated in 1962 that the adsorption or desorption of a gas on the surface of zinc oxide thin film layers results in changes in its conductivity [27]. Several materials have been used as the active layer in fabricating metal oxide semiconductors gas sensors such as Cr_2O_3, Mn_2O_3, Co_3O_4, NiO, CuO, SrO, In_2O_3, WO_3, TiO_2, V_2O_3, Fe_2O_3, GeO_2, Nb_2O_5, MoO_3, Ta_2O_5, La_2O_3, CeO_2, Nd_2O_3 [28]. The selection of a certain material for the gas sensing application depends on the electronic structure of the material. Due to the fact that the range of electronic structures of oxides is so wide, metal oxides can be divided into two main categories, transition-metal oxides and non-transition-metal oxides. The difference between the two categories depends mainly on the size of the band gap of the materials in each category.

Gas sensing in the metal oxide semiconductors is originated from redox reactions between the target gases and the oxide surface [29]. The redox reaction occurs when O^- distributed on the surface of the materials would react with molecules of target gases leading to an electronic variation of the oxide surface. Such variation is then transduced into an electrical resistance variation of the sensors [30].

MOS gas sensors are characterized by their low cost and high sensitivity. However, this high sensitivity is mainly based on high operating temperature. The main reason of the high temperature is the reaction temperature of O^-. In order to increase the probability of adsorbing a certain molecule onto the surface of the active layer, it should be pre-heated at an elevated temperature.

SnO_2 is among the most popular sensing materials used in MOS gas sensors mainly because of its high sensitivity. The working temperature of SnO_2 based sensors varies from 25 °C to 500 °C. The best sensing temperature is different from one gas to the other, which render such material as ideal selective material. If the difference between

the optimal temperature for detecting two different gases is large, a single sensor could be also designed to detect two kinds of target gases at the same time [31]. Nevertheless, the selectivity of the MOS gas sensors is still rather low. Selectivity could be improved by doping the active layer with a suitable catalyst material [32] [33]. Another common method to improve the selectivity of gas sensors in general is using sensor array based on different sensing elements [34] [35].

The main disadvantage of the MOS gas sensors is their high-energy consumption. In order to obtain high sensitivity it is always required to heat up the sensing element at a certain elevated temperature, which is dependent on the target gas. Such a criteria restricts the development for MOS gas sensors for certain application where the operation at room temperature is highly demanded. Additionally, this kind of gas sensors is characterized by long recovery time after each gas exposure, which restricts employing these kinds of sensors in applications where the concentration of the gases change rapidly.

2.1.2 Polymer Gas Sensors

Utilizing organic polymers as the sensing material in gas sensors has been demonstrated since the early 1980s [36]. Organic polymers can be classified into two groups:

- Conducting polymers
- Non-conducting polymers

In this discussion we focus on the first group, which is conducting polymers due to its high relevance to the results presented in this work. Conducting polymers such as polypyrrole (PPy), polyaniline (Pani), polythiophene (PTh) and their derivatives showed improved characteristics when compared to metal oxides. They are characterized by short response time, high sensitivities and operate at room temperature rather than an elevated temperature. The detection procedure in polymers-based gas sensors is either by a change in the physical (e.g. volume changes upon exposure) or chemical (e.g. oxidation state) properties [37]. The interaction between gas molecules and conducting polymer films are multiform and can be divided into two main categories as follow:

- Chemical reaction between analytes and conducting polymers
- Weak interaction between analytes and conducting polymers

The former category depends on the change in the physical properties of the active material upon gas exposure. Conductive polymers are strongly dependent on their doping levels. Nevertheless, the doping levels can be easily altered when exposed to different

gaseous analytes by chemical reaction at room temperature. Changing the doping level results in electron transfer from/to the analytes, which subsequently cause change in the resistance or the work function of the polymer. The latter category relies on the weak interaction between many organic analytes, such as benzene, toluene and other volatile organic compounds (VOCs), and the conductive material at room temperature. Detection of such analytes by their chemical reaction is quite difficult. However, they influence the properties of the active layer since they involve absorbing or swelling the polymer matrix.

Conductive polymer based gas sensor can be realized in two main configurations. The first configuration, which is commonly used, is chemiresistors, where the electric resistance of the sensing material is sensitive to changes in the chemical environment. The second configuration is based on a transistor, commonly using organic thin-film transistors (OTFTs). In that case, the gas detection procedure is quantified by changes in the transfer characteristics of the transistor.

In general, polymer based gas sensors show poor selectivity towards the different gaseous analytes. Nevertheless, one approach to improve such behavior is by applying alternating (AC) signal to the chemiresistor, which results in measuring not only the resistance but also the capacitance and the inductance upon gas exposure. Due to the fact that the value of dissipation factor (resistance/absolute value of reactance) changes with the current frequency, and the peak in the dissipation-frequency curve shifts when the sensor is exposed to different gases [30]. The peak position is unique for different gases and useful in distinguishing them [38] [39].

Another main disadvantage of such kind of gas sensors is its long-term instability as well as its poor recovery. Moreover, the response of the polymer based gas sensors are highly affected by the working environment. Although, polymer based gas sensors deliver several advantages, further research and development are required in order to render them as a strong candidate to replace the commonly used metal oxide semiconductors based gas sensors.

2.1.3 CNT Gas Sensors

Random Carbon nanotube (CNT) networks have attracted a broad community of researchers since their discovery by Ijima in 1991 [40]. Their impressive structural, mechanical and electronic properties have been exploited in wide range of applications in science and engineering [14] [15] [37] [41]. The inherently reduced dimensionality and, hence,

high surface-to-volume ratio, which, together with outstanding gas adsorption capabilities, renders CNTs as ideal candidate for environmental sensing applications. In general, CNTs could be classified into single-walled carbon nanotubes (SWCNTs) and multi-walled carbon nanotubes (MWCNTs). Devices incorporating both kinds of CNTs have been repeatedly proposed as sensors for a variety of gases [42] [43] [44] [45] [46] [47].

CNTs show p-type conduction under ambient conditions [48], adsorption of electron-donating molecules results in an increase of charge carrier recombination and hence a decrease in conductance. The adsorption of electron-withdrawing molecules on the other hand will result in an increase of the hole concentration and hence an increase in device conductance [42]. Sensing in CNT films could be attributed to the contribution of two mechanisms, charge transfer causing intra-tube modulation and inter-tube modulation by gas adsorption [49]. Intra-tube modulation involves charge transfer in individual nanotubes, where as the inter-tube modulation it occurs at the nanotube-nanotube junctions. Nevertheless, the complete sensing mechanism of CNT based gas sensors is not yet fully understood and the theories explaining it are sometimes quite controversial.

CNT-based gas sensors are potentially flexible, low-weight and low-cost devices, thereby being attractive for single use applications as well as portable applications such as smart packaging and environmental monitoring. They showed high sensitivity to wide range of gases such as NH_3, CO, NO_2, CO_2 and O_2 in addition to the detection of volatile organic compounds (VOC) such as acetone, methanol, ethanol, benzene and toluene. Similar to polymer based gas sensors, these kind of gas sensors can be realized in two main configurations, chemiresistor [50] [51] and based on field effect transistor (FET), commonly called chemFET [52] [53]. The gas detection process in the former realization is measured by the change occurs in the resistance of the deposited CNT thin-film upon gas exposure, while the latter measures the change in the transfer characteristics of the transistor upon gas exposure. It is worth noting here that chemFET provide more parameters for measurement, which results in more insights on the semiconducting nature of the CNT sensing materials. Additionally, the signal amplification of the transistor provides more detection limit relative to the chemiresistors. Nevertheless, the fabrication process of the chemFET is rather complex. Figure 2.1 illustrates a schematic for the chemFet and the chemiresistor architechture

Short response and recovery time are the main characteristics of CNT based gas sensors, which differentiate them from the other technologies. Moreover, different target gases result in different response and recovery time. Employing such a feature could result in obtaining selective CNT based gas sensors, as we will show in chapter 6. Furthermore,

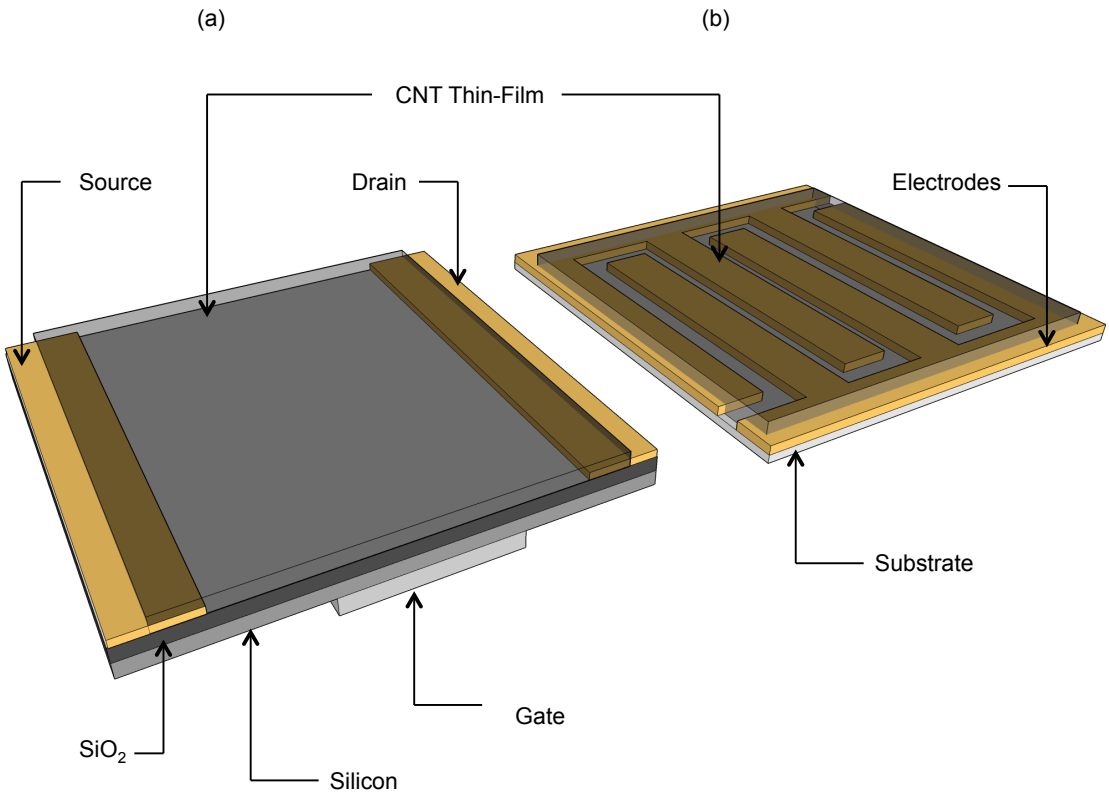

Figure 2.1: Schematic drawing for the common architectures of the CNT based gas sensors, ChemFET (a) and Chemiresistor (b)

CNT based gas sensors outperform conventional sensing materials in term of their great adsorptive capacity [30]. Their gas detection procedure operates at room temperature which eliminates the need for additional heater to operate normally.

Although, the existence of several methods that tries to enhance the selectivity of the CNT based gas sensors, selectivity is considered one of the main drawbacks of these kind of sensors. In the upcoming sections we discuss such methods in more details and evaluate their performance as well. The fabrication cost of CNT based gas sensors are relatively higher than other gas sensors based on materials like metal oxide semiconductors. This can be attributed mainly to the fact that metal oxide materials are produced in larger scale, which decrease the total fabrication cost. In order to decrease the cost of the CNT-based gas sensors, it is necessary to achieve high-throughput, low cost production technique onto a wide variety of substrate material. Employing a fabrication technology such as spray deposition is capable to fulfill such requirements. Different technologies used in fabricating CNT layers will be discussed in details later in next section.

Figure 2.2 summarizes evaluation scheme we used to compare between the three commonly used technologies for the fabrication gas sensors based on electrical variation of

the sensing material. The technology utilized in this work is highlighted as well as its main disadvantage, which is our main focus.

2.2 CNT Thin-Film Deposition Technologies

CNTs have been produced by three major methods; arc-discharge, laser ablation and chemical vapor deposition (CVD), where the latter is the most common method for direct growth of CNT thin-films. CVD process involves catalyst nanoparticles acting as seeds for the growth of the CNTs. Although CVD produces high quality films, the high vacuum/temperature requirement for the growth process is not suitable for several applications where low-cost and flexible substrates are required. CNTs can be as well processed from solution of well-dispersed nanotubes. Solution-based process has several advantages when compared to the direct growth methods. It is a low temperature process, which results in depositing CNTs on rigid as well as flexible substrates. Additionally,

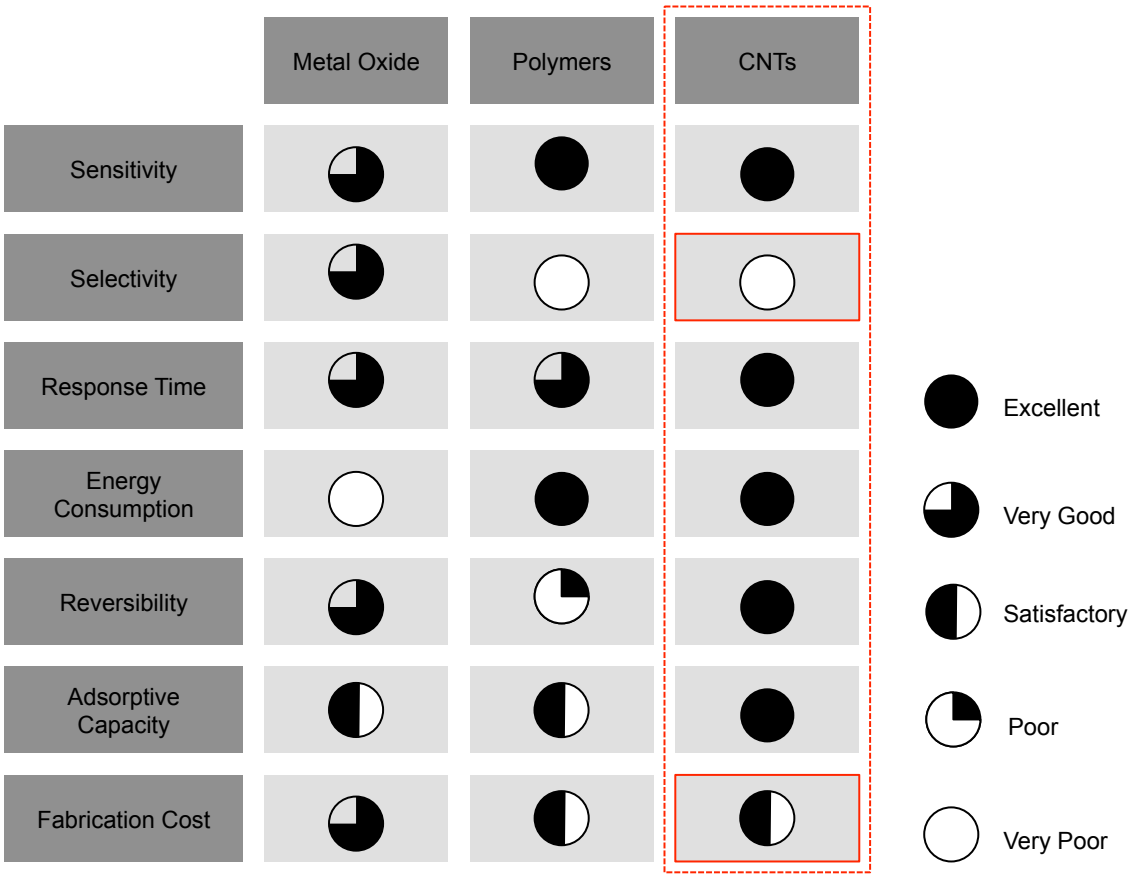

Figure 2.2: Chart summarizes the evaluation scheme for the three common technologies used in fabricating gas sensors while highlighting the technology used in this work which is CNT.

it doesn't require high-vacuum system, which reduces the fabrication cost significantly. Our focus in this work is on the solution-based CNTs. In the following discussion, we will present several common techniques used to coat solution-based CNTs onto different substrates, which are vacuum filtration, dip-coating, spin-coating and spray deposition.

2.2.1 Vacuum Filtration

Vacuum filtration is considered the most common method in fabricating CNT thin-films, due to its simplicity and processing consistency [54]. The filtration method involves vacuum filtering a dilute suspension of CNTs in a solvent over a porous filter membrane with pore size id 20-200 nm [15]. As the solution sifts through the membrane filter, CNTs are collected on the surface, forming an interconnected network. After filtration, the film is washed with copious amount of water to remove residual surfactant absorbed on the CNT surface. Filtration leads to highly uniform and reproducible films. Filtration is a scalable method under the condition of providing large filters. Fabricating CNT thin-films using this method provides extreme precise control over the film density. Such a property renders this method to be used in studying and investigating the different characteristics of CNTs. Its main disadvantage is that the fabricated films are deposited onto filter substrates, which is not an ideal substrates for wide range of applications. In order to overcome such a drawback, typically vacuum filtration technique is employed in transfer printing process, where CNT thin-films are firstly deposited onto the filter substrate and then transferred to other target substrate [55].

2.2.2 Dip-Coating

Dip Coating is a reliable technique in obtaining thin, uniform and partially aligned CNT films [56] [57]. The process scalability, cost effectiveness and its feasibility to be applied in roll to roll printing gives it several advantage over vacuum filtration technique[15]. The quality of the produced films is dependent on the solution viscosity, the interaction between the substrate and the solution as well as the coating speed. The process works as follow; the substrate is immersed in the CNT solution for 2 minutes and then it is withdrawn with a constant speed and left to dry in ambient nitrogen. After drying, this step is repeated until the required thickness and sheet resistances are obtained. With every additional coating the thickness of the film increases, thus the sheet resistance and the transmittance decrease. The thickness of the film can be controlled as well by changing the concentration of the CNT material in the prepared solution. Given that CNTs are intrinsically hydrophobic, it results in poor film adhesion with the substrate.

Typically, 3-Aminopropyltriethoxysilan (APTES) treatment is applied to the substrate to facilitate uniform nanotube bonding. It is worth mentioning that one main disadvantage of the dip coating method is that both sides of the substrates are coated, which may not be preferred for certain applications and cause excessive waste in the solution. A schematic illustrating the dip-coating process is shown in fig. 2.3

2.2.3 Spin-Coating

Spin Coating is a common process that is used to apply uniform thin-films to flat substrates [58]. It is a highly reproducible process that is widely used in the microelectronics industry during the application of photo-resists on silicon wafers. Typically, such process involves dropping a small amount of the solution onto the substrate to be coated, which is subsequently rotates at high speeds producing centrifugal forces that spread the solution uniformly over the surface. Several factor influence the thickness and the surface topography of the produced film such as; rotational speed, solution concentration and solution viscosity. The thickness of the film is controlled through the rotating speed of the substrate. Increasing the speed decreases the thickness. It can be also controlled

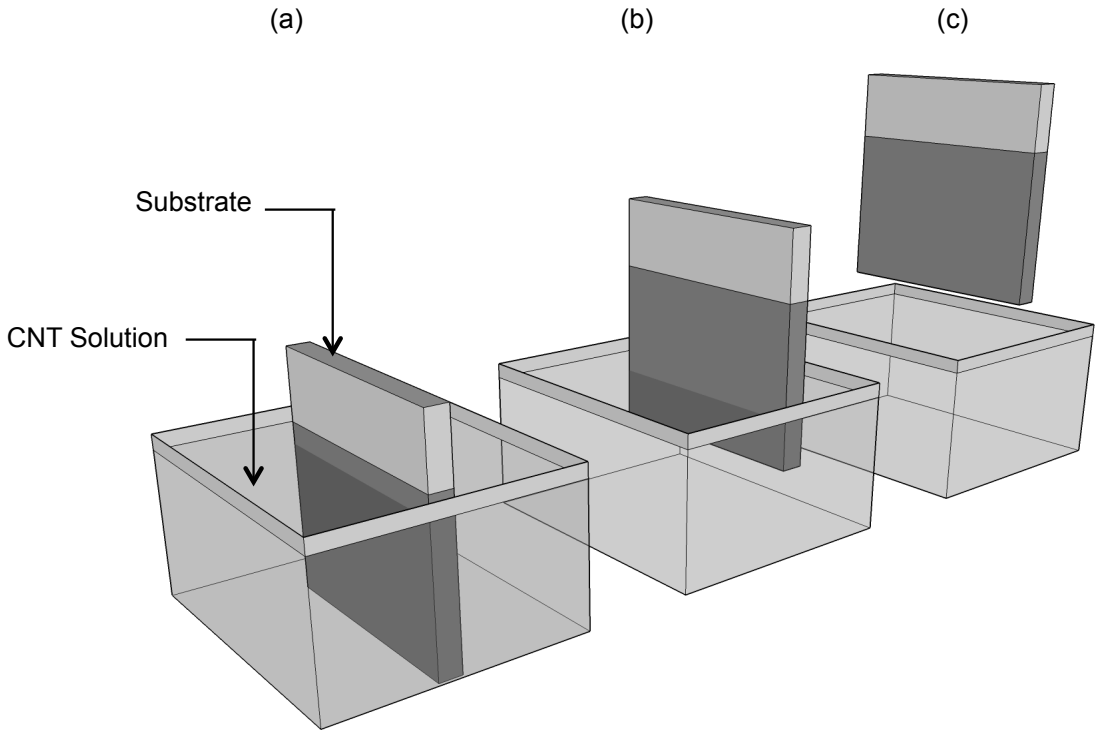

Figure 2.3: A schematic drawing showing the different steps of the dip-coating process, immersing the substrate in the CNT solution (a), pulling-out the substrate at a constant velocity (b) and drying the substrate (c)

through the number of times the spin coated layer is allowed to dry to allow a successive layer to be coated on the top of it. The main disadvantage of the spin coating technique is the non-uniformity of CNT distribution along the radial direction, which results in severe problems when trying to scale up the process. Moreover, roughly 90% of the ejected material is wasted during the process. In general, this method shows successful reproducible results when applied in small-scale (e.g. research laboratories) but not in the industrial level. A schematic illustrating the spin-coating process is shown in fig. 2.4

2.2.4 Spray Deposition

Spray technology has been used in wide range of application including surface coating, combustion and humidification. The concept of the spray process is simple: a colloidal suspension is sprayed uniformly over a substrate and the dispersing fluid is evaporated by heating, thus leaving the colloidal deposit to form the coating. Spray deposition is the process of forming liquid droplets onto the target substrate. Breaking up the bulk liquid into droplets (mist) is often referred to as atomization. A spray gun or atomizer nozzle is the device which perform the atomization process. Such process is usually performed by an atomizer nozzle (spray gun). Typically, the liquid jet or sheet is disintegrated using the kinetic energy of the liquid itself. Several methods can be applied to perform the atomization process. Accordingly, spray nozzles can be classified into three main technologies, air-assisted, ultrasonic and aerosol jet.

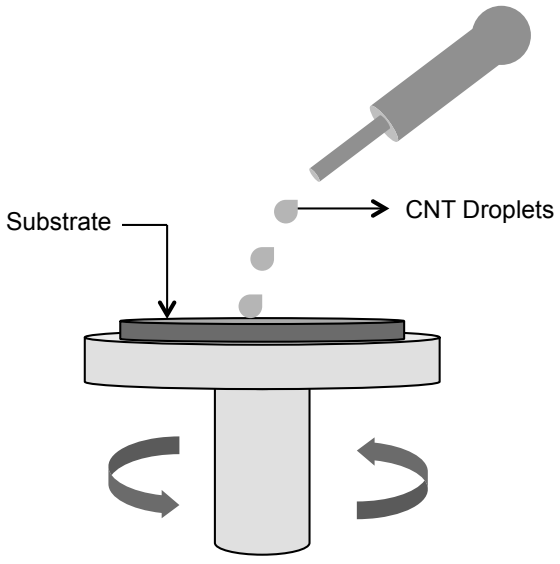

Figure 2.4: A schematic drawing showing the spin-coating process

In air-assisted nozzles, often called air spray nozzle, atomization is produced by relying on a high-speed air stream or gas, typically N_2. The fluid is fed to the material nozzle by gravity and mixed into the gas stream. The energy of the gas disrupts the fluid into droplets causing atomization. Ultrasonic nozzle works with entirely different principle. Piezoelectric transducer, driven by an electronic power generator, produces waves at ultrasonic frequencies, which causes vibration in the nozzle body. The formed liquid film at the vibrating surface, which is fed through the liquid passage, becomes unstable causing the ejection of mist of small droplets from the surface. In that case, the disintegration of the liquid is performed without applying any pressure. The frequency of these kind of nozzles are typically between 25 kHz and 130 kHz.

The performance of the air-assisted and ultrasonic spray nozzles is strongly dependent on different parameters, the size and geometry of the nozzle itself in addition to the physical properties of the liquid being atomized as well as the gaseous medium surrounding the droplets. Density, viscosity and surface tension are among the most important fluid properties. The variation in these properties affects directly the droplet size as well as the spray angle. For instance higher viscosity, which is equivalent to greater attraction between the liquid molecules, results in increased resistance for molecules to move away from each other. This consequently delays the disintegration process and increases the average size of the droplet. For the fabrication of all the devices presented in this work, we utilized an air-assisted spray nozzle. These kinds of nozzles, along with the ultrasonic spray nozzles, provide a fine degree of atomization [59], which in turns results in a more uniform and homogenous film.

Unlike air-assisted and ultrasonic nozzles, aerosol jet process, which is a concept introduced and patented by the company OPTOMEC, can deposit with feature sizes down to 10 microns and high placement accuracy. Such a process does not only disintegrate the fluid causing atomization, it also uses aerodynamic focusing for the high-resolution deposition of the fluid. The aerosol jet system consists mainly of two components. The first one which is the droplet generator where the atomization process takes place. Atomization can be performed using air-assisted or ultrasonic atomizer. The second module is for focusing the aerosol and depositing the droplets. Aerosol jet technology enables the possibility of patterning directly onto different substrates without the need for masks or resists. Nevertheless, when compared to the former methods, aerosol jet technology is relatively more expensive.

Typically, CNT solutions are sprayed through an air gun onto a heated substrate. The temperature of the substrate depends on the solvent and the surfactant used to disperse the

CNTs. Besides influencing the surface topography; the spraying parameters have a direct impact on the optical and electrical characteristics of the fabricated films. Figure 2.5 shows a schematic for the spray deposition process indicating the different parameters of the system. Further discussion on the effect of these parameters on the deposited film is performed in chapter 3.

Spray deposition was shown recently to be the best choice when low cost and large scalability films are required [59] [60] [61]. It guarantees efficient material usage at the cost of higher surface roughness when compared to spin-coating or dip-coating techniques. In spite of the effectiveness and the high quality films obtained from the latter techniques, they lack several aspects, which are essential for producing large-scale films. One additional advantage of spray deposition over the other techniques is its applicability to rough or patterned surfaces.

Figure 2.6 illustrates the comparison between the different deposition techniques, where it evaluates the performance of each technique according the criteria, scalability, film-roughness, thickness control, substrate choice and material usage.

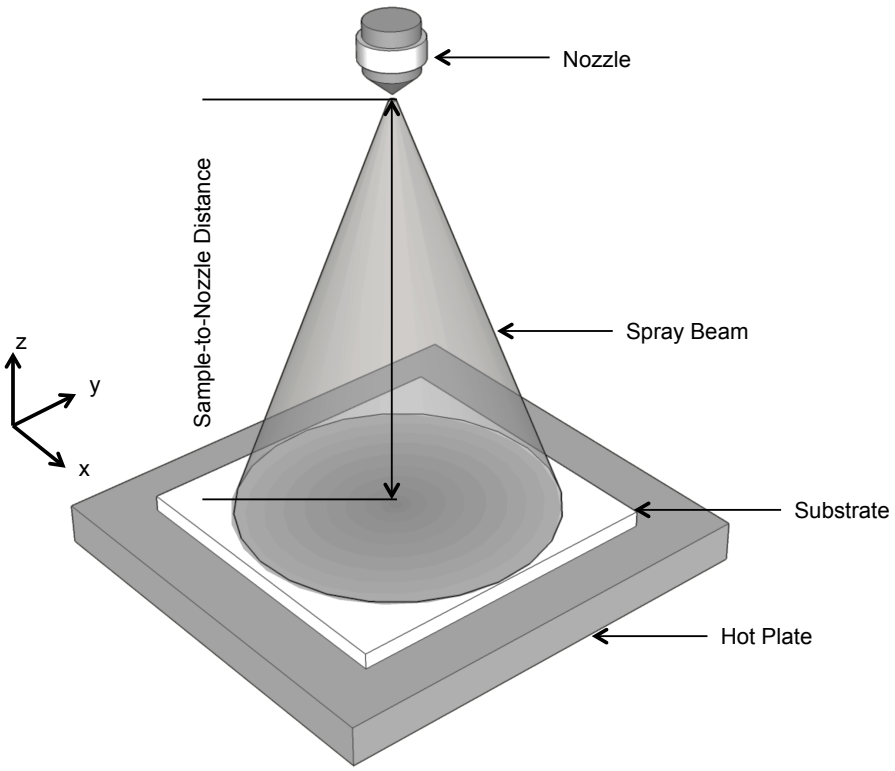

Figure 2.5: A schematic drawing for spray setup indicating the different spray parameters

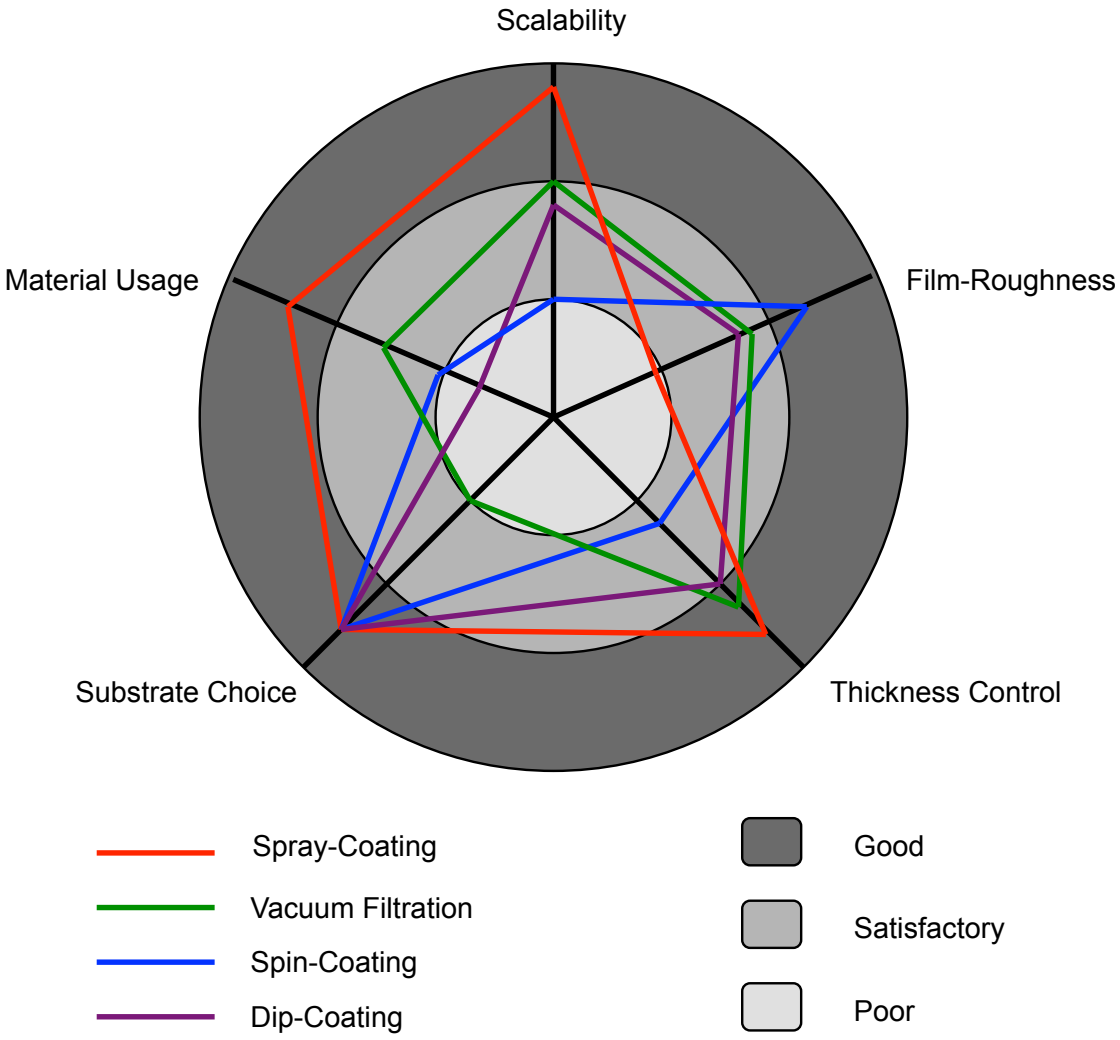

Figure 2.6: A comparison between the common techniques used in preparing CNT thin-films, spray deposition, spin-coating, dip-coating and vacuum filteration. The evaluation criteria of the different techniques is based on the discussion presented here

2.3 Techniques for Selective CNT Gas Sensors

As we discussed earlier, the main aspect that is still lacking in CNT-based gas sensors is there ability to differentiate between different gas analytes. Adding such a feature to the outstanding properties of CNTs render them as the ideal candidate for low cost, low weight and high performance gas sensing application. We can define two main approaches in order to fulfill the requirements of obtaining selective CNT based gas sensors. The first approach is related to the fabrication process, where additional steps are involved in the fabrication process of the CNT gas sensors. The second approach is related to the characterization procedure, where advanced characterization techniques are

performed on the CNT based gas sensors. In order to evaluate the different approaches, we define four main aspects for the evaluation process; accuracy, total cost, life time and practicality.

2.3.1 Fabrication Approach

Performing this alternative requires changes or modifications in the fabrication process of the CNT gas sensors. Changes in the fabrication process could result in changes in the characterization procedure or in the data processing as well. Nevertheless, the core change remains in the fabrication process of the CNT gas sensors. In this context, changes in the fabrication process means building an array of sensors for gas detection rather than a single sensor. A gas sensor array is made up with two or more sensing elements in order to detect targeted gas with data of higher dimension. Such step requires integrating several sensors on the substrate while keeping the total area of the array as minimum as possible, otherwise one main feature of the CNT based gas sensors could be lost, which is the possibility in miniaturization for portable applications. Moreover, in order to achieve the expected results from the sensor array, the response of each individual sensor in the array should be altered in a certain manner towards the different analytes. This is an additive fabrication step, which is performed after the deposition of the CNT layer.

Several methods can be deployed in order to alter the response of the CNT layer of each sensor in the array. Here we highlight and discuss three common techniques which are metallic nanoparticles (NPs) deposition, polymer coating and building the sensor array based on different kinds of CNTs rather than a single kind.

2.3.1.1 Metallic NPs Deposition

Deposition of metallic NPs is the most common method and widely used among many researchers [37]. The main attraction of such technique is its selective capability but also because it extremely enhances the sensitivity of the single CNT gas sensors. Materials such as Au, Pd, Pt, Cr, Rh, Al and Ag are previously reported to deliver a selective behavior from the CNT-based gas sensors [51] [62] [63] [64] [65]. Several techniques are used in order to functionalize CNT layer with metallic NPs such as thermal evaporation [66] [67], sputtering [64] and electrochemical deposition [68]. Many influencing factors affect the performance of the sensor after the functionalization process, such as the shape, size and the load of the deposited NP and thus decide the response towards the

different gases. Controlling such parameters is essential in order to obtain the expected results. Such effects are covered in details in chapter 4.

In principle, deposition of different metallic NPs on top of the different sensors in the array deliver quite accurate results in terms of the obtained distinction between the different analytes. The main problem facing such a technique is lacking the understanding of the sensing mechanism of the CNT after the functionalization process. Subsequently, finding the optimum combination of metals to be deposited on the same array is not an easy task. Understanding the interaction between the deposited NPs and the CNT layer is the corner stone in order to build high performance CNT gas sensor array.

Due to the fact that metallic functionalization usually depend on expensive materials such as Au and Pt, the fabrication cost of such technique is considered to be high relative to the other techniques. On the other side, this method has a longer operating life time when compared to polymer coating for example.

2.3.1.2 Polymer Coating

Recently, enhanced gas sensing by combining CNTs with organic polymers has been demonstrated [37]. Polymer coating is another type of functionalization, which also aim to modify the surface of the CNT layer but using polymers rather than metals. Spin-coating, spray deposition, dip-coating and drop-coating are among the common processes to coat the surface of the CNT with polymers.

Unlike metallic NPs, certain polymer such as polyethylenimine (PEI) can alter the properties of the CNT layer from p-type to n-type. Such a transformation is with a great benefit in blocking certain analytes while bonding with others. For instance, such functionalization on CNT chemFET resulted in detection of less than 1 ppb NO_2 while being insensitive towards NH_3 [69]. On the other hand, the same group showed that functionalization with Nafion (a polymeric perfluorinated sulfonic acid ionomer) results in gas sensors insensitive to NO_2 while exhibiting a good sensitivity towards NH_3. Similar to conductive polymer based gas sensors, such functionalization technique suffers from the short life time of the device. In general, devices and applications based on polymers usually requires encapsulation step after the fabrication process to increase its life time but such step is quite difficult to perform in an application like gas sensing. Additionally, defining the exact area to be coated on the array is a rather complex step with the commonly used techniques. This results in limiting the application of this technique to single CNT based gas sensors rather than array which affects the whole performance of the device negatively. The main advantage of polymer coating is its

low cost, nevertheless such an advantage is not sufficient to depend on that technique in delivering accurate and high performance CNT based gas sensor array.

2.3.1.3 Different Kinds of CNTs

Fabrication of gas sensor array based on different kinds of CNTs rather than a single kind is a technique, which shows high potential, yet not fully explored. The difference between the CNT could be in the tube length (short or long), the percentage of semiconducting tubes (67% or 90%), type of CNTs (single-walled or multi-walled) and functionalization (COOH or OH). The advantage of such technique that it does not require any additive fabrication process, it includes only the deposition of the different layers of CNTs which render such technique to be the cheapest relative to the others. One more advantage of such technique as well is its durability; the degradation in the sensitivity of the CNT layer is rather low.

The main problem faces such technique is the accuracy in differentiation. Due to the fact that all the sensors in the array depends more or less on the sensitivity of the CNT layer, the performance of the CNT gas sensor array is not expected to be the highest. Nevertheless, in applications where accuracy is not as important as low cost and long lifetime, such technique could be ideal.

2.3.2 Characterization Approach

Discrimination can be also achieved by obtaining different recovery or response time for the CNT film towards the different gases. Such a kind of measurement investigate the adsorption dynamics of the different gases at the CNT films. Hafaiedh et al [70] reported the possibility of obtaining discrimination between different VOCs based on their response time. Our group as well showed similar comparison between four gases (NH_3, ethanol, CO and CO_2) in terms of their recovery time and showed also the possibility to discriminate between at room temperature [71].

Such kind of characterization can be further performed at different frequencies not only at DC, which could deliver better discrimination between the gases and gives more insight on the sensing mechanism of the CNT film. In order to monitor the response and recovery time at different frequencies, we have first to understand the behavior of the CNT layer under different frequencies in terms of the changes that occur to the resistance and the reactance of the film. Such kind of investigation is discussed in chapter 6. This advanced characterization technique is often called impedance spectroscopy

measurement, which is a well-known technique commonly used to understand and gain insights on any electrical system [72].

The advantage of such a characterization technique is mainly its low cost, due to the fact that no changes occur to the fabrication process of the single CNT gas sensor. On the other hand, there is a lot of disadvantages for such technique. This technique is highly dependent on the experimental and environmental conditions. It is highly sensitive to small changes in the temperature or the humidity of the environment, which affects directly its repeatability. In crucial applications like toxic gas detection, depending on the recovery time of the sensor to identify the nature of the gas is unpractical. Such criteria limits the application where such technique can be applied. Nevertheless, applying this kind of characterization gives a lot of insights on the behavior of the CNT layer in general, which can be helpful in developing new methods to discriminate between different analytes. Figure. 2.7 summarizes the evaluation scheme for the proposed approaches as well as highlighting the techniques utilized and developed in this work.

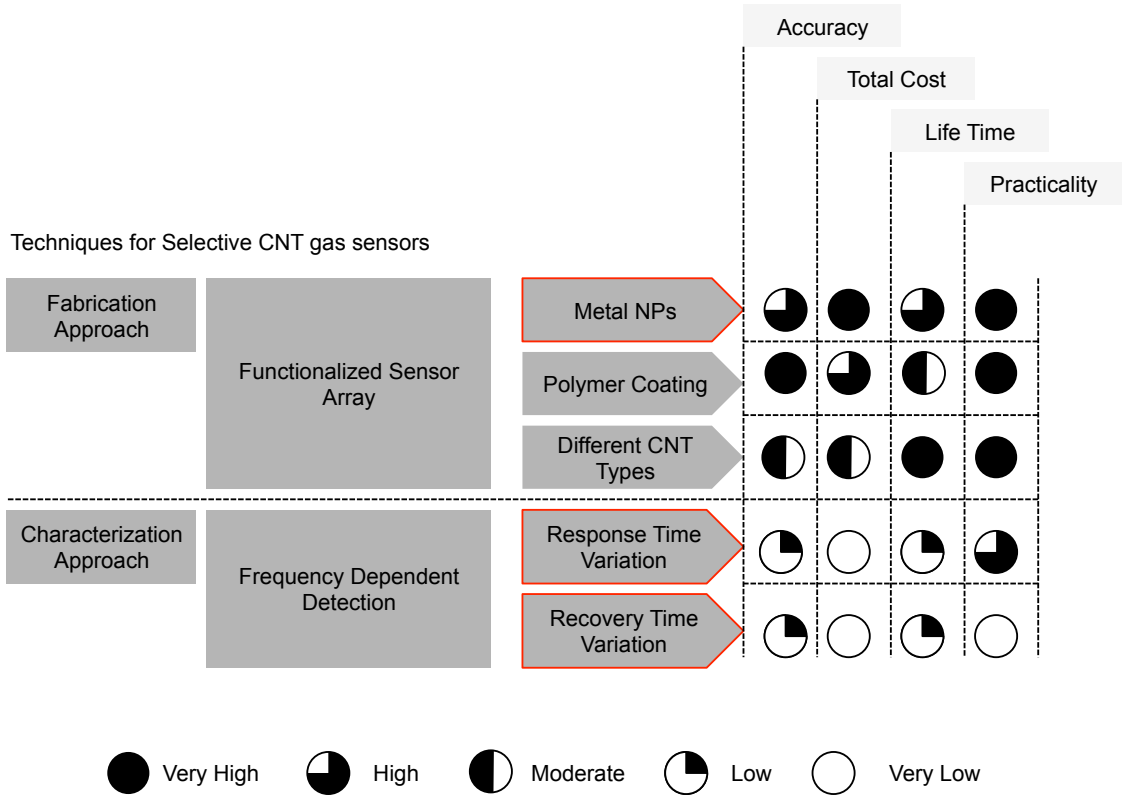

Figure 2.7: Chart summarizes the evaluation scheme for the proposed alternatives to achieve a selective CNT based gas sensors. The three techniques utilized and developed in this work are highlighted

2.4 Process Development Framework

In this section, we present the process development framework utilized for manufacturing of the different CNT based devices presented in this work. Figure 2.8 summarizes the different steps of the process development framework utilized for the manufacturing of the different CNT devices presented in this work. Developing and optimizing the process of producing CNT based devices involves four major steps. The choice of the application is the corner stone that the whole process development is built upon. In this work three kind of application are utilized, CNT thin-films for conductive electrodes, CNT based gas sensor and CNT based gas sensor array.

According to the application choice, the appropriate substrate is chosen. For instance, CNT thin-films for conductive electrodes are typically deposited on glass or plastic substrates rather than Si substrates. The material of the substrate influences the different parameters in the fabrication process as well. Subsequently, the fabrication processes in-

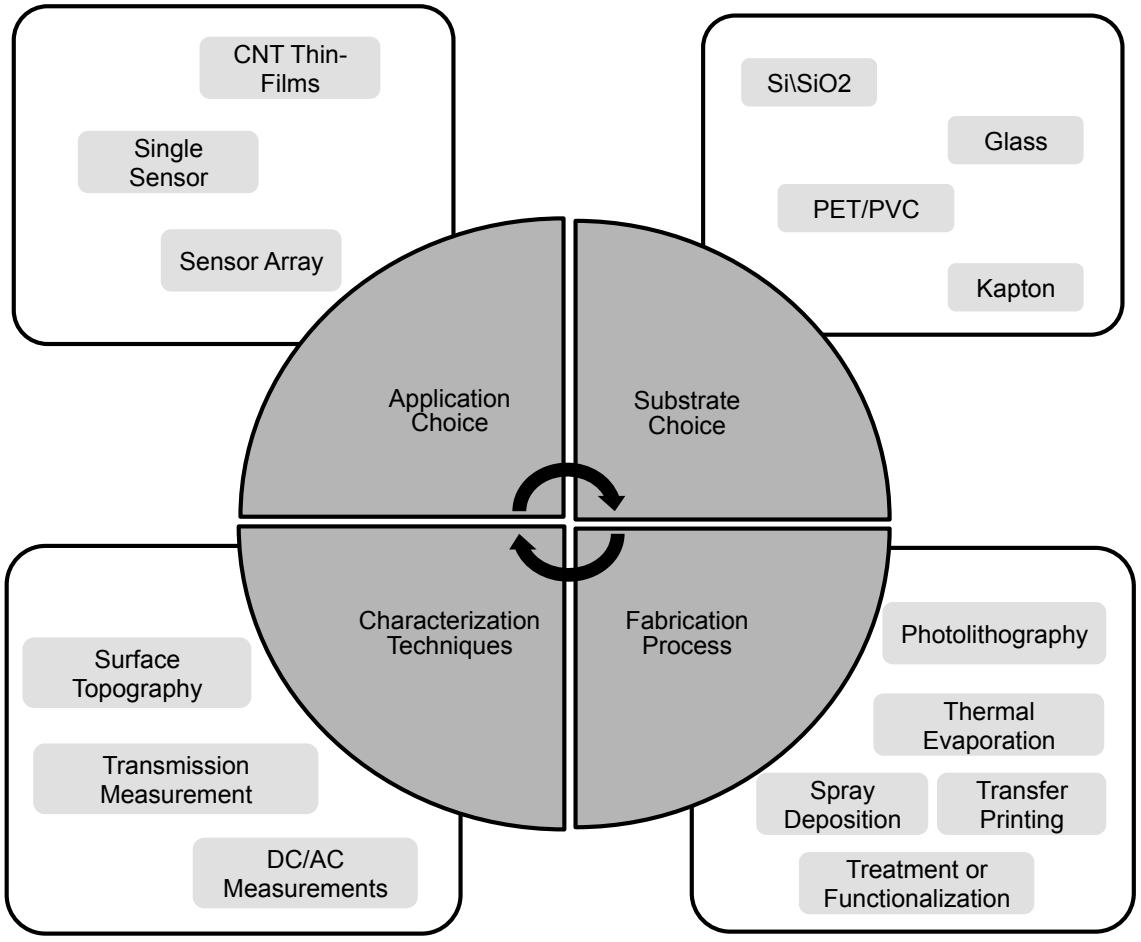

Figure 2.8: Chart summarizes the process development framework utilized in this work for the fabrication of the different CNT based devices

volved in the development process is dependent on the choices of the former steps. CNT thin-films for conductive electrodes require only spray deposition then post-deposition treatment. On the other hand, the process of fabricating CNT based gas sensor arrays involve several fabrication steps, photo-lithography, thermal evaporation, spray deposition and finally metal functionalization.

Calibrating and optimizing the different processing parameters is an integral part of the process development. In order to collect the feedback of the performance of the fabricated device, different characterization techniques are required.

The characterization techniques can be divided into two main parts, basic characterization and advanced characterization. Basic characterization involves sheet resistance measurement, optical transmission measurement and surface topography. These kinds of measurement are applied to CNT thin-films for conductive electrodes as will be discussed in chapter 3. Advanced characterization involves complex impedance characterization, which monitor the behavior of the device within a certain frequency range as well as modeling that behavior with an equivalent circuit. Such kind of characterization is applied to CNT based gas sensors, which will be discussed in chapter 6.

2.5 Summary

In this chapter, we presented an overview for the different technologies utilized as gas sensors based on the electrical variation of the sensing material. We evaluated the performance of the three commonly used technologies, metal oxide semiconductors, polymers and CNT, according to certain criteria. We presented as well the four commonly used techniques to prepare CNT thin-films, vacuum filtration, dip-coating, spin-coating and spray deposition. While highlighting spray deposition technique, which the technology utilized in this work, we evaluated these different techniques according to a proposed scheme. Finally, we showed the process development framework used for fabricating the devices presented in this work.

Chapter 3

CNT Thin-Film Technology: Spray Deposition and Transfer Printing

One step towards the realization of flexible electronics devices based on CNTs, is mastering and optimizing the different fabrication techniques of CNT networks on flexible substrates. In this chapter, we demonstrate the fabrication of high quality CNT thin-films through a reliable, reproducible and low cost spray deposition technique. CNT solutions were prepared using carboxymethyl cellulose (CMC) and sodium dodecyl sulfate (SDS) as dispersive agents. We investigated the effect of using each dispersive agent on the performance of the fabricated layer in terms of surface morphology, optical and electrical characteristics. CNT thin-films with an average surface roughness of 5 nm with a sheet resistance of 170 Ω/sq at a thickness of 50 nm , are presented. Furthermore, transmittance of 86 % at a wavelength of 550 nm with a sheet resistance of 250 Ω/sq is achieved.

We introduce as well a transfer printing process for the fabrication of CNT thin-films on plastic. CNT thin-films are firstly deposited on glass using spray deposition process and then through a low temperature and reproducible process is transferred to plastic. By comparing the performance of the CNT thin-films before and after the transfer printing process, we reached almost a similar quality in terms of surface morphology, Raman spectrum, optical and electrical characteristics. The transfer printing process results in CNT thin-films on plastic with lower surface roughness when compared to the directly spray deposited on plastic.

3.1 Overview on CNT Thin-Films on Different Substrates

The discovery of CNTs was seen as a possibility of revolutionizing the electronic research as CNTs show superior performance because of their impressive structural, mechanical and electronic properties [15] [73] [74]. Initially, a lot of work was concentrated on the electronic, optoelectronic and sensing behavior of individual CNTs [73]. More recently, the attention has shifted towards assemblies of CNTs, rather than single ones. One of the most common applications of CNT films involves electrodes for solar cell, photo detectors or organic transistors [15] [74]. CNT thin-films with density close to the percolation threshold show semiconducting behavior and can be used as an active layer in thin film transistors [75][76]. Additionally, CNT thin-films exhibit high optical transparency, which renders them as an ideal candidate to replace the relatively expensive ITO [77]. The main advantage of CNTs over ITO is their capability to be fabricated on flexible substrates [78]. Despite of the great potential of CNTs in the field of flexible electronics, there are still a lot of problems facing this new rising technology. Several techniques were reported for the deposition of CNT films on plastic. Direct deposition using spray coating or spin coating produced films with lower conductivity when compared to ITO [61]. Spin coating has the further disadvantage of limited film thickness [79]. Chandra et al. [80] reported the fabrication of CNT transistor on flexible substrates. CNT was directly deposited on pre-fabricated bottom-gated TFT structures on flexible substrate using surface functionalization. Moreover, Rogers et al. [81] reported a medium scale integrated circuit on flexible substrate composed of up to nearly 100 transistors. Zhang et al. [41] adopted a vacuum filtration method to prepare CNT films and transfer them to a flexible substrate using PDMS stamps. PDMS stamp is used to peel the film off the filtration membrane and release it onto the desired substrate, but this transfer process requires constant heating at 100 °C in order to improve the adhesion of the target substrate.

Zhou et al. [55] reported a similar method for transferring CNT thin films to flexible or glass substrate using also vacuum filtration process. They also succeeded to pattern the film during the transfer process, but again the process requires a relatively high temperature. Liu et al. [82] made use of the self-releasing feature that occurs to SDS based CNT films. They succeeded in transferring CNT films to other substrates without using PDMS. The technique depends on allowing the ultra-thin CNT films to non-destructively self-release into freestanding films on the water surface. Then, it could be easily transferred to the substrate of interest while retaining their original sizes and

network structures. Although this technique results in high quality CNT films, it requires delicate handling to the deposited layer in order to be reproducible.

Here, we investigate the performance of CNT thin-film layer deposited by spray-coating technique. A comparison between the SDS and CMC based CNT thin-films is presented as well. SDS based CNT thin-film is deposited on flexible substrates by a reproducible and simple transfer printing process. The results achieved from such process is compared with the directly sprayed layers on the same substrate.

3.2 Materials and Methods

3.2.1 Solution preparation

CNT solution-based spray deposition is a low temperature process that has several advantages when compared to direct growth methods. Several factors are affecting the solution-based deposition process: CNT material quality, degree of CNT dispersion, choice of surface treatment and activation of substrates and removal of dispersing aids after deposition. CNTs are intrinsically subject to strong van der Waals forces [15]. Overcoming these forces and consequently breaking up the CNT bundles is the first challenge towards the preparation of CNT solutions. With the aid of high power sonication such as probe sonicator or bath sonication, purified CNTs in powder form can be dispersed into solvent for further solution processing. Two common approaches are pursued in dispersing CNTs: dispersion in organic solvents and surfactant based aqueous dispersion [79]. In this work, all the experiments are based on CNT aqueous solutions.

Most surfactants are water soluble and are capable of individualizing CNTs at high concentration. Additionally, they can be rinsed off in subsequent washing of the film. Triton X-100, sodium dodecyl sulfate (SDS) and CMC are the most widely used surfactants. The mechanism of the surfactant works as follows: The hydrophobic end of the surfactant attaches to CNTs, while the hydrophilic end helps pulling the CNTs into water [83]. The interaction between the surfactants and CNTs depends on the chemical characteristics of CNTs, the surfactant itself and the solvent. Sonication helps in breaking the van der Waals forces between the nanotube and in turn attaching the surfactant to the tube.

In our work, SDS or CMC were dissolved in distilled water to make 0.5 wt% aqueous solution. It should be mentioned that increasing the amount of the surfactant increases the viscosity of the solution, which later affects the deposition process. The CMC solution is stirred overnight in order to uniformly dissolve the surfactant in water. After that, 5 mg

of CNTs are added in 10 g of 0.5 wt% CMC-aqueous solution to make 0.05 wt% CMC based aqueous CNT solution. Sonication of the CMC based solution is performed for 20 minutes using probe sonicator at 50% power (~ 48 Watt). On the other hand, SDS dissolves in water after only one hour of stirring. Sonication of the SDS based solution is performed for 30 minutes using probe sonicator at 50% power (~ 48 Watt). Solutions are centrifuged for 90 minutes at 15000 rpm and 80% of the centrifuged solution is taken from top to be used for the deposition.

3.2.2 Substrate preparation

Substrate surface treatment is required in order to achieve a uniform, homogeneous and stable CNT film. The substrate should be cleaned from any contaminants. This is done by immersing the substrates into acetone and subjecting it to an ultrasonic bath for 10 minutes and then repeating the step with isopropanol instead of acetone. In preparing plastic substrates the acetone step is skipped due to the degradation that acetone causes to plastic. Plasma cleaning is followed in order to convert the substrate surface from hydrophobic to hydrophilic. This step enhances the surface adhesion and allows the deposition of uniform surface coating. Plasma cleaning conditions varies depending on the substrate used. In case of glass, plasma cleaning was done for 1 minute. Plastic substrates require only 30 seconds at a lower power. CNT films are characterized by their weak adhesion to the substrates [57] [84]. We noticed that plasma cleaning is not sufficient to produce stable CNT films on glass, as the plasma effect vanishes after

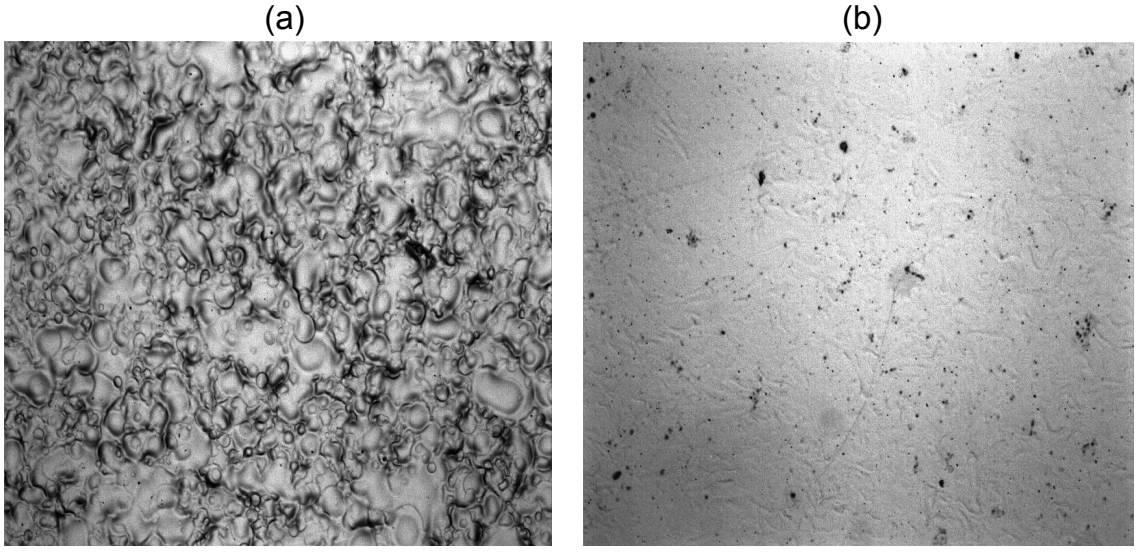

Figure 3.1: Optical image of spray deposited layer of CMC solution at the dry (a) and intermediate (b) regime

few hours from the cleaning. Thus the CNT films can detach easily from the substrate after the post treatment process and the removal of the surfactant. In order to enhance the adhesion between the substrate surface and the CNT film an intermediate surface treatment step has been introduced based on 3-Aminopropyltriethoxysilan (APTES) [15]. 1 wt% of APTES was added to isopropanol solution and the substrates are soaked in the solution for 15 minutes after the plasma cleaning.

3.2.3 Spray Deposition Process

A commercially available automatic air atomizing spray gun (Krautzberger GmbH, Germany) was used in depositing CNT thin-films. The spray gun contains an internal pneumatic control system which is activated by an electrochemical 3/2-way valve connected to a timer for precise spray time adjustment. The performance of any kind spray nozzle is strongly dependent on its size and geometry as well as the physical properties of the liquid being atomized and the gaseous medium surrounding the droplets. Here, a 0.5 mm nozzle orifice diameter was chosen. Other spray gun settings that were varied to obtain the desired spray characteristics are material flow rate, atomizing gas (N_2) pressure and nozzle-to-sample distance. Boiling point and vapor pressure of solvents are of great influence to the drying behavior of droplets in spray and hence the layer formation.

In all our experiments we kept the sample to nozzle distance at 27 cm. The other spray parameters varied according to the type of the surfactant used and the material of the substrate. In spraying CMC based CNT film on glass, the substrate temperature is set to 80 °C and the atomizing gas pressure is kept below 1 bar. On the other hand, in spraying SDS based film on glass or plastic, the hot plate temperature is set to 60°C and the atomizing gas pressure is kept below 0.5 bars in order to achieve the low deposition rate required in spraying SDS solutions.

We sprayed both SDS and CMC based CNT solution on glass substrates in order to compare the results of both films with the state-of-the-art CNT films mentioned in literature. Spray deposition can be performed in three different regimes: Dry regime, intermediate regime and wet regime. The wet regime can be obtained by either decreasing the hot plate temperature or decreasing the nozzle-to-sample distance. Such parameters results in a layer with wet droplets on top of the substrate, which as a consequence produce layers with non-uniform thickness distribution. The dry regime is obtained through either increasing the nozzle-to-sample distance or increasing the hot plate temperature. Such arrangement allows the solvent to evaporate before reaching the

substrate, which results in non-homogeneous and non-overlapping layers of CNT thin-film, thus can be easily de-laminated in the post treatment process. The intermediate regime is the one more suitable for depositing CNT thin-films. Such regime results in uniform and homogeneous layers where good overlapping between the droplets and precise control of the film thickness is achieved. Figure 3.1 shows an optical image comparing between a spray deposited layer of CMC at the intermediate and dry regimes. Due to the fact that the solution properties is more dependent on the surfactant properties rather than the CNTs, we calibrated the spray process parameters by depositing the surfactant solution (without CNT) on the target substrate.. Such a strategy is very efficient and can be generalized for any newly used surfactant.

Both surfactants were sprayed at the intermediate regime. CMC based solutions were sprayed at temperature of 80 °C in order to deposit films of the desired characteristics. SDS based solution on the other hand, was deposited on lower temperature of 60 °C, lower air pressure and lower deposition rate. Due to the foam formation for the SDS material, changing any of the mentioned parameters would change the spraying regime. This results in the formation of irregular features in case of the wet regime and dark spots at the interface of the droplets in case of the dry regime.

3.2.4 Post-Treatment Process

The post-treatment process is required in order to remove th surfactant from the deposited CNT thin-films. CMC requires treatment for 16 hours in diluted HNO_3 (4M) while SDS based solution requires only soaking the film in distilled water for 10 minutes. The post-treatment process for CMC based CNT thin-films is highly sensitive to the amount of the HNO_3. Depositing thick CNT layers requires either higher acid concentration or longer post-treatment time. The long post treatment process of CMC solution in HNO_3 did not allow us to deposit it on other substrates rather than glass. We found that SDS based films can be easily detached from the substrate directly after the post deposition treatment which is not the case in CMC based films. This feature can be exploited in transferring SDS based CNT films from one substrate to the other as will be shown in the next section. Figure 3.2 summarizes all the steps included in the process of spraying CNT thin films based on CMC as well as SDS.

3.2.5 Transfer Printing Process

Beside direct deposition, there are several alternative ways to obtain CNT films on flexible substrates. One of the reported methods is based on the transfer of a CNT film

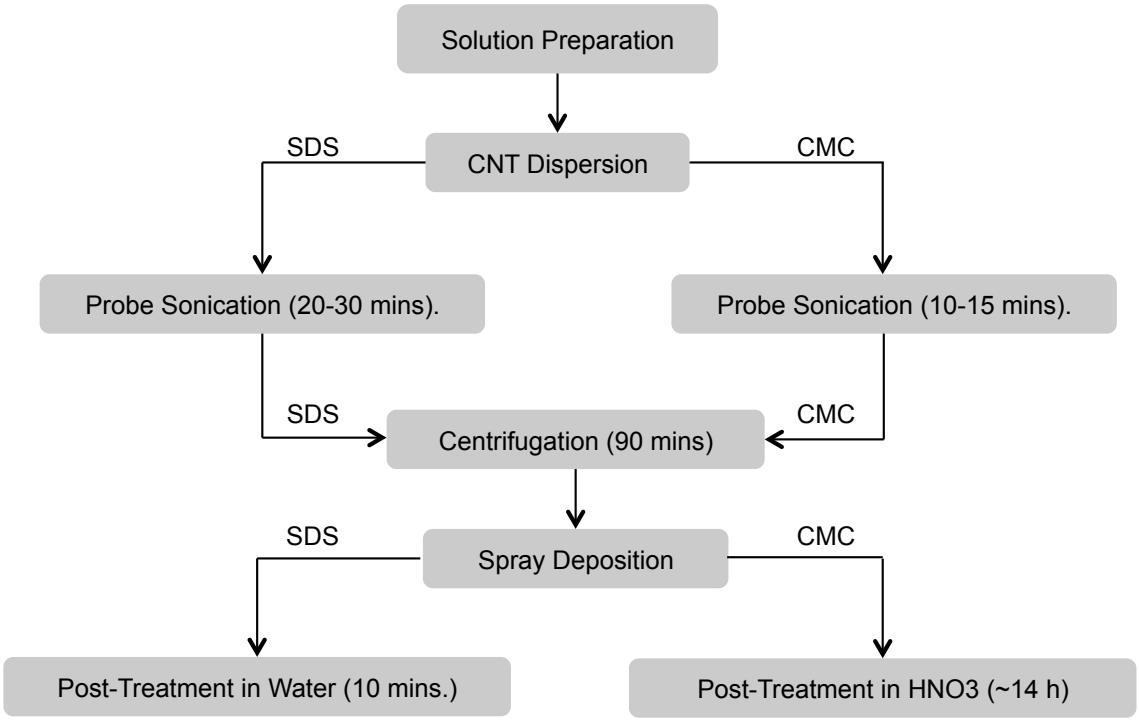

Figure 3.2: Chart summarizing the main steps in using CMC and SDS based CNT thin-films

on PDMS followed by the transfer from PDMS to the desired substrate. The original film can be either directly grown on the original substrate [85] or deposited by vacuum filtration technique[83]. In our case, the film is obtained via an optimized and highly reproducible spray process on glass, which is described in the previous section.

Figure 3.3 shows the steps required for the transfer printing process. Transferring SDS derived CNT film from glass to PDMS is achieved by sticking carefully the PDMS layer on the glass substrate where the film is deposited making sure that no bubbles occurs at the interface. This step is followed by immersing the stack in water for 30 seconds. Water helps in dissolving the remaining SDS that binds the film to glass. The smooth surface of the PDMS and its conformal contact makes it easier for the CNT layer to attach to it. PDMS layer with the transferred CNT film on top of it is then placed carefully onto the plastic substrate, which should has already been chemically treated with APTES for 15 minutes. The stack is placed on a hot plate adjusted at 65 °C for 5 minutes. Minimal pressure is applied during this step. Then, the PDMS layer is removed carefully from the plastic substrate.

Transferring the films from PDMS to the desired substrate depends mainly on how good the PDMS conforms to the aimed substrate avoiding any air enclosure at the interface. PDMS adhesion gets worse at high temperatures [86]. Thus, temperature is a key

parameter in transferring CNT thin-films. When transferring to plastic substrates, e.g. polyvinyl-chloride (PVC) or poly-ethylen-terephthalat (PET), temperature can also cause deformation to the plastic material, therefore it has to be kept sufficiently low.

3.3 CNT Thin-Film Deposition on Glass Substrates

Figure 3.4 shows the relation between the sheet resistance and the optical transmittance of spray deposited CNT thin-films on glass substrate. The square curve is CNTs with ~ 67% semiconducting tubes and with average tube length of 1μm dispersed in CMC solution, while the triangle curve is the same type of CNTs but dispersed in SDS. Taking a close look at the characteristics of SDS based films reveal reasonable performance in terms of sheet resistance at any given transmittance, with the lowest data point corresponding to 177 Ω/sq at 78%. The results indicate comparable performance in terms of sheet resistance and transmittance for the same type of CNTs and little effect due to the two different dispersant employed. It's worth mentioning here that the data points plotted for CMC based films reach significantly lower values since the film thicknesses achieved are higher.

Another method to quantify and compare transparent conductive thin films is via equation 3.1, where σ_{op} is the optical conductivity and Z_o = 377 Ω is the impedance of free space [87].

$$T = \left(1 + \frac{Z_o}{2R_{sh}} \frac{\sigma_{dc}}{\sigma_{op}}\right)^{-2} \tag{3.1}$$

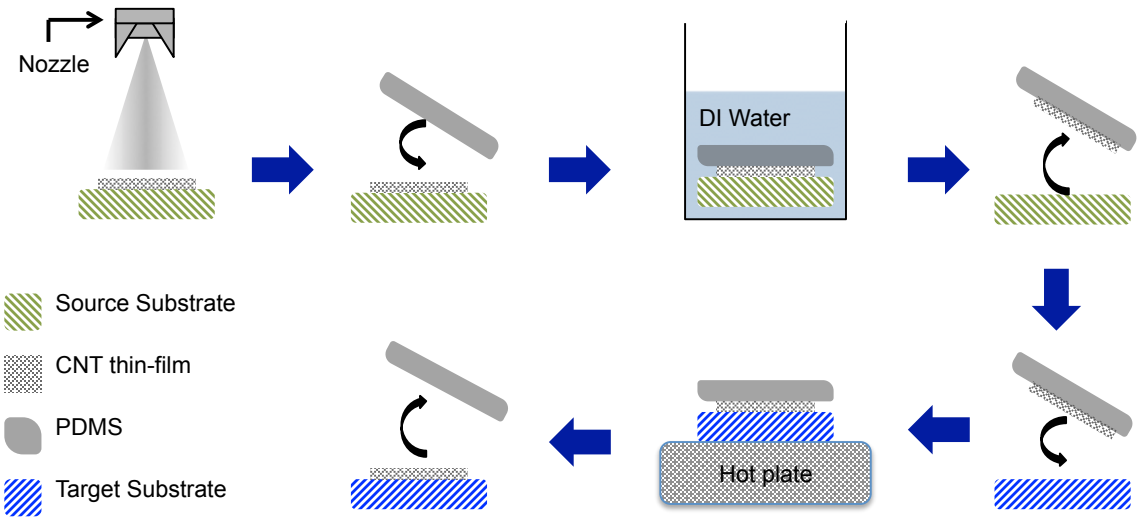

Figure 3.3: A schematic shows the steps for the transfer printing process

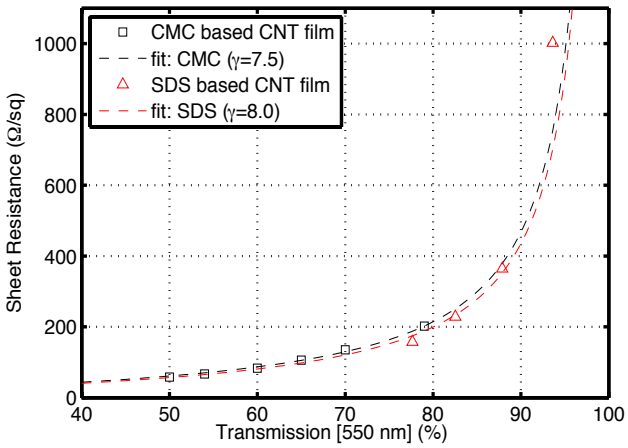

Figure 3.4: Comparison of sheet resistance and optical transmission obtained for CNT films deposited from SDS and CMC based dispersion.

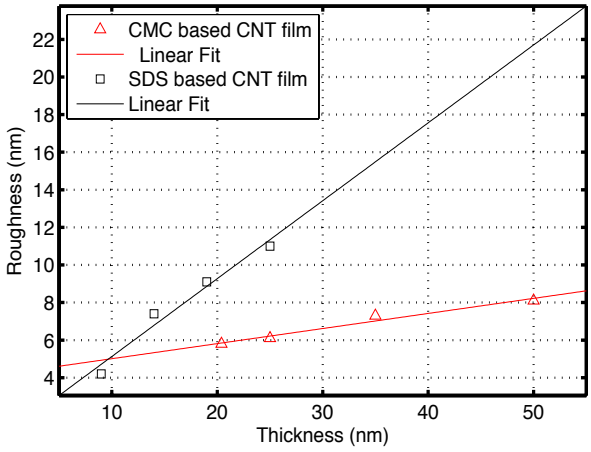

Figure 3.5: The relation between film thickness and surface roughness shows a nearly linear behavior within the measured thickness for both SDS and CMC based CNT films, where SDS based films exhibit higher surface roughness

This formula is generally applied to thin metal films where the absorption of the material is significantly lower than the reflectance and the thickness is much smaller than the wavelength of interest. Typically, the value for the optical conductivity of CNT thin-films at 550 nm is chosen to be 200 S/cm, as determined by Ruzicka et al. [25]. Since the optical conductivity is independent by the doping levels, this value is assumed to be constant even among differently processed films. By fitting the data plotted in fig. 3.4 with this equation a value of 7.5 is obtained for the ratio $\gamma = \frac{\sigma_{dc}}{\sigma_{op}}$ for CMC based films and 8 for SDS based films. This ratio is often used as a figure of quantitative comparison of CNT thin film performance.

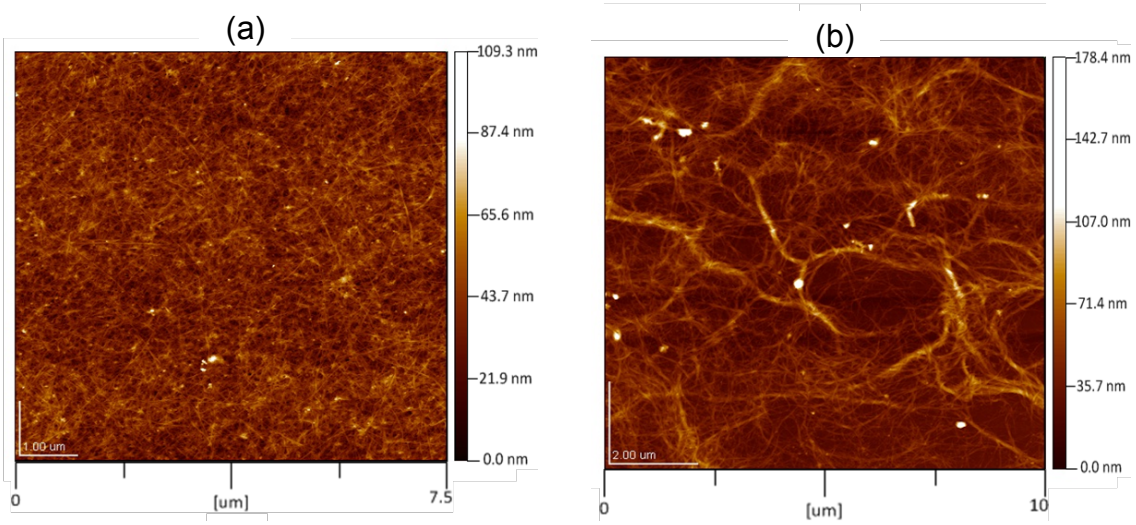

Figure 3.6: AFM images of two CNT films directly deposited on glass dispersed in CMC (a) and SDS (b)

Figure 3.6 shows two AFM images for CNT films deposited on glass based on CMC and SDS dispersive agents. Using CMC as a dispersive agent results in fewer number of bundles in the deposited CNT film. This is due to the fact that CMC is a better dispersive agent than SDS. Actually, achieving a completely de-bundled CNT solution is quite complicated, since longer sonication process breaks down the nanotubes rather than de-bundling them. Moreover, CMC based CNT thin-films showed lower surface roughness than SDS based films with the same thickness as shown in fig. 3.5. As consequence of the low deposition rate required in spraying SDS based solution, as described in the experimental section, more spraying time is required to obtain the same film thickness compared to the CMC based film.

3.4 CNT Thin-Film Deposition on Flexible Substrates

After achieving high performance CNT films on glass, we then sprayed the CNT solution directly on plastic. Two kinds of plastics were used PVC and PET. Depositing CNT directly onto plastic could be quite difficult especially in case of CMC surfactant. The process of depositing CMC based films requires keeping the substrate at relatively high temperature, which, in turn, might cause some deformation to some plastic substrates. Moreover, the post deposition treatment is performed in HNO_3 for at least 24 hours, which has a negative effect on the properties and the characteristics of plastic. We have therefore concentrated on SDS-based CNT solution. Since the spraying parameters developed for glass were kept, we can assume that the obtained film thickness remains

unchanged as long as we apply the same spraying time. Figure 3.7 shows the relation between optical transmission and sheet resistance for both PET and PVC films before doping. PVC shows lower sheet resistance at the same transmission, which could be attributed to the smoother PVC surface with respect to PET. The samples were soaked in concentrated nitric acid for 1 hour. The sheet resistance decreased largely after the doping reading comparable results as for the glass case as shown in fig. 3.8 . It is worth mentioning that doping plastic in nitric acid could affect the substrate negatively, thus the doping time should be optimized with caution.

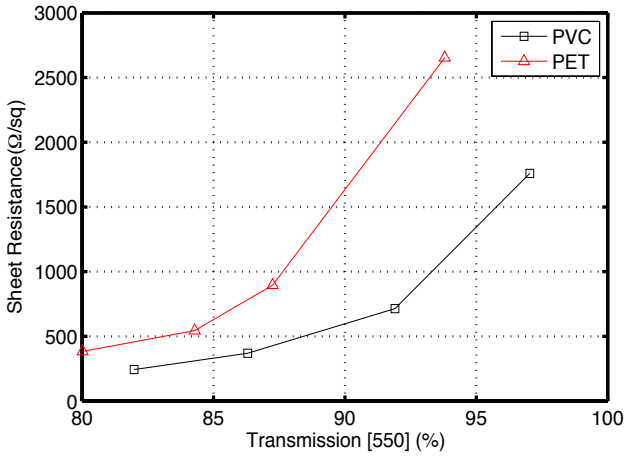

Figure 3.7: Relation between sheet resistance and optical transmission for CNT films deposited on different plastic substrates (PET and PVC)

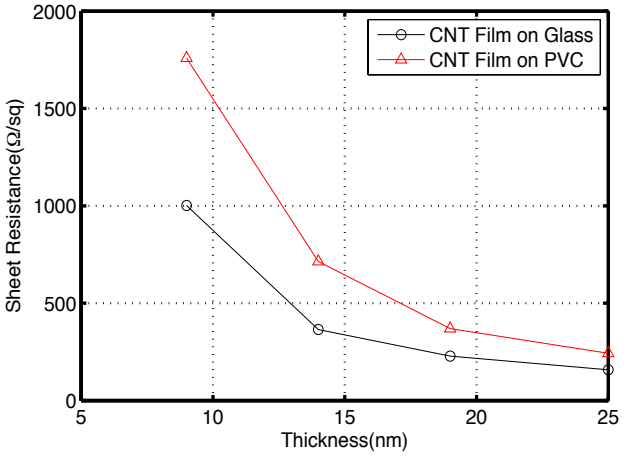

Figure 3.8: Comparison of the sheet resistance of films deposited on glass as well as PVC with respect to the thickness of the film

3.5 Transfer Printing of CNT Thin-Films

3.5.1 Optical and Electrical Characteristics

The efficiency and the performance of the transfer process rely on how the conductivity and the transmission of the film are affected by the process. Although, the performance of films on PVC was better than those on PET, we found that PVC cannot sustain the temperature applied during the process and slightly deforms. In order to overcome this deformation we decided to use an enhanced PET material, which is as thin as the PVC, but it is more resistant to higher temperature. Films were deposited using CNTs with average tube length of 10 μm and with 67 % semiconducting tubes from Hanwha Inc. Figure 3.9 shows that the sheet resistance of the film increases by 16 % from its original value after the transfer while the inset picture shows the deposited film on PET. This effect could originate from non-complete transfer for the CNT film. Such effect can be compensated by soaking the film in concentrated HNO_3 for 1 hour. The amount of time spent in the acid depends mainly on the characteristics of the plastic substrate and it's chemically resistance to the acid treatment. Doping before the transfer process was not possible in this case, since APTES treatment is not done and the film would simply detach from the glass during doping. The characteristics of the transferred CNT films on PET are compared to the directly deposited films on PET and also with films deposited on glass substrate as shown in fig. 3.10. Transferred films shows lower sheet resistance values than those directly deposited on PET. The transferred films were originally deposited on glass where they have lower sheet resistance. The reduced roughness of the glass with

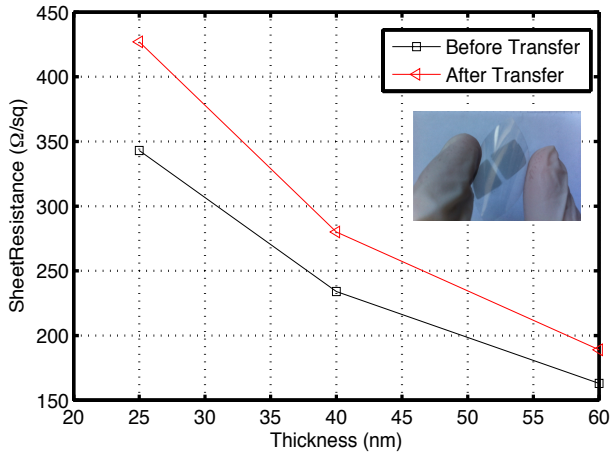

Figure 3.9: Comparison of the sheet resistance of CNT films before and after the transfer process. Inset picture is the fabricated CNT film on PET substrate

respect to the plastic substrate and the transfer of the film from one substrate to the other are responsible for the difference in performance.

3.5.2 Surface Morphology

Figure 3.11 shows the surface topography of the CNT film transferred to plastic. When comparing it to fig. 3.6b we can notice that there is no significant change in the film morphology. Transferred films shows slightly lower surface roughness than those directly deposited on plastic, since, they were originally deposited on glass which inherently produces films with lower surface roughness than plastic.

3.5.3 Raman Spectroscopy Measurement

Another way of evaluating the quality of the transferred CNT film is the Raman spectroscopy measurement. Figure 3.12 shows the Raman spectra of CNT films; i) directly deposited on glass, ii) directly deposited on PET and iii) transferred from glass to PET. By taking a closer look at the curves, one can notice a small D-band (1340 cm^{-1}) is obtained for the CNT films deposited on glass which implies the presence of few defects in the fabricated film [88]. The corresponding G/D ratio for that film is ~ 21. In fig. 3.12b and 3.12c, the fact that PET consists of carbon molecules introduced new peaks beside the normal carbon nanotube peaks [89]. This is indicated by the blue curves in both figures. Moreover due to the large defects that are inherently present in PET [90] [91], we can notice the high D-band in both figures. Since the defects in PET were the dominant

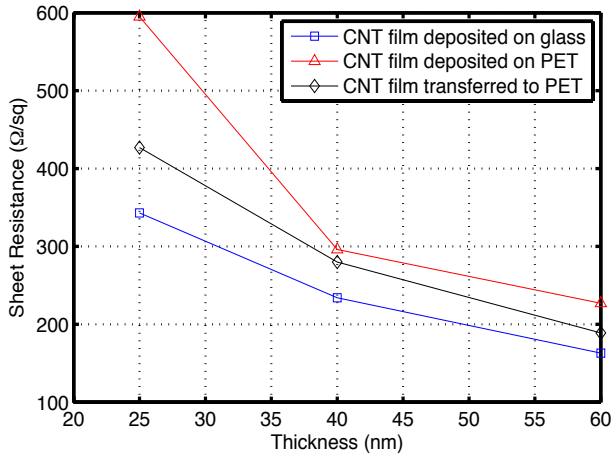

Figure 3.10: Comparison of the sheet resistance of the CNT film deposited on glass (blue squares), deposited on PET (red triangles) and deposited on glass and then transferred to PET (black circles) with respect to the film thickness

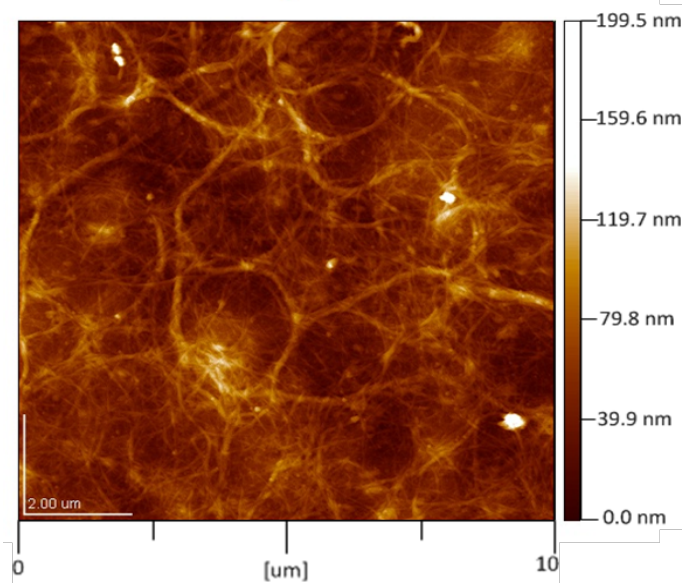

Figure 3.11: An AFM image for a CNT layer transferred onto a plastic substrate

effects in the measurement, it was hard to evaluate the defects present in the carbon nanotube. Although the G/D ratio calculation was quite difficult due to the mentioned PET defects, it points to relatively small defects in the carbon nanotubes which agrees with the results obtained for films deposited on glass.

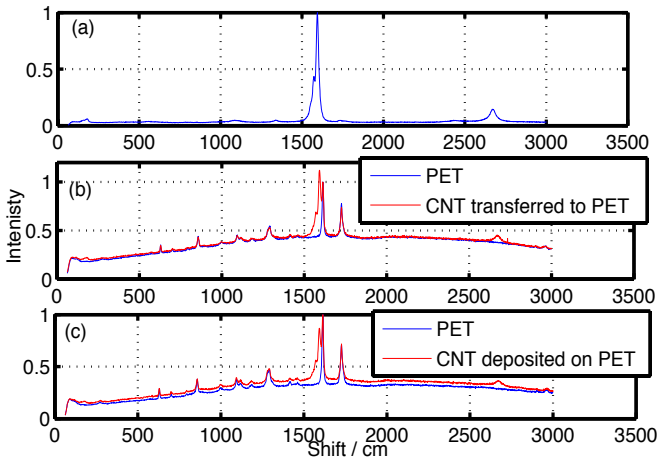

Figure 3.12: Raman spectra for CNT films directly deposited on glass (a), transferred to PET (b) and directly deposited on PET (c). The blue curves in (b) and (c) show the Raman spectra for PET only.

3.6 Summary

We fabricated CNT thin-films on different substrates and with different dispersive agents. We presented two techniques for fabricating CNT film on flexible substrates: direct spray deposition on plastic and transfer printing of already deposited film from glass onto plastic. SDS based CNT solution was utilized in both techniques. CNT films transferred to plastic showed superior performance with respect to the others which are directly deposited on the same substrate. Moreover, we compared between SDS and CMC in terms of process parameters as well as film characteristics. The new optimized low cost and low temperature transfer printing process introduced in this chapter opens a new horizon in the flexible electronics field. The performance of the fabricated films could be improved by employing higher quality plastic substrates that can sustain higher temperature and further fabrication steps.

Chapter 4

CNT-Based Gas Sensors: Pristine and Functionalized

We report the fabrication and characterization of CNT-based gas sensors with an exceptional as well as immediate response towards different test gases at room temperature. The response of the CNT gas sensors towards gases such as NH_3, CO, CO_2 and ethanol is examined. Testing towards such gases enable the fabricated sensors to cover different areas of applications such as environmental monitoring, toxic gases detection as well as the food packaging industry. In order to fully exploit the potential of such sensors, it is necessary to achieve high-throughput, low-cost production onto a wide range of substrates materials. One promising technology capable of fulfilling such requirements is spray deposition. Spray deposition technique is deployed for the preparation of all the samples characterized in this chapter

We present as well CNT gas sensors functionalized with metallic nanoparticles (NPs) which enhance the response of the sensor vastly. The sensors are functionalized with Au, Pd and Ag at different loads. The NPs were deposited by a thermal evaporation process. It is shown that metal functionalization of the CNT layer can alter the performance of the sensor towards different test gases, and hence can enable differentiation between different gases. Au functionalization results in exceptional response to NH_3, CO and ethanol, while Pd functionalization improves the sensor response to CO_2 exposure. We recorded a sensitivity of CNT sensor functionalized with 1.5 nm of Au up to 92%, 32% and 22% when exposed to NH_3 with concentration of 100 ppm, ethanol with concentration of 100 ppm and CO with concentration of 50 ppm respectively. The normalized response for Pd functionalization CNT layer with a nominal thickness of 0.5 nm reached 3%, 6%, 12% and 17% under concentrations of 500 ppm, 1000 ppm, 2500 ppm and 5000 ppm of CO_2 respectively.

In order to understand the interaction between the different types of NPs and the CNT layer several characterization techniques should be held. We investigated the change in the optical properties of the CNT layer after the deposition metallic NPs. Au and Ag introduce surface Plasmon (SP) on the surface. The frequency of the SP is dependent on the nominal thickness of the deposited metal as well as the size of the formed NPs. Upon thermal annealing a shift occurs in the frequency of the induced SP on the CNT surface due to the changes in the surface morphology. We found that thermal annealing affects the response of the CNT based gas sensor as well. Additionally, we show that depositing Au NPs on top of the CNT layer introduce changes in the work function of the formed layer.

4.1 CNT-Based Gas Sensors Overview

Kong et al were among the first to demonstrate fast and sensitive ChemFETs employing a single semiconducting CNT working under ambient conditions [42]. Their system exhibited p-type transistor characteristics and significant change in conductance could be measured upon exposure to NO_2 abd NH_3. ChemFET sensors based on a random network of SWNTs were successfully used by Novak et al. [92] for the detection of dimethyl methyl phosphonate, a simulant for the nerve agent Sarin. Sub-ppb concentration levels were detectable and fast recovery of the sensor could be achieved by applying a positive gate bias. On the other hand, chemiresistive sensors based on random CNT networks, deposited by plasma-enhanced chemical vapor deposition, were fabricated by Valentinin et al. [93]. Their sensor was capable of detecting NO_2 concentrations as low as 10 ppb at an operating temperature of 165 °C. The utilization of CNT networks in both device types, ChemFETs and chemiresistors, can be considered a simple approach to overcome limitations in reproducibility and manufacturing scalability of single CNT devices.

Despite their high sensitivity with respect to several gases, pristine CNT films lack the capability to differentiate between different gas molecules. The lack of selectivity of the CNT based sensors can be partially overcame by metal functionalization of the CNT surface [51] [94] or by polymer coatings [95]. Several methods were used in order to deposit metallic NPs on top of the CNT network such as thermal evaporation [66] [67], sputtering [64] and electrochemical deposition [68].

Penza et al. employed sputtering technique to deposit Pt nanoclusters at tuned loading of 8, 15 and 30 nm [64]. The sensors were exposed to different gases such as NO_2, NH_3, CO_2 and CH_4. CNT sensors with Pt load of 8 nm showed the highest normalized response in case of NO_2 and CH_4 while CNT sensors with Pt load of 15 nm showed

the best normalized response in case of CO_2 and NH_3. The main drawback is that the operating temperature of the sensors was 120 °C. The same group also reported CNT sensors functionalized with Au nanoclusters [63]. The highest response obtained was 10%, 16% and 14% for 10 ppm concentration of NO_2, 1000 ppm concentration of NH_3 and 10 ppm concentration of H_2S respectively. These results were obtained at an operating temperature of 200 °C. Similarly, Zenolli et al. fabricated CNTs based sensors functionalized with Au NPs and oxygen plasma and exposed them to different pollutants such as NO_2, CO and C_6H_6 [96]. They showed that Au functionalization results in better sensing abilities towards the detection of specific gases (NO_2 and CO) while in the case of C_6H_6 Au NPs do not seem to play a crucial role in the sensing process when compared to pristine CNTs functionalized with oxygen plasma.

Although the formation of metal NPs on top of the CNT film improves greatly the response of the sensor towards different gases, the interaction between the metal NPs and CNT film is still not fully understood. Kim et al. were among the first to demonstrate the formation of nano-Schottky barrier (also referred to as 'non-traditional Schottky barrier') at the interface between the deposited Al NPs and the CNT film [97], which in turn modulates the molecular adsorption. Moreover, Kauffmann et al. reported that upon electrochemical growth of Au NPs on top of CNT film, an electron transfer occurs from CNT to the NP species. Transfer of electronic density accompanies the adsorption of CO molecules on the NP surface back into CNTs [98]. They also reported that the magnitude of electron transfer into the CNT valence band scaled with the work function of the functionalization metal [99]. Mubeen et al. also reported the formation of nano-Schottky barrier at the Au NPs CNT interface which is modulated upon the exposure of H_2S [68]. Furthermore, they stated that the sensitivity of the sensor is strongly dependent on the number and the size of the Au NPs but the sensing mechanism is independent of it.

Another series of studies concentrated on physical changes induced on a given surface by metal NPs. Serrano et al. discussed for instance the surface plasmon resonance (SPR) in Au films deposited onto glass substrates and annealed in air at different temperatures [100]. They showed that the resonant absorption of extended surface plasmons of the deposited Au films depends on the thickness of the film. Moreover, the morphology of the film and its optical properties is dependent on the film's initial thickness which can be altered according to the annealing temperatures. Sun et al. reached the same conclusion by investigating the temperature dependence of morphological evolution and the corresponding SPR properties variation of Au films with nominal thicknesses of 5 nm upon rapid thermal annealing for 180s at different temperatures ranging from 100 to 700 °C [101]. Gingery et al. reported the evaporation of Au NPs on top of multiwall carbon

nanotubes (MWCNTs), which are grown by chemical vapor deposition [67]. They stated that the size and the distribution of the NPs are affected only by the nominal thickness deposited, with no influence of the evaporation rate or the substrate temperature during the evaporation process.

In this chapter, we present the fabrication and characterization of pristine as well as functionalized CNT-based gas sensors. All the fabricated sensors we examined towards four different test gases, NH_3, ethanol, CO and CO'$_2$. We functionalized the CNT layer in order to alter the response of the sensor and enhance its sensitivity. Different metallic NPs were used to functionalize the CNT layer. The functionalization process was performed by thermal evaporation. we investigated as well the interaction between the deposited NPs and the CNT layer in term of surface morphology, optical transmission and work function measurements.

4.2 Materials and Methods

The samples fabricated in this chapter are based on spray coating technique, where CNT solutions are sprayed through an air gun onto a heated substrate. The temperature of the substrate is a process parameter that depends on the solvent and the surfactant used to disperse the CNTs. Besides influencing the surface topography; the spraying parameters have a direct impact on the optical and electrical characteristics of the fabricated films. The deposited CNT layers were sprayed by air atomizing nozzle. These kinds of nozzles, as well as the ultrasonic spray nozzles, provide a fine degree of atomization [59], which in turn results in a more uniform and homogenous film. A commercially available automatic air atomizing spray gun (Krautzberger GmbH, Germany) was used in depositing the CNT films. The samples fabricated in this chapter followed the same spraying regimes discussed in chapter 3.

4.2.1 Solution preparation

The CNT network is composed of commercially available unsorted Single Wall Nanotubes (SWNT), which are 33% metallic and 67% semiconducting. In order to dissolve CNTs in an aqueous solution, a high molecular weight cellulose derivative, sodium carboxymethyl cellulose (CMC), is used. This kind of surfactant has been reported previously as an excellent agent for dispersing CNTs in water [102]. Further discussion about the effect of different kinds of surfactants on the prepared CNT solution was presented previously in chapter (Transfer). CMC is dissolved in distilled water to make 0.5 wt% aqueous solution. The solution is stirred overnight in order to uniformly dissolve the

surfactant in water. After this, 5 mg of CNTs are added in 10 g of 0.5 wt% CMC aqueous solution to make 0.05 wt% CMC based aqueous CNT solution. Sonication of the CMC based solution is performed for 20 minutes using a probe sonicator at 50% power (~ 48 Watt). Solution is centrifuged for 90 minutes at 15000 rpm and 80% of the centrifuged solution is taken from top to be used for the deposition.

4.2.2 Sensor Fabrication

Si wafers with 200 nm of thermally grown SiO_2 are used as substrates. An inter-digitated electrode structure (IDES) consisting of a 5 nm thick Cr layer, which promotes Au adhesion on SiO_2, followed by a 40 nm Au layer is evaporated on top of the SiO_2. 100 μm is chosen to be the spacing formed between the two electrodes of the inter-digitated structure. The substrates are exposed to oxygen plasma for further cleaning and then they were immersed in 1 wt% of APTES in isopropanol solution since APTES acts as adhesion promoter. On top of the IDES a CNT film is spray deposited in order to form the resistive network for the gas sensing. Figure 4.1 shows a schematic for the sensor structure and an AFM image for the typical CNT layer deposited on top. Chemical post-deposition treatment is required to remove the CMC-matrix embedding the CNTs, thus converting the network behavior from insulating to conducting. To this purpose, the samples are soaked in 4M HNO_3 solutions for > 12 hours at room temperature for complete removal of the surfactant, rinsed in DI water and then dried. For the functionalizing CNT network, metallic NPs are deposited by thermal evaporation process from a tungsten boat. Au with an equivalent nominal thickness of 1.0 nm, 1.5 nm and 2.5 nm is evaporated over the entire structure coated by CNTs, while Pd was evaporated with nominal thickness of 0.5 nm, 1.0 nm and 1.5 nm. Note that all metals were evaporated with the minimum evaporation rate which is 0.1 Å/s.

4.2.3 Sensor Characterization

The complete sensor module is composed of the CNT sensor, mounted on a carrier glass together with a Peltier heating element for temperature control and a Pt100 sensor for in-situ temperature monitoring. The heating element is located beneath the glass carrier, while the Pt100 sensor is placed next to the CNT sensor on top of the glass carrier. Figure 4.2 shows a schematic for the module used in characterizing the gas sensors fabricated in this chapter. This arrangement allows precise determination of the actual temperature reached by the CNT sensor and enabling heating the sensing element during gas exposure and/or recovery cycles up to 150 °C. Sensor performance was investigated by exposure

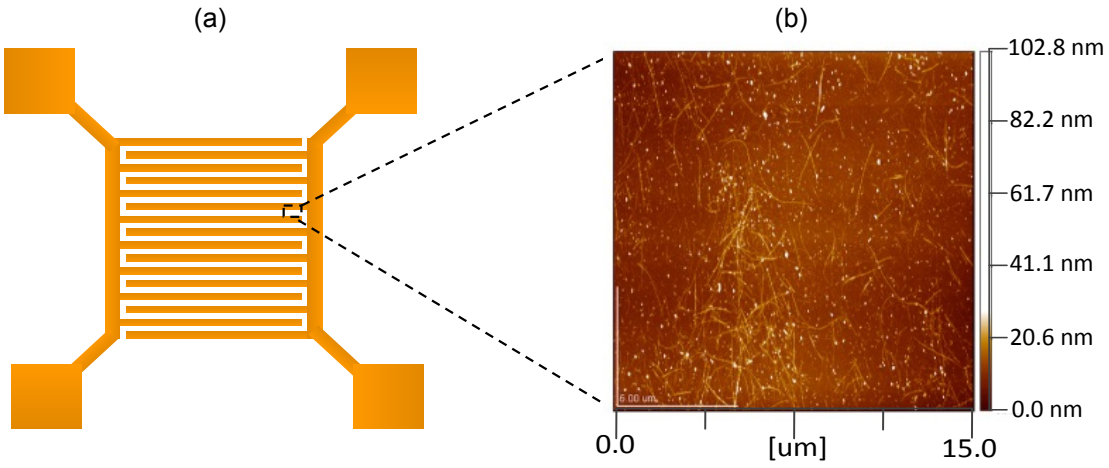

Figure 4.1: (a) Schematic of the sensor architecture showing the IDES structure (b) AFM image of a typical low density CNT layer deposited on top of the IDES structure.

to different concentrations of the test gas (NH_3, CO_2, CO and ethanol). The desired concentration is achieved by dilution of the test gas with a carrier gas while maintaining the total gas flux constant. Pure nitrogen is used as the carrier gas for NH_3, CO and ethanol while air is used as the carrier gas for CO_2. The duration of the exposure cycle was chosen to be 100 s for all test gases. The exposure cycle is followed by an active recovery cycle for 900 s. In this cycle we heat up the sensor up to 80°C in order to desorb all the gas molecules before the next exposure cycle. It is worth mentioning here that passive recovery (no heat applied) can be also applied but longer time is required for complete gas desorption. Passive recovery is used to investigate the intrinsic recovery time for the gas sensor towards different test gases . Such kind of characterization will be presented in more details in chapter 6.

4.3 Characterization of Pristine CNT-Based Gas Sensors

When using CNT films for gas sensing, the network density is one of the critical parameters affecting the device performance [71]. The gas sensors presented in this chapter utilize CNT films with rather low tube densities. At such densities, the film operates near its percolation threshold, thereby reducing the amount of metallic pathways in the network and amplifying the contribution of semiconducting pathways.

Figure 4.3 shows the variation in the resistance with time for the pristine CNT gas sensor

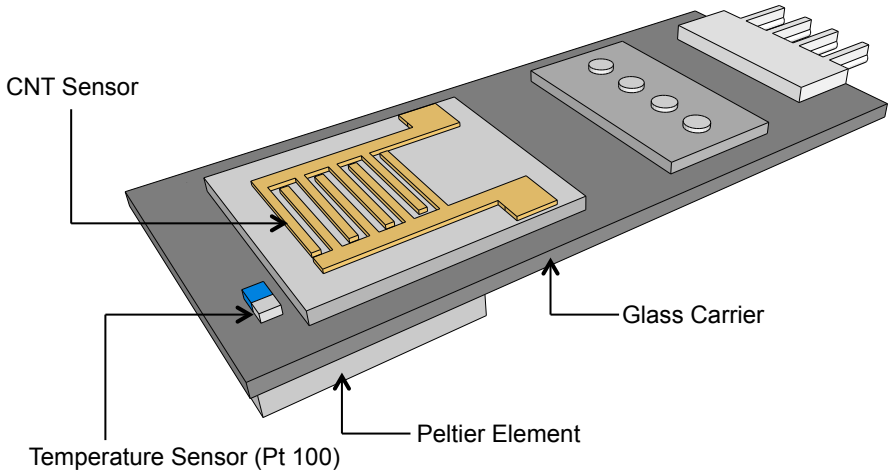

Figure 4.2: A schematic for the sensor module and its different components.

towards the four test gases. Concentrations between 10 and 100 ppm for NH_3 and ethanol and between 5 and 50 ppm for CO have been considered. These concentrations are achieved by diluting the test gas with pure N_2 as carrier gas. For CO_2, the concentrations tested cover a range between 500 and 5000 ppm and is achieved by diluting the test gas with normal air as carrier gas. Note that in case of CO_2 measurement, normal air used as carrier gas typically contains 390 ppm of CO_2, which is the reason for the high concentration range covered in our tests. Each cycle consists of an exposure interval followed by a recovery interval. During exposure, the test gas enters the chamber along with the carrier gas at room temperature at a constant flux of 200 ml/min for the desired duration. We chose 100 s exposure time for all test gases, which is to our knowledge shorter than the usual exposure intervals reported in literature.

Recovery is then introduced by heating the sensor module to 80 °C and increasing the carrier gas flux to 1000 ml/min for 300 s, after which heating is stopped. The high flux is maintained for another 300 s to accelerate cooling of the sensor and purge any residual test gas molecules out of the chamber. Recovery is then completed by a final 300 s interval under sensing conditions to restore the initial resistance. The increase in thermal energy during the heating cycle is necessary to enhance desorption of gas molecules attached to the CNT film and enable full recovery.

The main figure of merit used to evaluate the sensor performance is the normalized response, defined in Eq. 4.1, as the relative change in resistance, where R_i and R_f are the initial and the final resistance value of the exposure cycle, respectively.

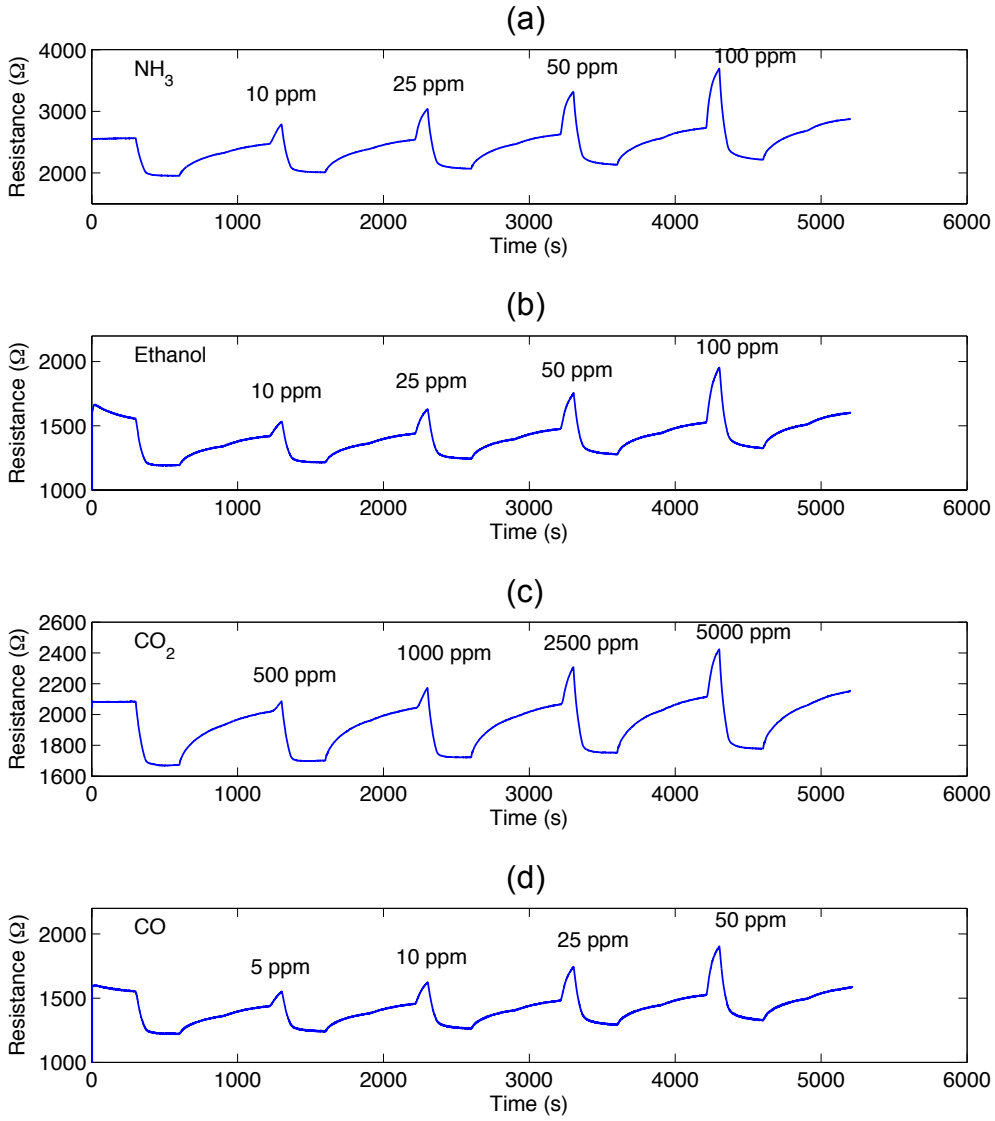

Figure 4.3: Plot of the measured sensor resistance over time. Each graph is divided into four segments which corresponds to the different exposure cycles. The four test gases are NH_3 (a), ethanol (b), CO_2 (c) and CO (d).

$$NormalizedResponse = \frac{R_f - R_i}{R_i} \tag{4.1}$$

Plotting the normalized response of each gas versus its corresponding concentrations as shown in fig 4.4, we can notice that the normalized response enhances with increasing the concentration of the gas , at least within the concentration range shown here. We found as well that the normalized response has rather a logarithmic dependence on the concentration , but differs between gases and depends on the concentration range recorded. The response towards NH_3 reached 15% to a concentration as low as 10 ppm. We can consider the normalized response towards NH_3 is exceptional, taking into account

the short exposure intervals of 100 s. Further enhancement in the normalized response towards the different gases can be achieved by functionalizing the CNT network with metallic NPs, which will be discussed in the following sections. For the rest of this chapter as well as the following chapter, the pristine CNT layer will be reffered as bare CNT layer.

4.4 Characterization of Functionalized CNT Thin-Films

In order to achieve better understanding of the modifications introduced by depositing the NPs on top of the CNT networks, we investigated first the characteristics of the functionalized CNT thin-films in terms of surface morphology, optical transmittance and work function. Such kind of characterization enabled us to identify the changes that are introduced to the CNT layer after the functionalization with different metallic NPs. Most of the discussion in this chapter focuses on the modification introduced by Au to the surface of the CNT layer. This is primarily attributed to the fact that Au introduce a lot of changes to the surface optically and electrically , moreover it achieves the highest enhancement in the sensitivity of the sensor when compared to the other metals.

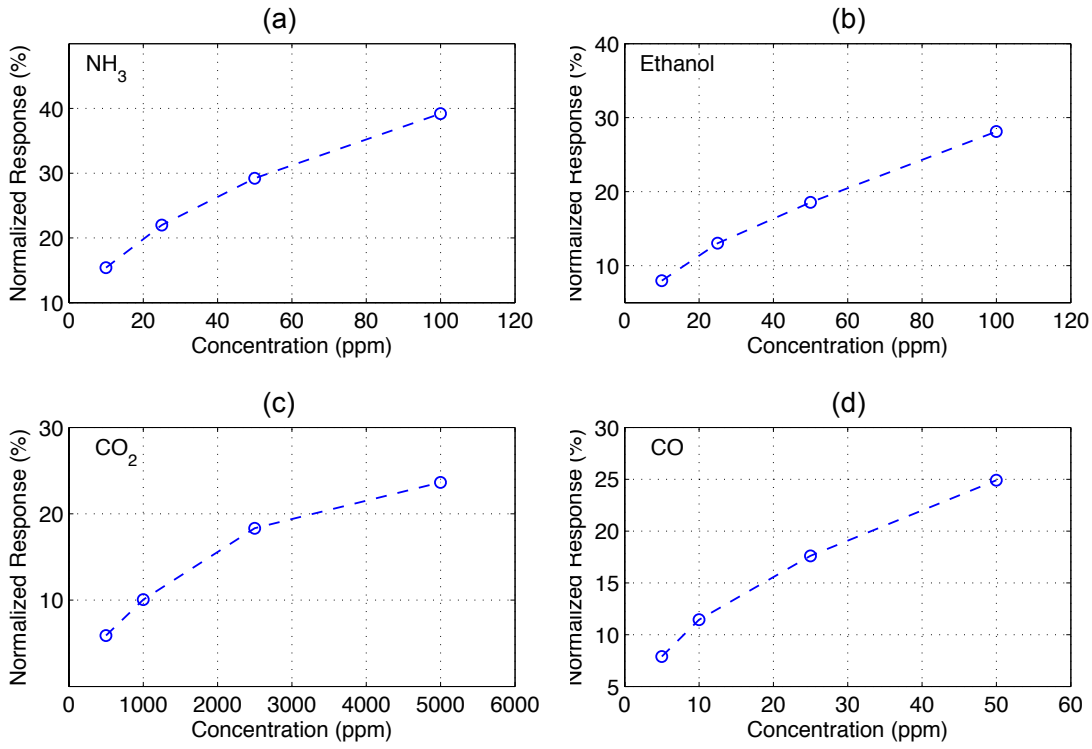

Figure 4.4: Relation between the normalized response and the concentration of different test gases NH_3 (a), ethanol (b), CO_2 (c), CO (d) for a CNT-based gas sensor.

4.4.1 Surface Morphology

Before depositing NPs on top of the CNT network, we investigated the formation of Au and Pd NPs directly on glass. Figure 4.5 shows an AFM image for Au and Pd with the same nominal thickness deposited on glass substrate. The formation of the NPs for both metals is completely different in terms of the clustering of the NPs as well as the distance between them. This could be attributed to the difference in stress distribution during the evaporation process of each metal. Such difference in the formation of the NPs has a direct effect on the performance of the CNT thin-film as well as the response of the gas sensor as we will show in the next section.

The morphology of the metal NPs on the substrates depends on the initial thickness of the film and the integrated stresses built at the interface between the substrate and the coating material [100]. The stress introduced during the evaporation of thin metal films has been studied for a long time [103] [104]. Briefly, the stress introduced in the film is composed of thermal stress, which is due to the difference in the thermal expansion coefficient between the substrate and the evaporated metal, and intrinsic stress, which is due to the accumulated flaws, which are built on the surface during the deposition process. Which effect plays the dominant role depends on the physical properties of the material and the evaporation conditions. In general, stress between the substrate material and the coating material result in stress distribution at the interface, which promotes the migration of the film away from the stressed areas upon heating. The relaxation of the film is a non-uniform process and leads to inhomogeneous nucleation on the surface.

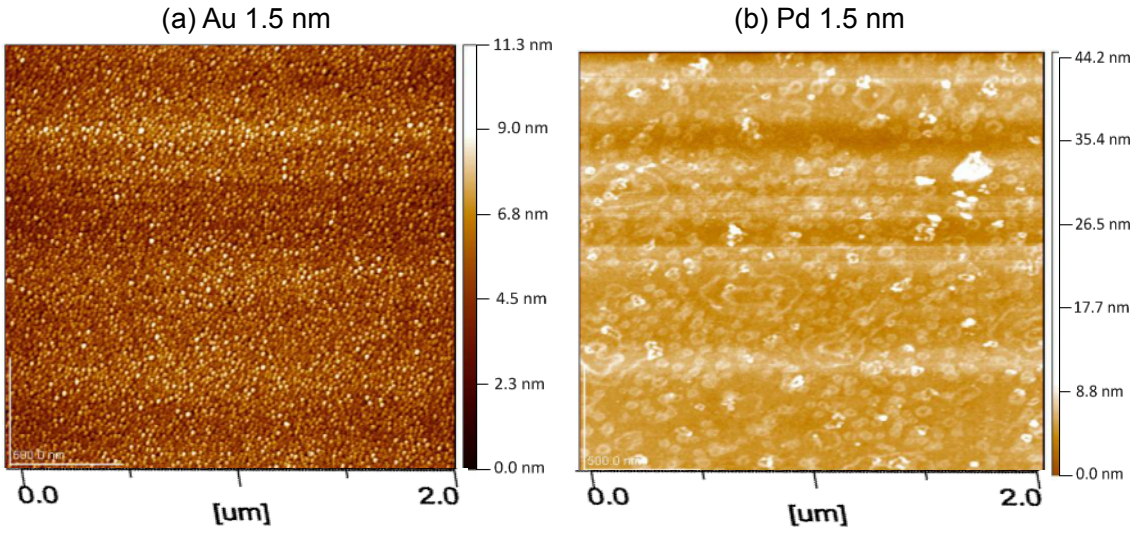

Figure 4.5: AFM images for the formation of Au (a) and Pd (b) NPs with the same nominal thickness (1.5 nm) on glass substrates.

This result in the formation of metal islands which tend to modify their shapes upon annealing, mostly becomes more rounded in order to decrease their surface energy.

Due to the fact that the films deposited in all the experiments in this chapter utilize CNT layers with rather low-tube densities, as described in the experimental section, the material of the substrate plays an important role in the formation and clustering of the NPs. Figure 4.6 shows the scanning tunneling microscopy images for a CNT layer functionalized with 0.5 nm of Au fabricated on Si substrate. The image shows that the formation of the Au NPs is uniform on the substrate. The deposited NPs tends to form round shaped in order to reduce the surface energy as discussed.

Thermal treatment is an important process step to stabilize and to de-dope the CNT network before gas exposure [63]. On the other hand, performing thermal treatment to functionalized CNT sensors, affects directly the NPs evaporated on top of the CNT films, thus affects the sensor performance. In order to investigate the effect of the thermal treatment process on functionalized CNT network, CNT thin films utilized in sensor fabrication were spray deposited on glass substrate with the same process steps described earlier and subsequently functionalized via thermal evaporation. The nominal thicknesses for Au deposition were 0.5 nm, 1.0 nm, 1.5 nm and 2.5 nm, respectively. The samples were thermally treated in air at 100 °C for 1h. Figure 4.7 a and b show the morphological change that occurs to the Au NPs at different loads after thermal treatment. Au NPs tend to form isolated islands of large particle instead of relatively small particles distributed on the whole surface after the thermal treatment.

By looking at the AFM images we can identify three parameters for the metal islands: i) height ii) size and iii) relative distance between them. Before annealing only the

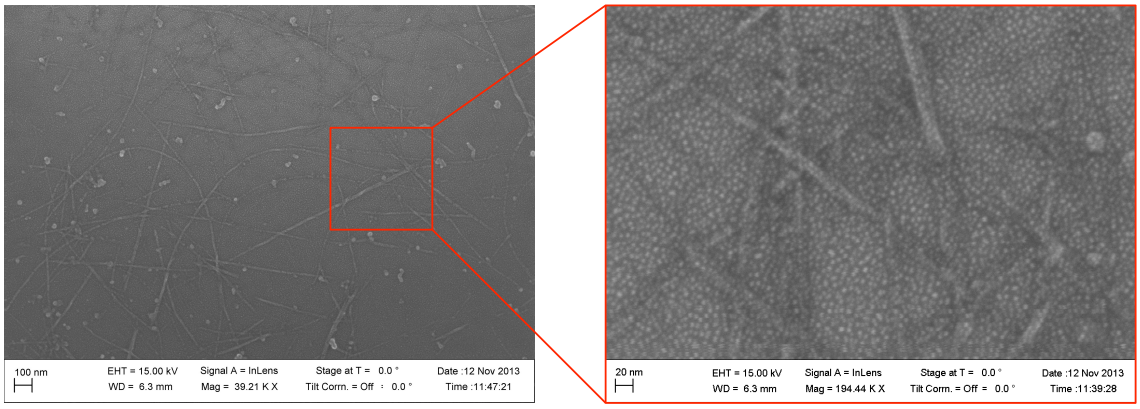

Figure 4.6: An SEM image of a spray deposited CNT thin-film onto Si substrate functionalized with 0.5 nm of Au along with a zoom-in acquired within the same area

CNT film is dominating the features of the image since the thickness of the CNT bundle diameter was higher than the nominal thickness of the evaporated Au. After annealing, the CNT film almost disappears underneath the formed metal islands. The max height of the formed metal islands becomes 128 nm, 133 nm, 101 nm and 87 nm for samples that had nominal thicknesses of 0.5, 1, 1.5, 2.5 nm, respectively. Moreover, the size of the islands and the distance between them decrease with increasing nominal thickness. The migration of the film from the stressed area to more relaxed ones is easier for thinner metal layer because a smaller amount of material needs to be displaced to create the metal island.

4.4.2 Optical Transmission Characteristics

The optical transmittance measurement shows the existence of SP in the fabricated samples within the visible range after the deposition of Au NPs. Au samples evaporated on top of the CNT films showed drop in the intensity of the optical transmission as shown in fig. 4.8. For Au with nominal thickness of 2.5 nm, the drop in intensity occurs around

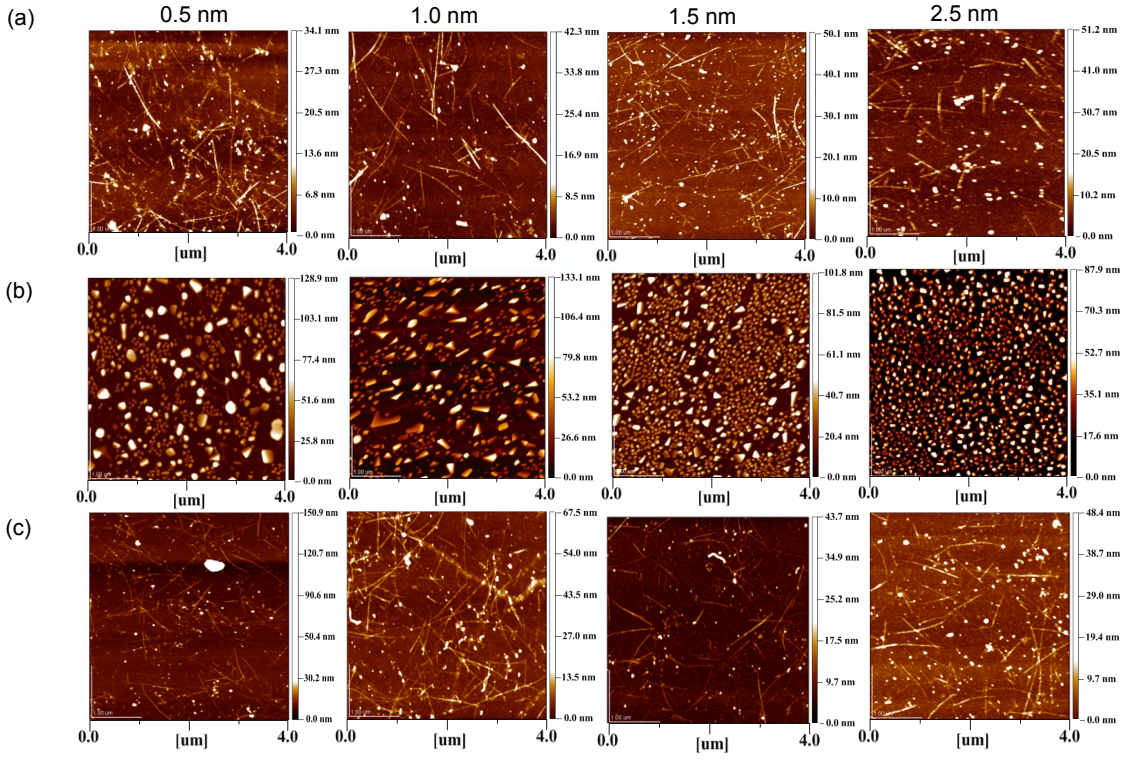

Figure 4.7: AFM images of CNT thin-films deposited on glass and functionalized with different loads of Au (0.5 nm, 1.0 nm, 1.5 nm and 2.5 nm). (a) As fabricated (b) Annealed continuously for 1 h at 100 °C (c) Annealed for 1 h in intervals of 10 minutes.

590 nm. A blue shift of ~ 50 nm can be observed upon annealing the samples for 1h at 100 °C. Qualitatively the same behavior is observed for the other samples. The variation in the optical transmission is dependent on the size of the metal islands which are formed after the thermal treatment and their distribution density as well. This agrees with the AFM analysis which showed the migration of the films from the stressed areas and the formation of metal islands upon thermal treatment.

We evaporated Ag NPs as well on top of CNT films sprayed on glass with nominal thicknesses of 1.0 nm, 1.5 nm and 2.5 nm, respectively using the same procedure described for Au. The change that occurs to the Ag NPs upon annealing is not that significant with respect to what occurred to the Au NPs. The maximum height of the metal islands for all Ag samples after annealing reached ~ 50 nm. The size of the Ag NPs increase and their shape became more rounded. The different load of the Ag samples did not have a significant effect on the morphological feature of the surface

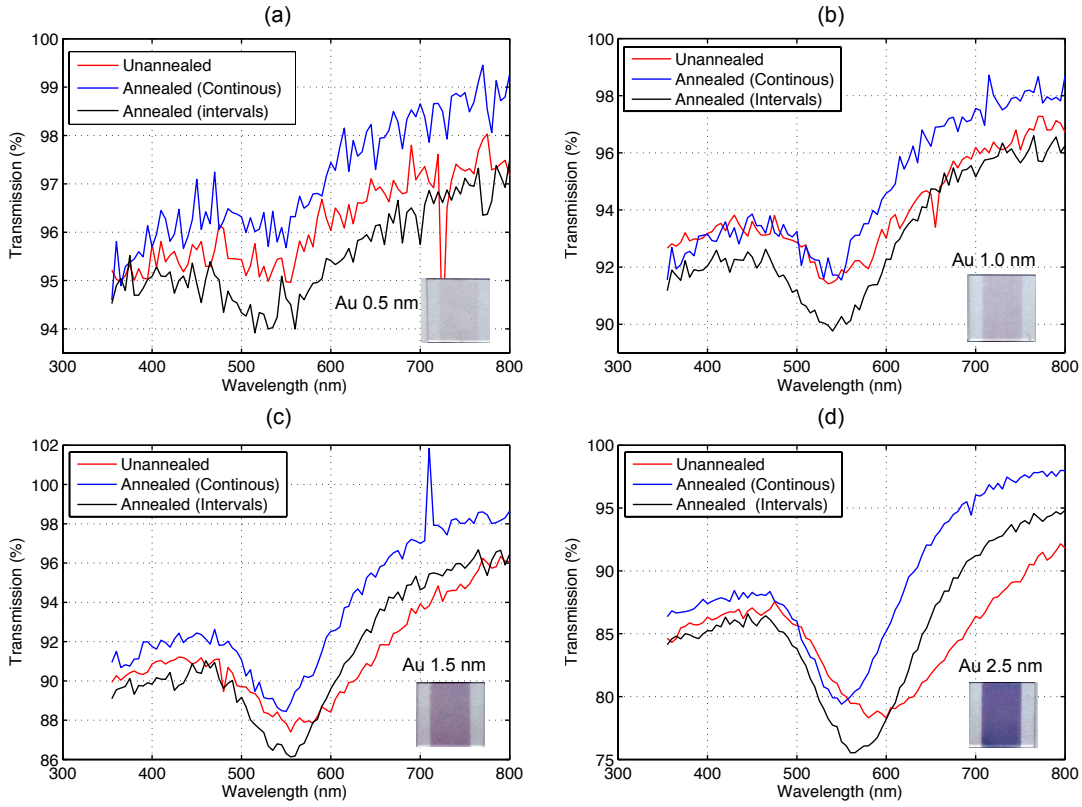

Figure 4.8: Optical transmission measurements for CNT networks functionalized with Au with loads of 0.5 nm (a), 1.0 nm (b), 1.5 nm (c) and 2.5 nm (d). Each graph shows the measurement for the as fabricated samples (red), annealed continuously for 1 h at 100 °C (blue) and annealed for 1 h at 100 °C in intervals of 10 minutes (black).

after the annealing. This implies that the Ag layers were more relaxed on top of the CNT than the Au layer. The difference in the physical properties between both metals could be one of the main reasons for this difference in behavior. The density and the melting point of the material directly affect the value of the built thermal stress during the evaporation process. Ag samples showed the same behavior as the Au samples but at different wavelength. A drop in the intensity of the optical transmission occurred at ~ 450 nm. Upon annealing at 100 °C for 1h, one can notice a small blue shift of ~ 10 nm of the SPR curve as shown in fig. 4.9. This confirms that the morphological features of the Ag NPs do not change dramatically upon annealing for this amount of annealing time at the given temperature.

The effect of the thermal treatment on the Au NPs was analyzed also using a different process. Instead of annealing the samples for 1h continuously, we divided the annealing process into intervals of 10 minutes. This process is repeated for 6 cycles and after each cycle the surfaces changes are monitored via AFM and optical transmission mea-

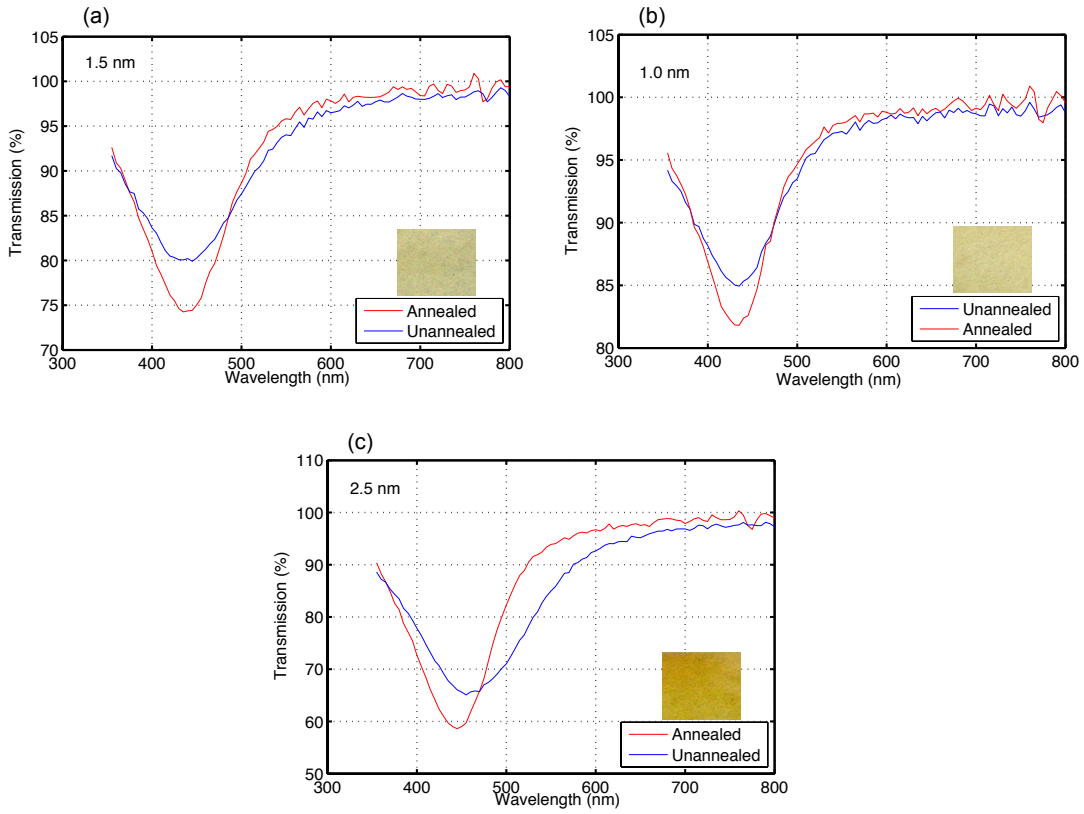

Figure 4.9: Optical transmission measurement within the visible range for CNT networks functionalized with Ag with loads of 1.0 nm (a), 1.5 nm(b), and 2.5 nm (c). Each graph shows the measurement for the samples before (blue) and after annealing (red).

surements. Figure 4.7 c shows that after of the stepwise annealing no dramatic change occurred to the surface. The morphological features as well as the optical transmission remained basically unchanged (fig. 4.7 a). The shift in the SPR curve is considerably smaller than that observed when the annealing was done continuously for 1h. A small blue shift of ~ 35 nm occurred. It is worth mentioning that this shift occurred after the first 10 minutes of annealing, while after that the optical transmission curve remained almost the same. The change in the optical transmission curve measured after each cycle is shown in fig. 4.10. As we will see later, the insensitivity of the functionalized APTES treatment has been shown to improve the adhesion between the glass substrates and the metal layer [1] by strengthening the film-to- substrate bond. The stronger the film-to-substrate bond, the stronger its capability to withstand the forces produced by the integrated stress throughout the film. Thus, when Au NPs evaporated on an APTES-treated glass are subjected to the same thermal treatment as when they are evaporated on a CNT film, no significant change occurred to the surface morphology. The different behavior with respect to the Au deposition on the CNT film is most likely attributable to the hydrophobic nature of the CNT film [57] [84], which causes a weak bond to be formed with the Au evaporated film and in turn a higher stress at the interface.

The different morphology of the Au NPs when directly deposited on APTES treated glass is reflected in the frequency of the SP that occurs at the interface. Figure 4.11 shows the optical transmission measurement of Au NPs on glass. The morphology of the Au NPs on APTES treated glass is different than those evaporated on top of the CNT film.

4.4.3 Work Function Measurement

Another critorion used to investigate the modification introduced to the surface by depositing NPs on top of the CNT layer is measuring the change occur to the work function w/o functionalization. We fabricated four new samples where CNT network is spray deposited on glass substrates and then we functionalized three of them with Au with loads of 1.0 nm, 1.5 nm and 2.5 nm, while the fourth sample is kept bare. Using a Kelvin probe force microscope, we measured the work function for all the samples and the obtained results are shown in fig. 4.12.

We recorded a value of 4.785 eV for the bare CNT layer which agrees with the work function value for CNT reported in literature [105]. The work function of the network decreases to 4.516 eV, 4.5495 eV and 4.5598 eV at functionalization load of 1.0 nm, 1.5 nm and 2.5 nm respectively. This implies that Au functionalization does not only change the surface morphology and the optical characteristics of the CNT network but also its

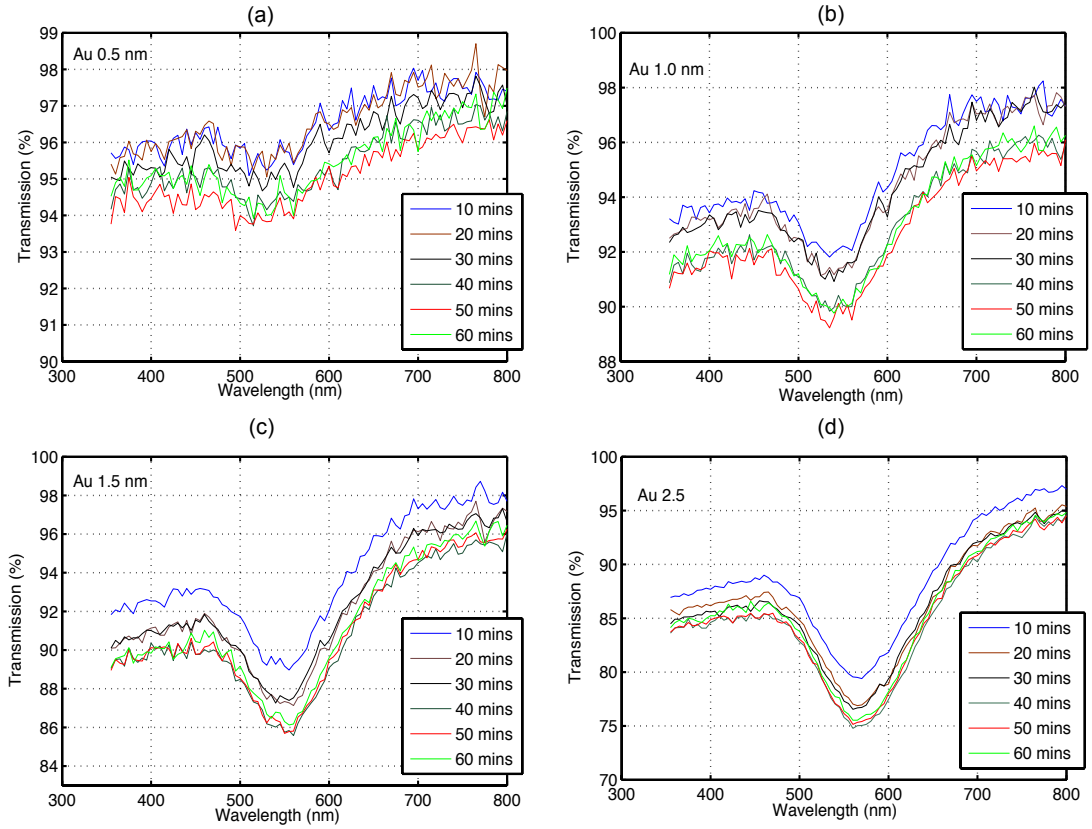

Figure 4.10: Optical transmission measurement within the visible range for CNT networks deposited on glass and functionalized with Au with loads of 0.5 nm (a),1.0 nm (b), 1.5 nm(c), and 2.5 nm (d). Each graph shows the change that occurs to the optical transmittance upon annealing in steps of 10 minutes.

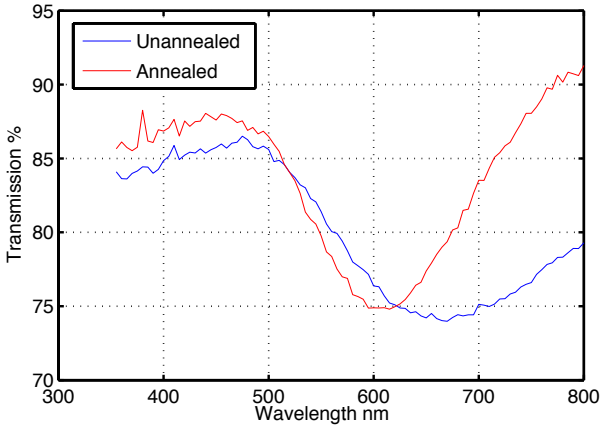

Figure 4.11: Optical transmission measurement within the visible range for Au NPs deposited on glass substrate before (blue) and after (red) annealing.

electrical characteristics. Taking a closer look at fig. 4.12, we can notice as well that by increasing the functionalization load the work function tend to increase by a small value.

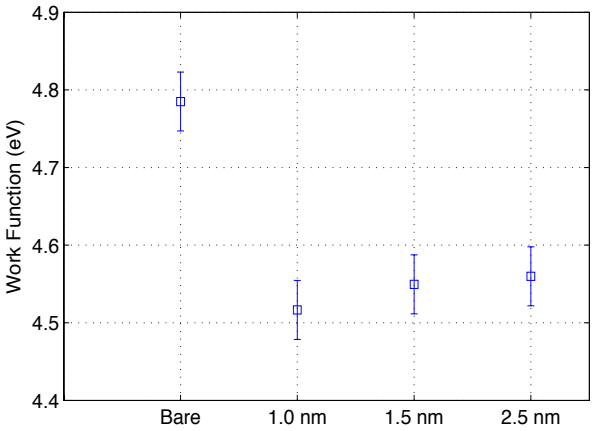

Figure 4.12: Plot of the measured work function for bare CNT layer and Au functionalized layer with loads of 1.0 nm, 1.5 nm and 2.5 nm.

Such behavior could be only due to the error in the measurement represented by the error bar in the plot. Nevertheless, it could be the case that by increasing the Au load the work function tend to approach the work function of bulk gold. At higher functionalization load, higher surface coverage by the NPs is obtained and hence, the NPs dominate the characteristics of the surface rather than the CNT layer.

4.5 Characterization of Functionalized CNT-based Gas Sensors

Metal functionalization of CNT network causes a slight decrease in the film resistance, which is in turn dependent on the load of the functionalization metal. Increasing the metal functionalization will tend to create a complete film on top of the CNT network, which will quench the sensitivity of the overall system. The change in resistance of the CNT gas sensors upon exposure to different gas species has been studied by several authors [106], [71], [107]. It has been attributed to two main reasons; i) Charge transfer between the adsorbed gas molecule and the CNT, and/or ii) modulation induced by the gas species at the Schottky barrier at the CNT/metal contacts (Au electrodes) interface. It has been previously shown that metal functionalization (especially Au) enhances greatly the response of the CNT gas sensors. Such effects was attributed to the catalytic action of the deposited layer which boosts the gas sensitivity of the CNT film[63].

It is well known that the adhesion between Au particles and CNT film is weak due to the hydrophobic nature of the CNT [48]. In our case, the post-deposition process in diluted HNO_3 can introduce defect sites and surface oxidization to CNT film [108],

thus allowing Au to bind to the CNT film via the carboxylic groups introduced on the surface.

The deposition of Au NPs on top of the CNT film cause the formation of 'non-traditional Schottky barrier' at the interface between the semiconducting tubes and the metal NP [98], [99]. One reason for the enhancement in the sensor response after the Au decoration could be the increase in the sites of CNT/metal Schottky barriers, which can be further modulated upon gas exposure. In case of NH_3, it coordinates with the formed Au NPs [109], hence charge transfer can take place through the formed NPs towards the CNT film. Possibly the Au NPs help in binding more than one NH_3 molecule to the same defect site instead of binding only one in case of pristine CNT film. The amount of charge transfer decreases with the increased size of the Au NPs because the catalytic activity of Au NPs diminishes considerably as the particle size exceeds a certain limit [110].

Upon annealing, Au NPs tend to migrate and form new nucleation sites in order to reduce the surface energy as we discussed earlier. This leads to two main effects i) increase in the film conductivity because the formed Au islands acts like a parallel metallic path to the CNT film, ii) partial uncovering of the CNT film which can interact directly with the exposed gas species. Which of the two effects is dominant depends mainly on the nominal thickness of the evaporated Au NPs.

Heating the sensor for small intervals doesn't affect the morphology of the metal NPs formed on top of the CNT film, as we discussed earlier. Nevertheless, we examined the effect of thermal treatment of 1 h at 100 ° C on the response of the functionalized CNT gas sensor. Figure 4.13 shows the effect of such thermal treatment on the resistance of the CNT sensors functionalized with Au at loads of 1.0 nm and 2.5 nm. Upon thermal treatment, a noticeable increase in the conductance is obtained. Larger effect is obtained for the CNT sensors functionalized with 2.5 nm Au nominal thickness. The plot shows that after annealing the resistance is dropped to almost one third of its value before the annealing. The effect of the annealing is not linear with the size of the NPs.

Figure 4.14 shows the effect of the thermal treatment on the response to NH_3 of both sensors. A considerably enhancement in the sensor response is obtained after the thermal treatment in the case of 1.0 nm Au coverage while the sensor response remained almost unchanged in the case of 2.5 nm of Au. This could be attributed to the different size of the Au NPs obtained after annealing.

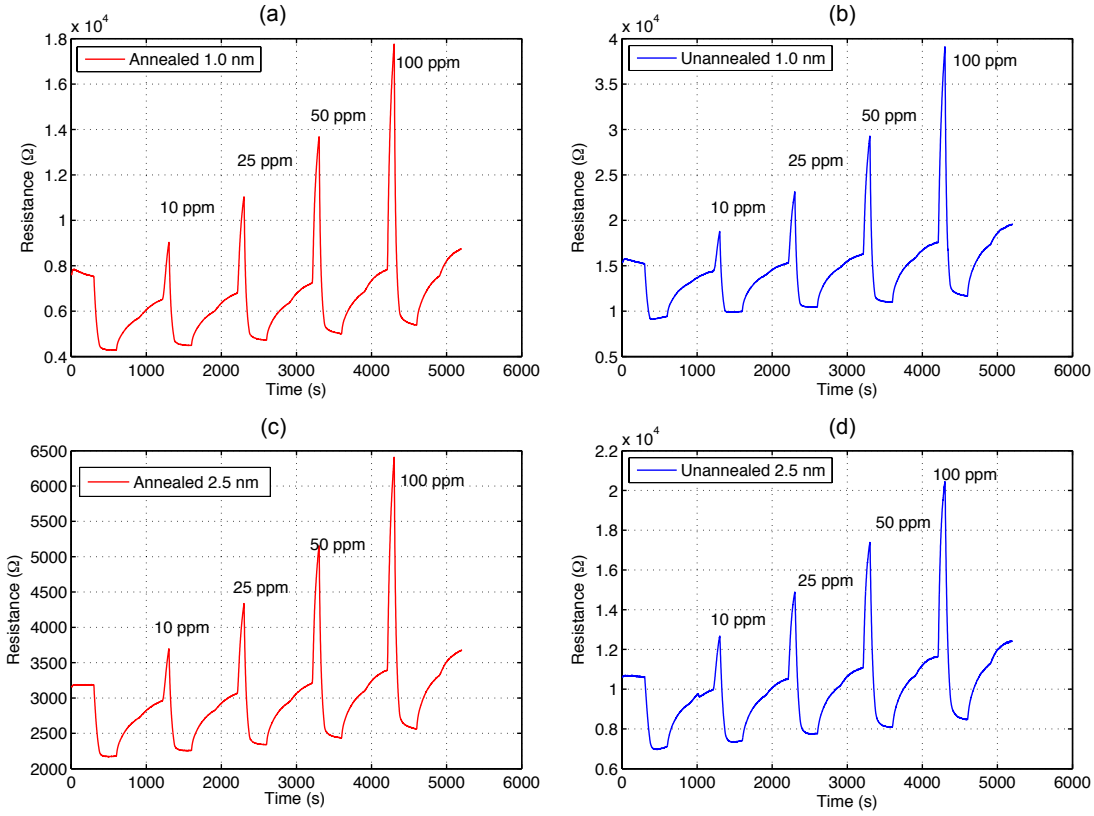

Figure 4.13: The change in resistance of CNT-based gas sensors functionalized with 1.0 nm and 2.5 nm of Au when exposed to different concentrations of NH_3 before and after annealing.

The functionalized CNT based gas sensors are examined towards the four test gas (NH_3, ethanol, CO and CO_2) with the same concentrations mentioned previously. The measurement setup remained unchanged and the active recovery is applied for 900 s after each exposure cycle.

Figure 4.15 shows the response to four different test gases obtained for the CNT gas sensors functionalized with Au and Pd with different nominal thicknesses. Taking a close look at the graphs, one can immediately notice that Au (1.0 nm) shows superior performance for NH_3, CO and ethanol. On the other hand Pd (1.0 nm) has the best response to CO_2.

CNT sensors functionalized with Au (1.0 nm) reaches a normalized response of 92%, 22% and 30% when exposed to 100 ppm of NH_3 and ethanol and 50 ppm of CO, respectively. CNT sensors functionalized with Pd (1.0 nm) reaches a normalized response of 17% when exposed to 5000 ppm of CO_2 and the normalized response is 2.1% with CO_2 concentration as low as 500 ppm.

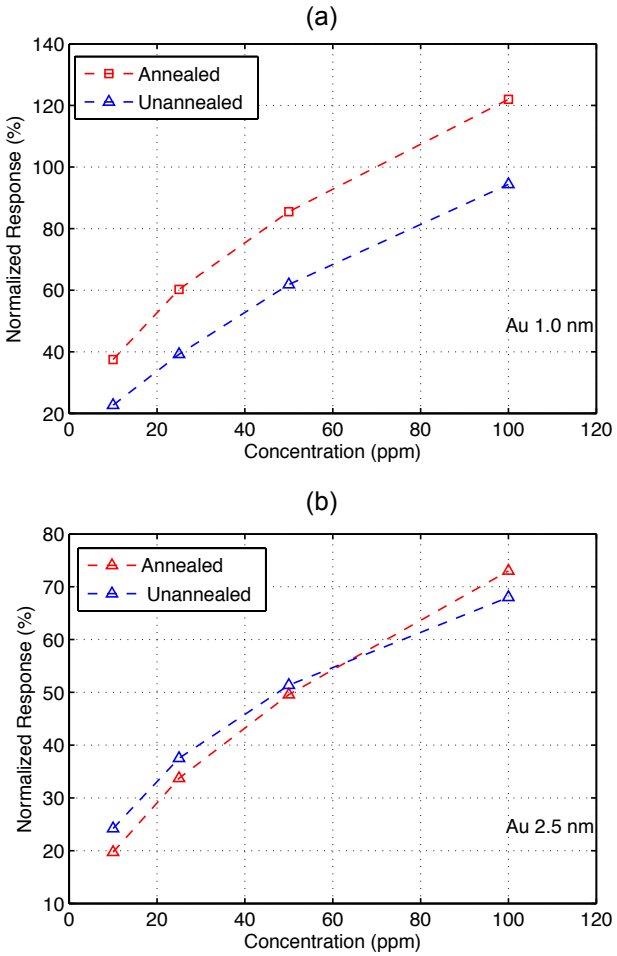

Figure 4.14: The relation between the concentration and the normalized response of CNT-based gas sensors functionalized with Au with loads of 1.0 nm (a) and 2.5 nm (b) when exposed to NH_3. Each graph shows the response before (blue) and after annealing (red).

Sensor response is found to have a rather logarithmic dependence on concentration. As expected, higher functionalization load does not result in higher sensor response, since the contribution of semiconducting CNT paths tend to decrease as a complete metallic film is formed. Each metal can achieve a maximum normalized response within a certain range of surface coverage. Figure 4.16 shows the relation between the functionalization load and its corresponding normalized response towards different concentrations of NH_3 for Au and Pd functionalization. The optimal range for Au functionalization is between 0.5 nm and 2.5 nm, while for Pd it is found to be between 0.5 nm and 1.5 nm. Although Au and Pd have quite similar work functions, which is reported previously to be a dominant effect in the formation of the potential barrier at the interface of the NP-CNT and also the response of the gas sensors [99], they behave differently when they are used for CNT sensors functionalization. This could be attributed to the difference in

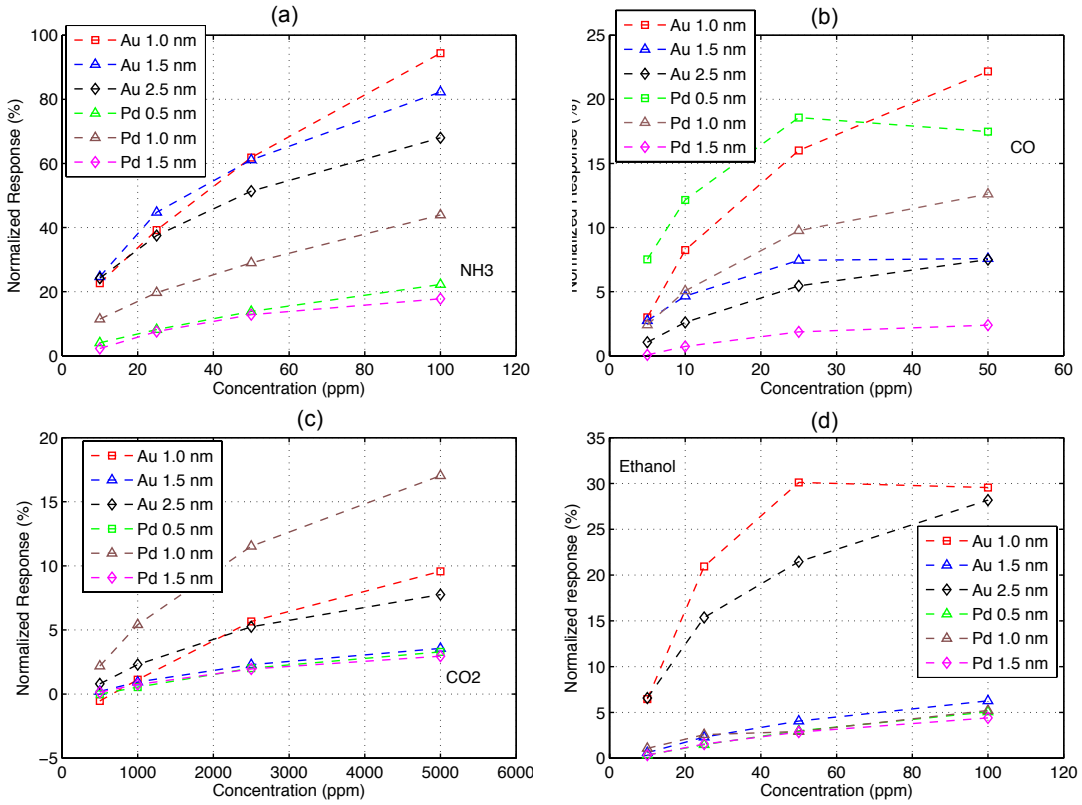

Figure 4.15: The relation between the concentration and the normalized response of functionalized CNT-based gas sensors when exposed to NH_3 (a), CO (b), CO_2 (c) and ethanol (d). Each graph plots the responses of the CNT-based gas sensors when functionalized with Au with loads 1.0 nm, 1.5 nm and 2.5 nm, and Pd with loads 0.5 nm, 1.0 nm and 1.5 nm.

stress distribution during the evaporation of each metal as discussed earlier.

Furthermore we fabricated CNT based sensors functionalized with Ag NPSs with loads 1.0 nm, 1.5 nm, and 2.5 nm. The sensors showed very weak response towards all test gases at all loads. The response towards the 4 test gases is shown in figure 4.17. One reason for this weak response could be that we chose the wrong working range of Ag functionalizations. The performance of the gas sensors was also investigated at different operating temperatures. Figure 4.18 shows the normalized response of a bare CNT gas sensor and a Au functionalized CNT gas sensor with a load of 1.0 nm. The exposure of the NH_3 gas was performed at two temperatures 50 °C (fig. 4.18 a) and 80 °C (fig. 4.18 b). Taking a close look at the graph, it becomes clear that the performance of the sensor deteriorates when compared to the results obtained in fig. 4.15 a. This could be mainly attributed to the increase in the gas desorption rate which increases with the increase in temperature. In other words, high operating temperature means that gas exposure and active recovery process are applied at the same time.

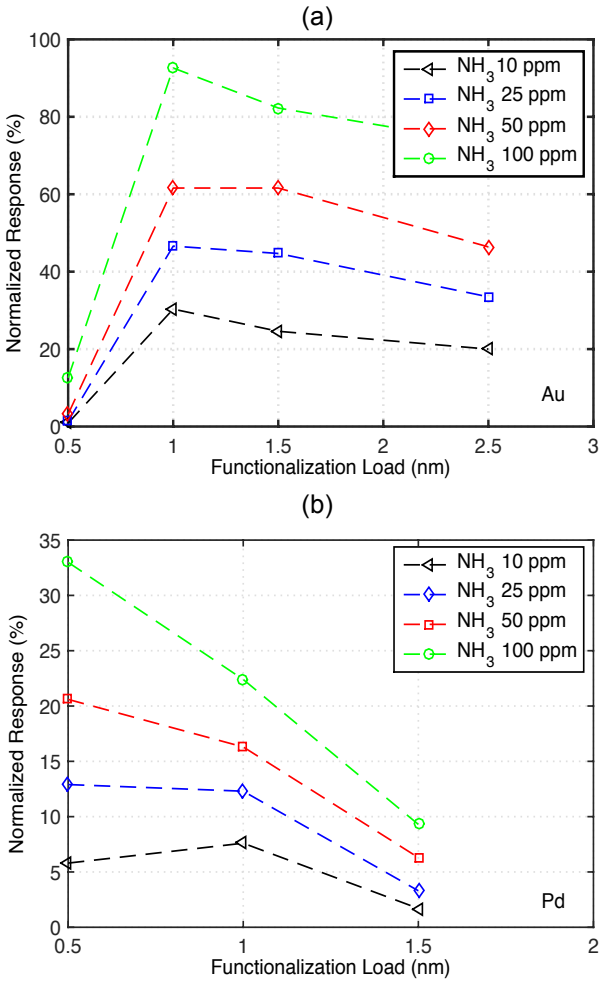

Figure 4.16: The relation between the functionalization load and the corresponding normalized response for CNT-based gas sensors functionalized with different loads of Au (a) and Pd (b).

4.6 Summary

We reported on the successful implementation of CNT based gas sensors with exceptionally high as well as immediate sensor response to four test gases (NH_3, CO_2, CO and ethanol). CNT films were prepared using a reliable and reproducible low cost spray process technique. We showed as well the importance of the functionalization process in order to enhance the response of the CNT layer. CNT gas sensors were functionalized by Au and Pd NPs through an thermal evaporation process. CNT based gas sensor functionalized with 1.0 nm of Au reached values of 25% for concentration as low as 10 ppm and 92% for concentration of 100 ppm under NH_3 exposure. Taking into consideration the short exposure time, which is 100 s, the values obtained for NH_3 can be considered exceptional. We also analyzed the effect of the thermal treatment

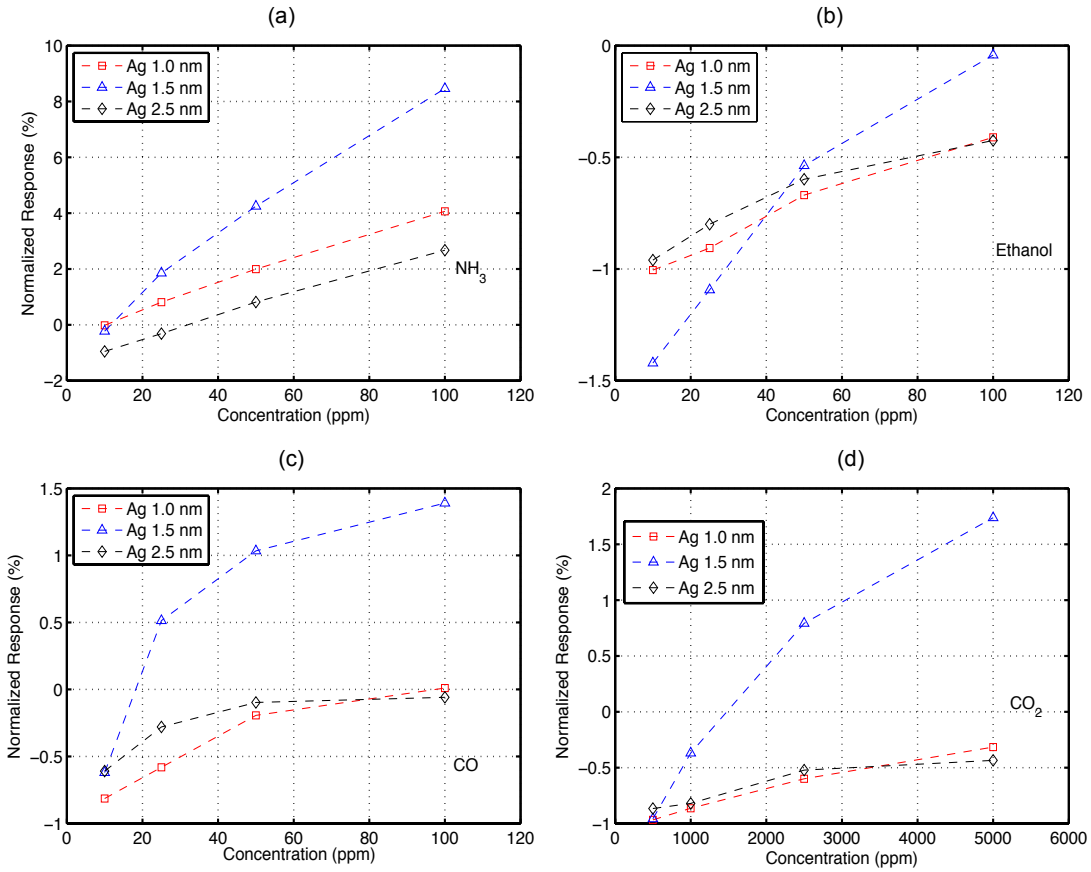

Figure 4.17: The relation between the concentration and the normalized response of CNT-based gas sensors functionalized with different loads of Ag (1.0 nm, 1.5 nm and 2.5 nm) under the exposure of NH_3 (a), ethanol (b), CO (c) and CO_2 (d).

on the performance of the Au functionalized CNT based gas sensors when exposed to NH_3. In case of Au with nominal thickness of 1.0 nm the sensor response can be as high as 120% with 100 ppm concentration of NH_3 after thermal treatment. On the contrary, for CNT based gas sensors functionalized with 2.5 nm of Au the response is not significantly affected by the thermal treatment. We investigated as well the changes that occur to the surface morphology, optical characteristics as well as the change in the work function of the CNT thin-film due to the deposition of NPs. Functionalization of CNT films deposited on glass with Au and Ag showed surface plasmon resonance effects that are dependent on the nominal thickness of the functionalization layer. Furthermore, morphological modifications occurred upon annealing lead to change in the optical and electrical characteristics of the functionalized CNT thin-films.

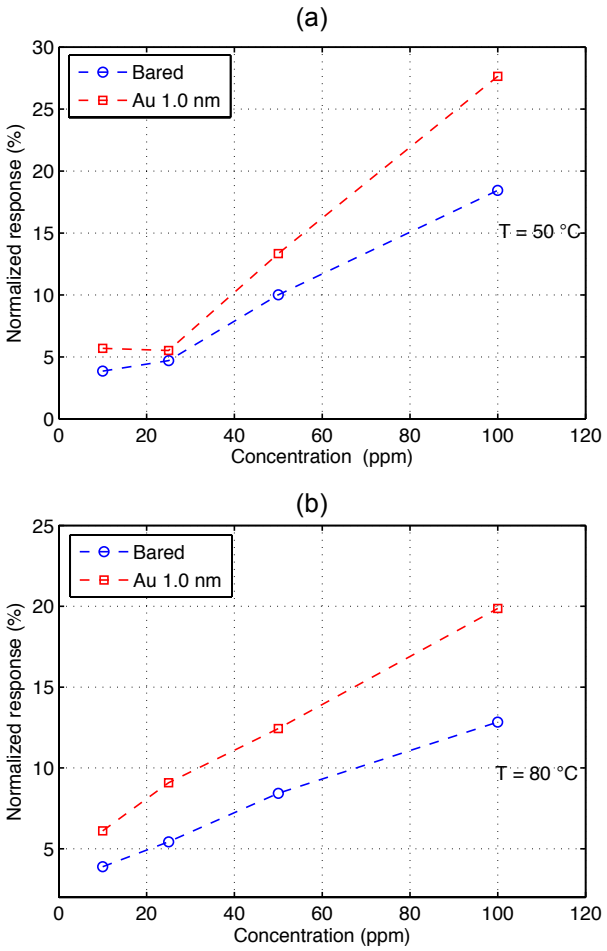

Figure 4.18: The relation between the concentration and the normalized response of CNT-based gas sensors at temperatures of T=50 °C (a) and T=80 °C (b) when exposed to NH_3. Each graph shows the response for a bare CNT layer (blue) and a CNT layer functionalized with 1.0 nm of Au (red).

Chapter 5

CNT-Based Gas Sensor Array

Functionalization of pristine CNT-based gas sensors enabled to tune the sensors' sensitivity towards different gas analytes. Nevertheless, achieving a clear distinction between the different analytes is still not reachable by depending on the response of a single sensing element. Such a criteria is highly required in certain applications like environmental monitoring, where the type of the detected analyte as well as its concentration are of great interest. In this chapter, we present the development of selective CNT-based gas sensor arrays on rigid as well as flexible substrate, which is capable of differentiating between four test gases (NH_3, ethanol, CO and CO_2). Different metals are utilized in order to alter the response of each sensing element towards the different gas analytes. We discuss as well the different possibilities and different combinations of metal functionalization for the sensors in the array. We present an efficient and quick framework strategy to achieve the optimum combination of the metal functionalization on the sensor array, that results in a clear distinction between the different gases.

CNT-based gas sensor array were fabricated as well on flexible substrate, where we functionalized the sensors with Au at different loads. The response of such array showed a clear distinction of NH_3 compared to the other gases. Furthermore, we investigate the response of the fabricated CNT sensor array towards a mixture of two gases. Such kind of characterization was performed by exposing the sensor array to a mixture of (NH_3, ethanol) and (NH_3, CO) at different ratios for each mixture.

5.1 CNT-based Gas Sensor Array Development Overview

Sensor array is a commonly used technique to enhance the selectivity of gas sensors in general. This technique was applied in metal oxide semiconducting [111] [112] as well as polymer-based gas sensors [113]. In principle, sensor array is a device that is composed

of several sensing elements. Each sensing element has a certain functionalization that provides a specific interaction with analytes in varying degrees. The combined response of all the sensing elements results in a unique pattern for each specific gas analyte. Pattern recognition techniques are required to discriminate between the different analytes. Several techniques have been reported to perform the pattern recognition process such as: discriminant function analysis [2] [4] least partial square regression (PLS) [2] [114] and principle component analysis (PCA) [2] [115] [116] [117] [118]. The latter is the technique employed for analyzing the data generated from the CNT-based gas sensor array presented in this work and it will be discussed in details in the next section. Star et al [119] were among the first to demonstrate the design, fabrication and testing for sensor arrays based on metal decorated CNT layers which were grown by CVD on Si/SiO_2. They fabricated FETs utilizing a CNT network as a channel decorated with different metal NPs. Metal decoration was done by thermal and electron-beam evaporation. They were able to distinguish between CO, H_2, H_2S, NH_3 and NO_2. Conductance response showed dependency on the type of the metal NP decorating the CNT. Lu et al [120] showed the fabrication of CNT based gas sensor array that consists of 32 sensing element. The sensing elements were pristine CNT, CNT loaded with metal clusters and CNT coated with polymers. Combining different kinds of functionalization enabled the fabricated sensor array to discriminate between different gases and vapors such as: NO_2, HCN, HCl, Cl_2, acetone and benzene. All sensors were detected in the ppm concentration levels in dry air. CNT-based gas sensor arrays are capable as well to be employed in the detection of lung cancer bio-markers. Peng et al [115] were able to detect simulated patterns of lung cancer bio-markers by CNT coated with non-polymeric organic materials. The sensor array showed excellent discrimination between VOCs found in the breath of patients with lung cancer relative to healthy controls.

In this chapter, we present the design, fabrication and characterization of a selective CNT-based gas sensor array functionalized with different types of metallic NPs. Such sensor array is capable to generate unique patterns for each test gas. The data analysis is performed by the mathematical tool principle component analysis. During the process of developing such sensor array, we investigate the relation between the stability of the film and its resistance from one side and the achieved sensitivity of the sensor from the other side. We present as well CNT-based gas sensor array on Kapton functionalized with different loads of Au NPs, which is able to discriminate between NH_3 and the other test gases. Based on the insights and understanding we obtained by functionalizing single CNT-based gas sensors, we developed a quick and efficient strategy framework for fabricating an optimum CNT-based gas sensor array. Finally, we investigate the response

of the fabricated sensor array upon exposure to a mixture of two different gases at the same time.

5.2 Materials and Methods

5.2.1 Sensor Array Design and Fabrication

The basic layout of the sensor array is shown in fig. 5.1. It consists of four sensors, with an active area of 3 x 3 mm each, which is the same area deployed for the single sensor in the previous chapter. Si wafers with 200 nm thermally grown SiO_2 and polyimide foils (Kapton 300 HN, 75 μm) are used as substrates. An inter-digitated electrode structure of 5 nm thick Cr layer and 40 nm Au layer is evaporated on top of the substrate. The inter-digitated structure has a spacing of 100 μm between the electrodes . The four sensors are connected to a common ground pad and another pad for each sensor, which make them five contacts in total. Note that the area of the whole sensor array (1 x 1 cm) was kept as the area of the single sensor layout introduced previously. This was intended for two different reason:

- In order to compare the response of each sensing element to the results obtained previously for the single gas sensors.
- Due to the limited size of the chamber used for gas testing.

The solution is prepared according to the method provided in the last chapter. For depositing the CNT layers for the experiments in this chapter we used dynamic spray system rather than static one. An automated spray system which consists of an industrial air atomizing spray valve (Nordson EFD, USA) in combination with an overhead motion platform (Precision Valve and Automation, USA) is used. Several parameters has to be adjusted in the spraying process in order to achieve the desired characteristics of the CNT layer. These parameters are material flow rate, atomizing gas pressure, nozzle-to-sample distance, substrate temperature and motion speed. The most significant dimension in air-assisted nozzles is the diameter of the orifice. For the used setup, the diameter of the nozzle is 0.3 mm. We used the same approach for spraying as introduced in chapter 3, in which we spray in the intermediate regime while heating up the substrate to the proper temperature. Such adjustment speeds up the drying process of the droplets arriving at the substrate and consequently results in uniform, homogenous and reproducible layers.

Functionalization of the CNT layer was performed via thermal evaporation process. PET mask that has one opening with the same size of the single sensor is used. This mask is

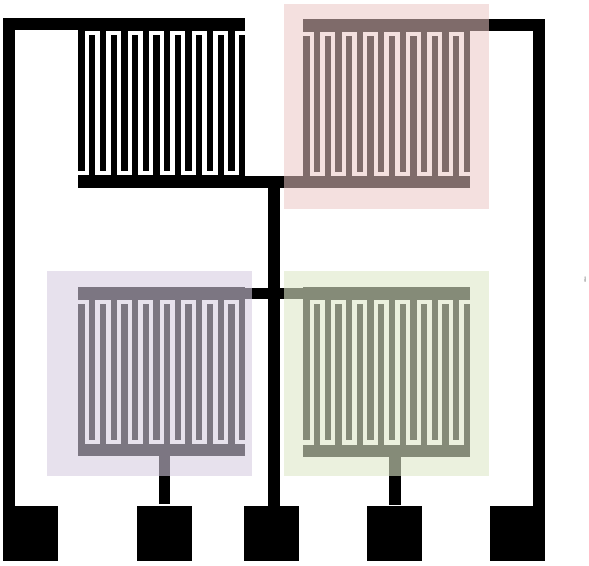

Figure 5.1: The design of the CNT-based gas sensor array fabricated in this chapter. The different color on each individual sensor indicates the different metallic NPs functionalization.

rotated three times for the different functionalization loads on each sensor in the array. The evaporation rate for all metals was kept at the lowest possible value (0.1 Å/s). Slow evaporation rate for the NPs, enhance and enables clustering of the metal on the CNT surface rather than forming a continuous layer.

5.2.2 Sensor Array Characterization

The sensor module had the same arrangement as the one used in the previous chapter in terms of the different components of the module and the operating conditions. We took one step further and we developed a new design for the sensor module to facilitate the handling of the sensor array during several measurements. In the new design, the sample is placed on a small piece of metal where the peltier element for temperature controlling and the Pt100 sensor for in-situ temperature monitoring lies directly beneath it.

For consistent, systematic and reliable results, the four sensors of the sensor array should be characterized simultaneously. In order to do so , the sensors read-out was performed by a Digital Multi-Meter (Keithley 2707) with an embedded multiplexer module which consists of 20 different channels. Such a setup, enabled us to multiplex between the four sensors each second and recording the resistances simultaneously.

The sensor array performance was investigated by exposure to different test gases with different concentrations. The test gases used are NH_3, ethanol, CO and CO_2. The desired concentration is achieved by diluting the test gas with the carrier gas. Pure N_2 is used as the carrier gas for NH_3, ethanol and CO while compressed air is the carrier gas for CO_2. Additionally, we investigated the performance of the sensor array upon the exposure to a mixture of two gases. In such case, we only mixed between the gases that has N_2 as its carrier gas.

5.2.3 Data Analysis

One of the most common methods for evaluating and analyzing the data generated by characterizing the response of the sensor array under the exposure of different gases is the Principle Component Analysis (PCA). PCA is a relatively simple mathematical method to reduce complex data sets to a lower dimension. The basic idea of such method is to express a given data set through another basis, which then allows the projection of the data to a lower dimensionality [121]. A step by step calculation of the principle components using the eigenvector decomposition can be found in appendix C.

In analyzing the data measured from the CNT-based gas sensor arrays fabricated in this chapter, we built a Matlab code, which perform the PCA. Briefly, the code reads the text files generated after measuring the response towards the four test gases, then built the sensitivity matrix. This matrix consists of 4 columns and 16 rows. Each column represents the response of one of the sensors in the array towards the four test gases with the four different concentrations for each gas, hence the 16 rows. The PCA is performed on that matrix after normalizing the data and subtracting its mean.

5.3 Sensor Array Development Framework

Functionalization of single CNT-based gas sensors with different metallic NPs gave us a lot of insights on the effects of the different types of metals on the performance of the gas sensors and the modifications that each metal introduce to the CNT surface. The results obtained in that aspect showed that the sensor normalized response enhances vastly towards all test gases. Nevertheless, single sensor functionalization does not result in a selective sensor response. In order to achieve such feature, sensor array is required. Such an array is composed of at least four sensors each is functionalized with different metallic NPs at a specific load, which in turn modify the response towards the different test gases. Thus, a selective pattern towards each gas could be achieved.

The main issue that we faced while fabricating the sensor array was the choice of the metal for each sensor as well as its corresponding load. In order to exploit such a problem in a systematic and consistent manner, we developed a framework strategy for the fabrication of the optimum CNT-based gas sensor array as shown in figure 5.2. The frame work can be described in three main steps.

- Step I: Same Metal, Different Loads
- Step II: Simulation of Virtual Sensor Arrays
- Step III: Fabrication of the Optimum Sensor Array

In the first step, we fabricate sensor arrays according to the process described earlier and functionalize each sensor in the array with the same metal but at different loads. For example if we choose Au for the first array, we functionalize three sensors in the array with loads 1.0 nm, 1.5 nm and 2.5 nm. The fourth sensor in the array was always kept bare (no functionalization) as a reference. The same procedure is applied for Pd, Ag, Ti and Cr. The load of the metal was chosen based on the knowledge we gained in the last chapter about the optimum operating range for each metal. This phase enabled us to have a general idea about the combined response of each metal towards the different gases. Additionally, it helped us to collect the response of large amount of sensors with different metal functionalization at different loads. The collected data were the corner stone for the starting of step II.

There is an infinite number of possible combinations for the different metal functionalization and the different loads that can be deposited on each individual sensor in the sensor array. In order to decrease such complexity, in step II we simulate the response

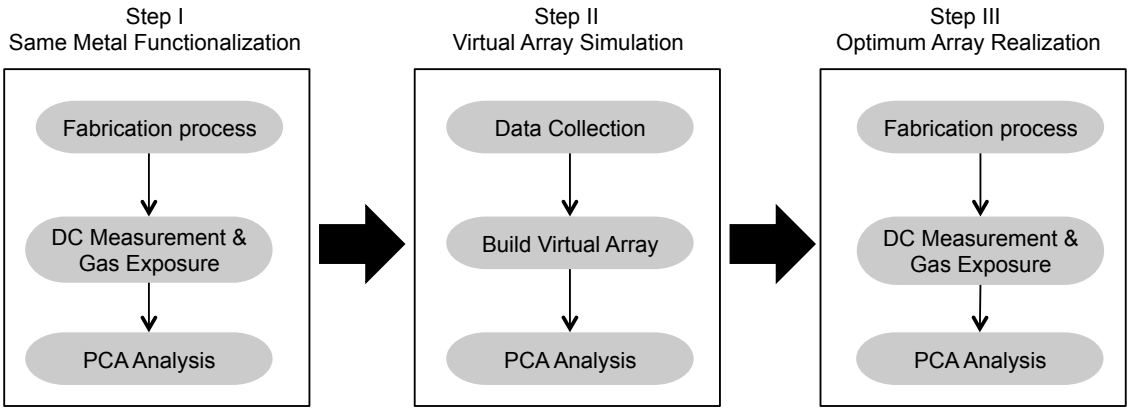

Figure 5.2: A chart summarize the different development steps of the CNT-based gas sensor array.

of different combination. Simulation seemed to be the optimum solution to decrease the development time. Different combinations of metals at different loads were used to build virtual sensor arrays. We developed a Matlab code to simulate the results of these different combinations. The choice of metals at different loads was based on the modification that such functionalization can introduce to the film resistance, moreover whether such metal at that specific load enhance or degrade the response towards one or more test gas. The optimum case is having a certain combination, where each individual sensor behaves completely different towards each one of the four test gases.

After different simulation iterations, we were able to reach the optimum combination of different metals at specific loads that can select between the four test gases. Step III is the fabrication and characterization of such combination as well as comparing the measured data to the simulation results.

5.4 Same Metal, Different Loads

5.4.1 CNT Thin-Films at Percolation Threshold

Applying the development framework described in the last section, we fabricated the first set of sensor arrays based on the fabrication procedure used in the last chapter. The sensor arrays fabricated utilize CNT thin-films with rather low tube densities. At such densities, the film operates near its percolation threshold, thereby reducing the number of metallic pathways in the network and amplifying the contribution of the semiconducting pathways. Such film density results in the highest possible sensor sensitivity towards the four test gases. The resistances of the individual sensors at such density were ~ 8 kΩ The metals used in this step with the corresponding load were as follows

- Au (1.0 nm, 1.5 nm, 2.5 nm)
- Pd (0.2 nm, 0.5 nm, 1.0 nm)
- Ag (0.2 nm, 0.5 nm, 1.0 nm)
- Cr (0.2 nm, 0.5 nm, 1.0 nm)
- Ti (0.2 nm, 0.5 nm, 1.0 nm)
- Al (0.2 nm, 0.5 nm, 1.0 nm)

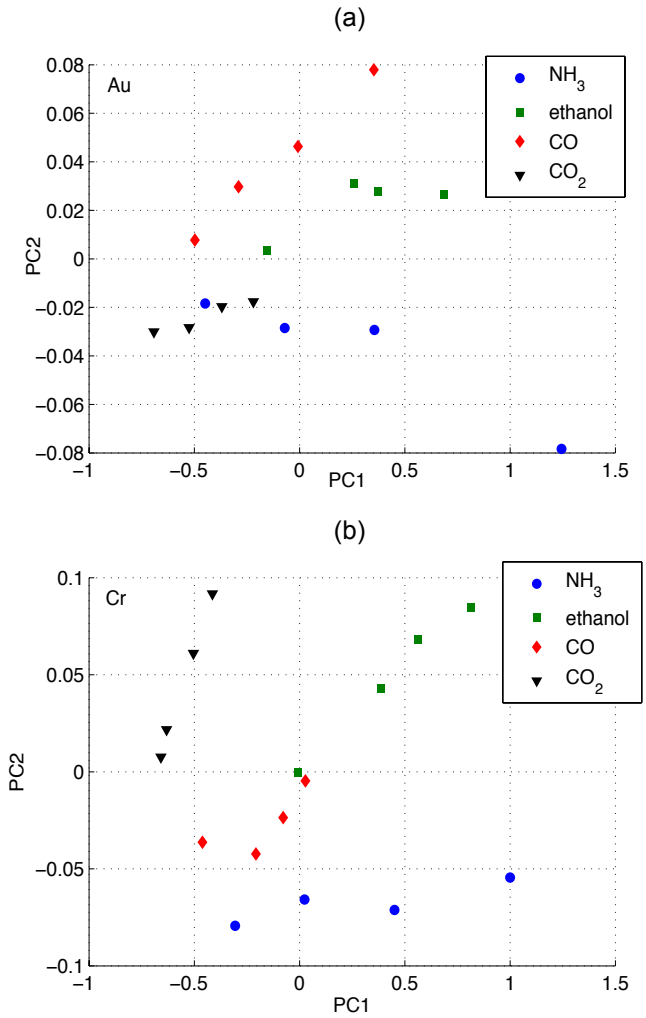

Figure 5.3: PCA for two CNT-based gas sensor arrays functionalized with different loads of Au (a) and Cr (b).

An example for the result obtained from these set of experiments is shown in fig. 5.3, which shows the PCA for two different arrays functionalized with Au and Cr. The sensor functionalized with Au shows a slight separation of NH_3 w.r.t the other gases. On the other side the Cr sensor array separates NH_3 and CO_2 from ethanol and CO, which are clustered in the midsection. One important figure of merit in evaluating the results of the PCA is the influence of the different principle components, which is represented by the variance percentage of the data in the direction of the principle component. In the results shown, the highest percentage is usually in PC_1 (>99.5%). This is due the fact that all the sensors respond in a similar way upon gas exposure (all functionalized with the same metal), which means that the obtained data are highly correlated. In our case the influence of the second and the third components is an important aspect for obtaining better distinction between the test gases. Although the results presented seem

promising, they are not reproducible. Figure 5.4 shows the variation in the results for two identical sensor arrays functionalized with different Pd loads. Similar variation in the results is obtained when repeating the fabrication process for the other metals as well. One possible reason for such a problem could be that the sensors before the functionalization process were not identical. By taking a closer look at the values of the resistances for Pd 1 and Pd 2 as shown in table 5.1 before the functionalization process, we can clearly see that the range of resistances for Pd 2 is almost double the values obtained for Pd 1. Additionally, within the same array there is relatively large variation between the resistances of the individual sensors. In order to investigate the effect of such variation in the resistance on the PCA results, we characterized two bared sensor arrays . The results obtained are shown in fig. 5.5 and the corresponding resistance of the individual sensor in each array s shown in table 5.2. We can observe two main points from the shown results:

- The results obtained from each array is not identical due to the difference range of resistance of the individual sensors in each array. This is consistent with the results

Table 5.1: Resistance variation for two sensor arrays each functionalized with different loads of Pd, where the CNT layer is deposited at percolation threshold

Indication	Functionalization	Resistance (before)	Resistance (after)
Pd 1	Palladium 0.2 nm	2.0 kΩ	2.0 kΩ
	Palladium 0.5 nm	1.5 kΩ	1.9 kΩ
	Palladium 1.0 nm	1.5 kΩ	0.312 kΩ
	Bare	2.1 kΩ	8.9 kΩ
Pd 2	Palladium 0.2 nm	4.5 kΩ	2.7 kΩ
	Palladium 0.5 nm	4.6 kΩ	1.9 kΩ
	Palladium 1.0 nm	5.0 kΩ	0.447 kΩ
	Bare	4.3 kΩ	5.1 kΩ

Table 5.2: Resistance variation for bare CNT-based gas sensor arrays deposited at percolation threshold

Indication	Functionalization	Resistance
Bare1	Bare	9.05 kΩ
	Bare	9.56 kΩ
	Bare	7.64 kΩ
	Bare	5.69 kΩ
Bare2	Bare	10.8 kΩ
	Bare	8.93 kΩ
	Bare	7.58 kΩ
	Bare	8.74 kΩ

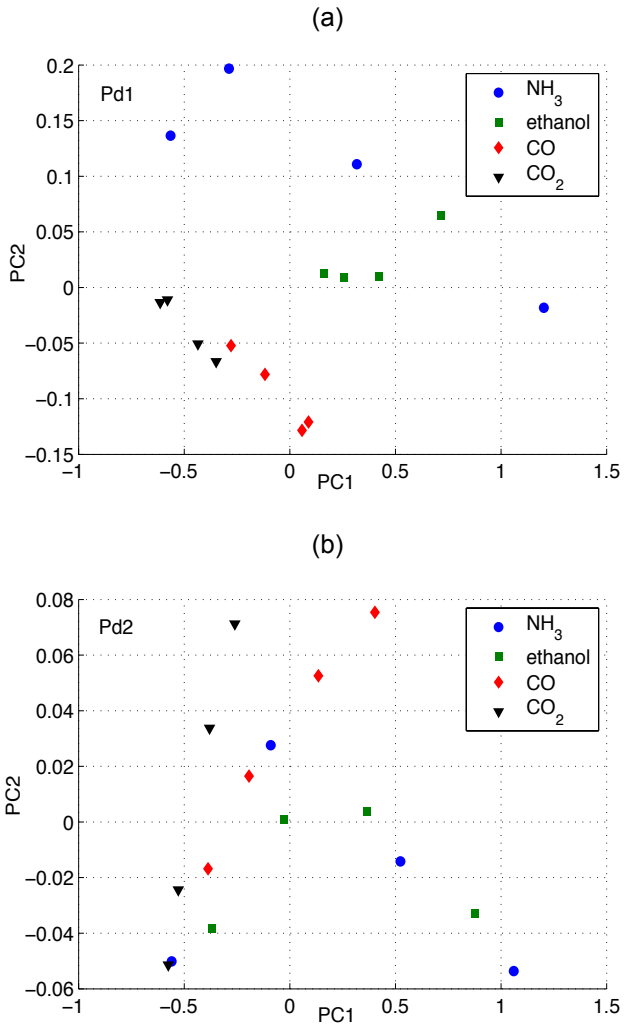

Figure 5.4: PCA plots for two CNT-based gas sensor arrays functionalized with Pd at loads of 0.2 nm, 0.5 nm and 1.0 nm.

obtained for the functionalized sensor arrays introduced above.

- PCA plot for the sensor array represented in fig.5.5b shows separation of NH_3, which should not be the case since all the individual sensors in the array are supposed to be 'identical'. This implies that the difference in the resistance of the individual sensors can result in separation in the PCA plot, hence gas selectivity

We further investigated the relation between the resistance of the individual sensors during the successive measurements towards the different test gases and their normalized response. In order to carry on that kind of investigation, we monitored the resistance of the individual sensors in the array at the moment before gas exposure at each concentration of the different test gases. We will show here only the resistance before the

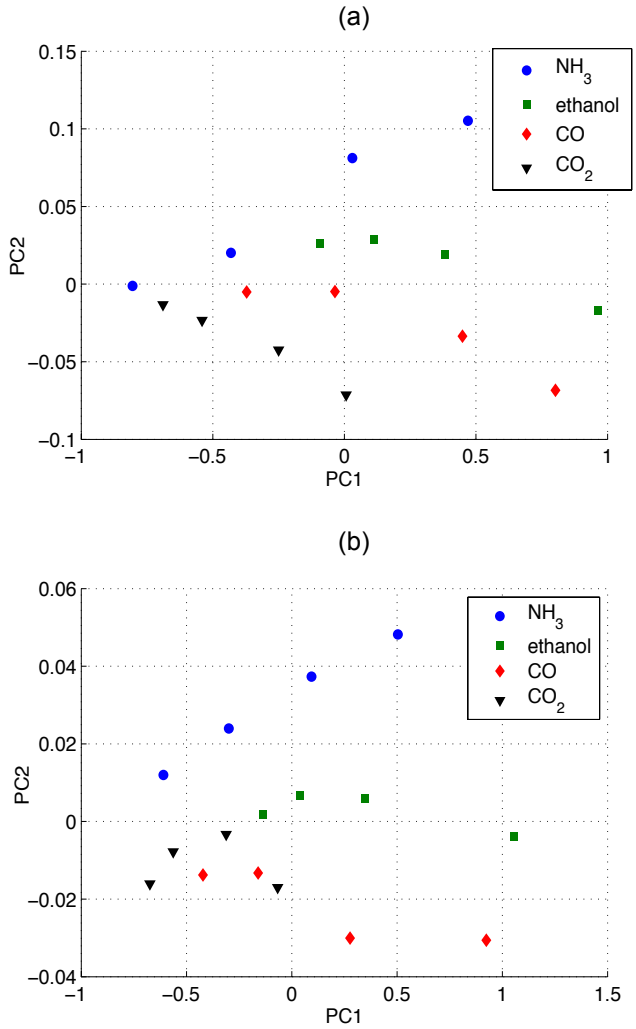

Figure 5.5: PCA plots for two bare CNT-based gas sensor arrays sprayed at the percolation threshold.

highest concentration, since we assume that most of the changes that occur during the measurement is reflected in the last exposure cycle.

Figure 5.6 shows the normalized response of the sensor arrays Pd 1 and Pd 2 as well as the resistances of the individual sensors at the chosen moments for the different measurements. It can be clearly observed that the resistance of the bare sensor in Pd 2 is by far higher than the resistance of the other sensors for the measurements with NH_3 and ethanol. The normalized response for these two measurements was also higher than the other two sensors. The resistance of the sensor decreases drastically at the CO and CO_2 measurements. Such a behavior could be one of the main reasons of having inconsistent PCA results from one array to the other. On the other hand, in array Pd 2 the bare sensor had the highest resistance and the highest normalized response as well.

The variation in the resistance of the CNT thin-film is one common feature when the layers are deposited at percolation threshold. At such low density the deposited layers are highly uniform but the resistance is highly sensitive to the number of deposited tubes. Depositing thicker films could omit such a problem but it would result immediately in decreasing the sensitivity of the sensor towards all test gases because of the domination of the metallic tube in that case. This implies that we have to trade-off the sensitivity in order to stabilize the resistance of the film.

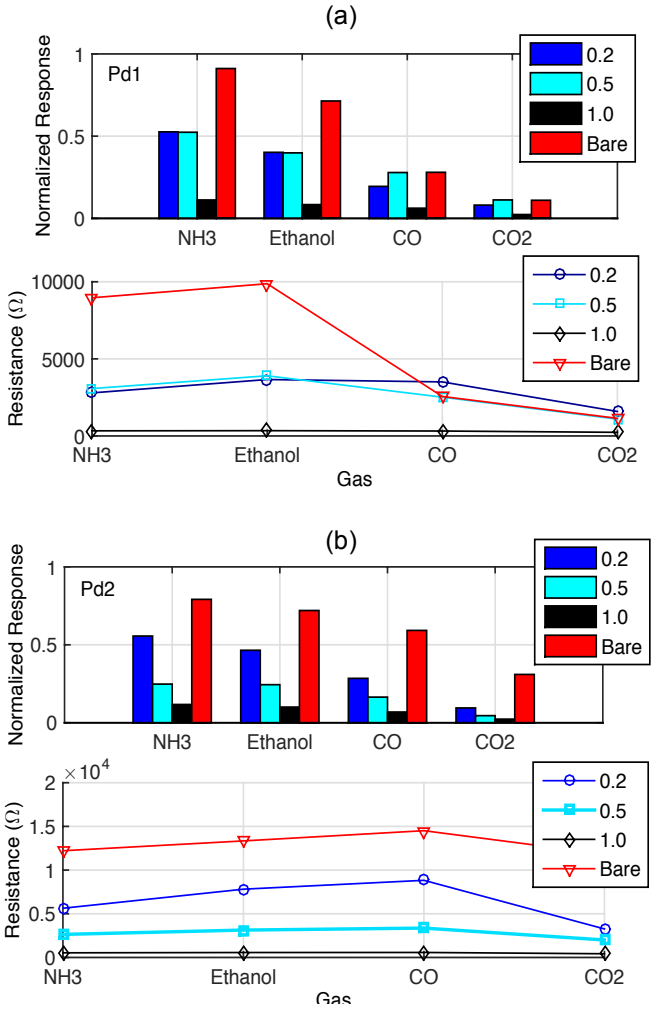

Figure 5.6: Comparison between two CNT-based gas sensor arrays functionalized with Pd at loads of 0.2 nm, 0.5 nm and 1.0 nm in terms of the normalized response towards the different test gases and the resistance of the individual sensors after the successive measurements.

5.4.2 CNT Thin-Films at Higher Thicknesses

Increasing the thickness of the sprayed sensors resulted in an average resistance of ~ 1 kΩ. In order to investigate the stability of the newly fabricated sensor arrays, we characterized two 'identical' bare sensor arrays as we did in the last section. Figure 5.7 shows the variation in the resistance during the measurement, the normalized response of each individual sensor in the array to the four test gases as well as the PCA results. By taking a closer look at the plots, we can clearly see that the resistance of each individual sensor is stable from one measurement to the other. Nevertheless, one array (fig.5.7 a and b) still shows separation of NH_3 and slight separation of ethanol from the other gases. Such behavior can be attributed to the fact that two sensors has almost the same resistance which is ~ 1.7 kΩ and the other two has a resistance ~ 1.2 kΩ. As aforementioned the change in the resistance of the individual sensors within the sensor array could eventually result in selectivity towards one or more test gas.

Further increase in the thickness of the CNT layer decreases the chances of obtaining selective sensor array consists of only bare sensors but also it decreases the sensitivity

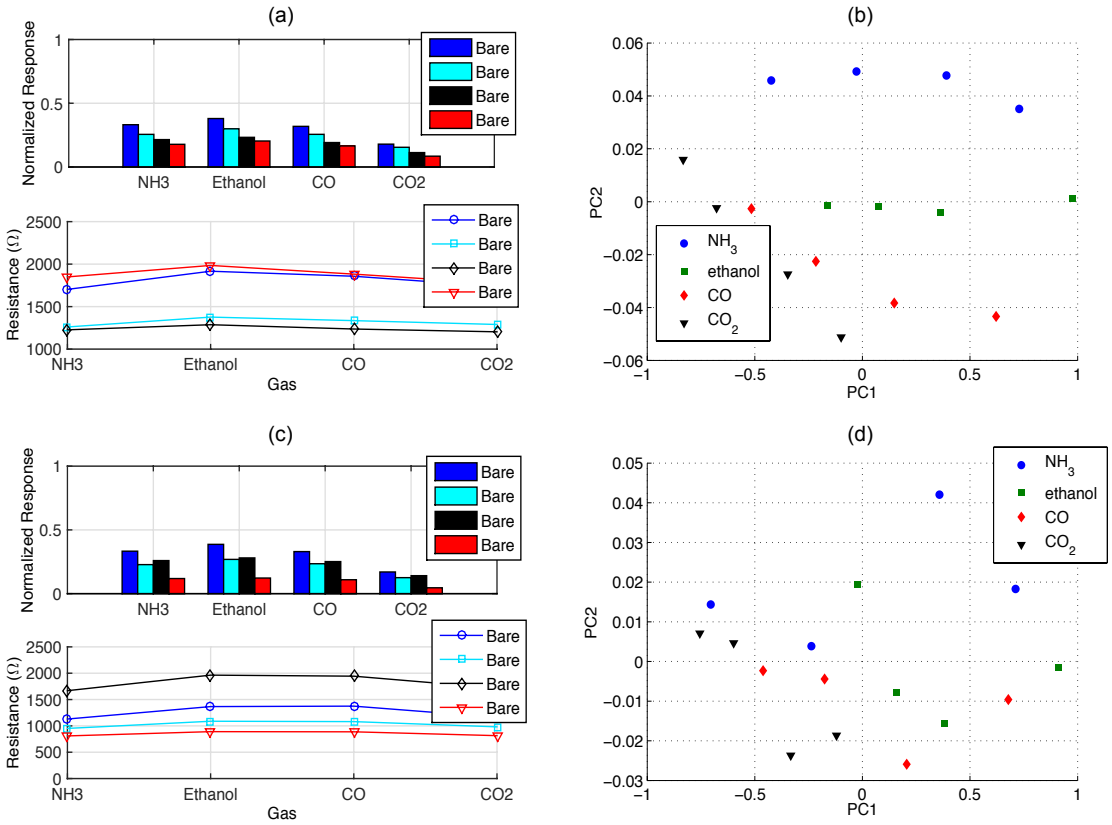

Figure 5.7: Comparison between PCA plots, the normalized response and the resistance of the individual sensors for two bare CNT-based gas sensor arrays.

towards all the test gases drastically. Even though, PCA plots (not shown here) for such high thickness CNT layers does not show any separation or clustering of the data points and the individual sensor resistances are all ~ 240 Ω, the sensitivity of all the individual sensors towards the four test gases is very low (< 5%).

The entire measurements carried out with the bare sensor arrays are presented in figure 5.8. The plot represents the relation between the resistance of the individual sensors and their corresponding normalized response (the mean normalized response of the four test gases). One can distinguish between three different film thicknesses: percolation threshold layer (circles), intermediate film thickness (squares) and high film thickness (rhombus). At the percolation threshold, a large variation can be observed in the resistance of the individual sensors as well as the corresponding normalized response. On the other hand, at the high film thickness the resistance and the normalized response are highly stable. Nevertheless, the obtained normalized response is very low towards all test gases, which in some cases lower than the noise level. The intermediate film thickness is the one more suitable for the sensor array fabrication. At such thickness the resistance of the film is relatively stable and the normalized response is sufficient to detect different gases.

5.4.3 Functionalized Sensor Arrays at Optimum Film Thickness

The best compromise between the film stability and the corresponding normalized response is achieved by depositing CNT layer at an intermediate thickness as we explained

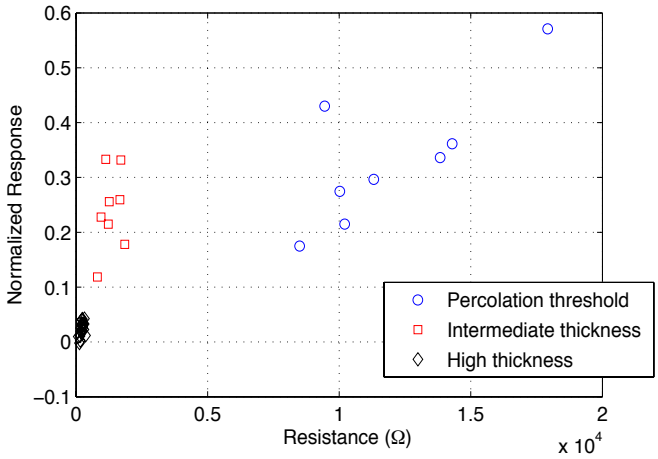

Figure 5.8: Relation between the resistance and the normalized response for the bare CNT sensing element in all the fabricated sensor arrays which are sprayed at different thicknesses: percolation threshold (circle), intermediate thickness (square) and high thickness (rhombus).

previously. We fabricated sensor arrays functionalized with Au, Pd and Cr according to the new adjusted film thickness. Four sensor arrays functionalized with Au, four sensor arrays functionalized with Pd and two sensor arrays functionalized with Cr were produced to check the reproducibility of the adjusted film thickness. Sensor arrays functionalized with the same metals revealed similar behavior in the resistance pattern during the measurement as well as similar PCA results. The bare sensor in the Au sensor arrays remains almost stable over all the measurement iterations. The normalized response show similar pattern in the different arrays as well. PCA plots for the four sensor arrays functionalized with different loads of Au are shown in fig. 5.9. Au functionalization enhances greatly the normalized response, especially towards NH_3 when compared to the bare sensor as we discussed in the previous chapter. For the other three gases: ethanol, CO and CO_2 the enhancement is not that noticeable as in the case of the NH_3. This could be the explanation for the separation of NH_3 in the PCA plots from the other test gases in all the Au functionalized sensor arrays.

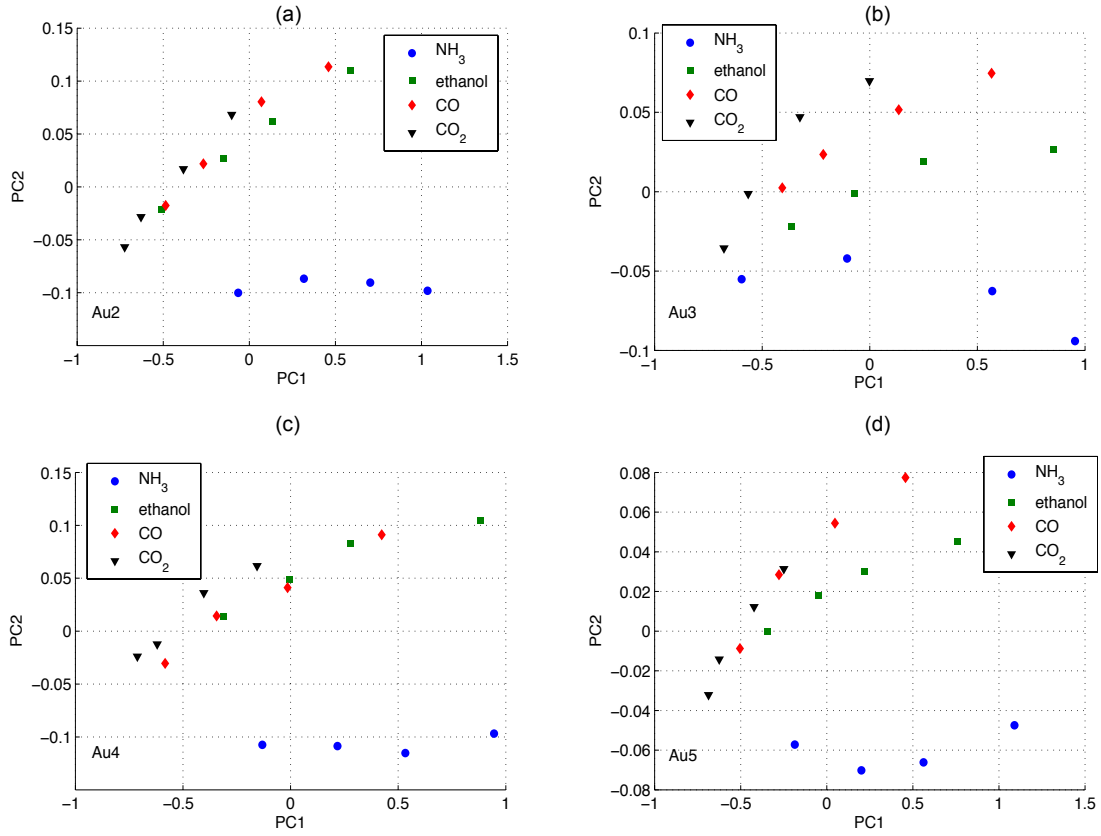

Figure 5.9: PCA plots for four CNT-based gas sensor arrays functionalized with Au. In each array three sensors are functionalized with loads of 1.0 nm, 1.5 nm and 2.5 nm while the fourth sensor in is kept without functionalization.

Similarly, the Pd sensor arrays showed consistent and stable results regarding the variation in the resistance during the successive measurements. The normalized response towards the test gases and the PCA plots are shown in figure 5.10. The PCA plots of the Pd sensor array showed all the same tendency in placing the CO_2 data points in the left part of the plot followed by CO. While the data points for NH_3 and are found to be close to each other unveiling a bad distinction for these two gases. This agrees with the result obtained in the last chapter for the Pd functionalized CNT-based gas sensors, which showed the highest sensitivity towards CO_2 w.r.t to the other three gases. The fact that Pd sensor array can separate CO_2 and CO from NH_3 and ethanol while Au sensor arrays separate NH_3 from the other gases renders these two types of functionalization as promising candidates for combination in one array as we will show later.

Cr sensor arrays showed as well consistent and stable performance. As shown in figure 5.11, Cr sensor arrays separated NH_3 from the rest of the test gases. PCA results of Cr sensor arrays were quite similar to the response of the Pd sensor array in terms of spreading and positioning the data points on the plot. Moreover, Cr (1.0 nm)

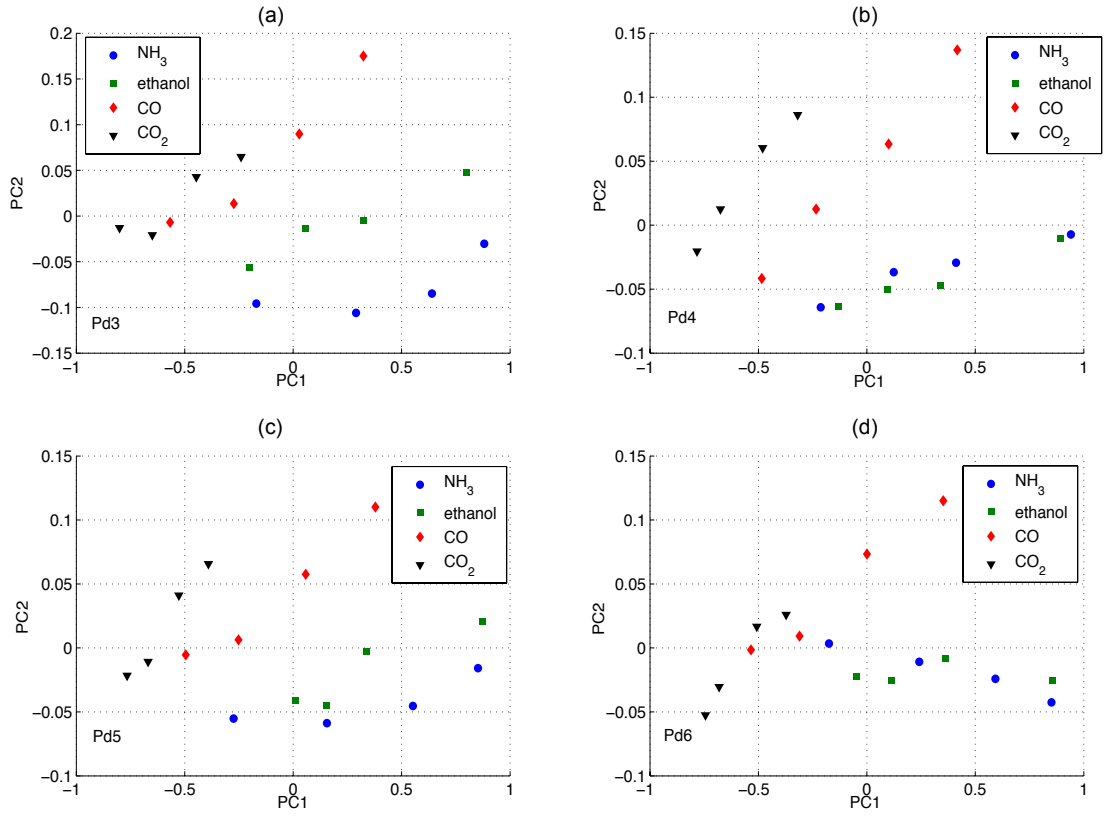

Figure 5.10: PCA plots for four CNT-based gas sensor arrays functionalized with Pd. In each array three sensors are functionalized with loads of 0.2 nm, 0.5 nm and 1.0 nm while the fourth sensor in is kept without functionalization.

showed superior normalized response towards all gases except for CO_2. Having higher resistance in all the measurements except for CO_2 could be the reason for such higher normalized response. It is worth mentioning here that Cr functionalization unveiled a consistent and interesting feature. The resistance of the CNT network increases after the functionalization process. Additionally, the higher the functionalization load, the higher the over all resistance of the network. This implies that Cr interacts completely different to the surface of the CNTs when compared to Au or Pd functionalization. Such a property is beneficial when combining different metals in one sensor array.

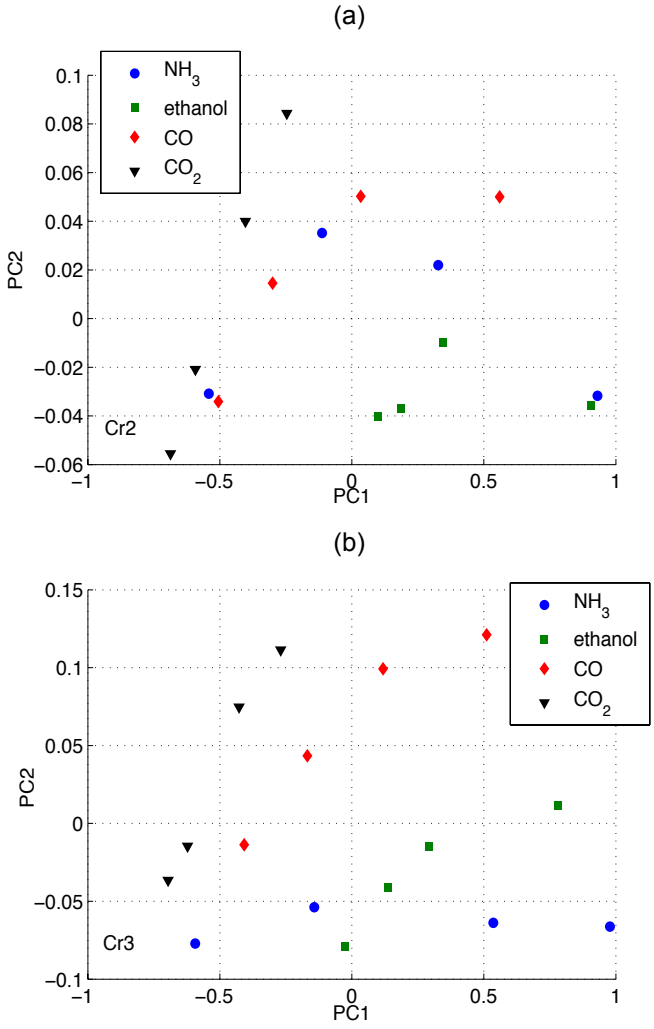

Figure 5.11: PCA plots for two CNT-based gas sensor arrays functionalized with Cr. In each array three sensors are functionalized with loads of 0.2 nm, 0.5 nm and 1.0 nm while the fourth sensor is kept without functionalization.

5.5 Simulation of Virtual Sensor Arrays

Each sensor array fabricated till now consists of four sensors, three are functionalized with the same metal at different loads and the fourth sensor was always kept bare. Effectively, these sensor arrays consisted only of two types of sensors, as we assume that each type of metal functionalization influences the CNT sensor in similar manner, although the functionalization load might be different.

In step II, we use the data we collected for the entire previously measured sensor in order to build a virtual sensor array to achieve the optimum combination of metal functionalization and their corresponding loads that can separate and select between the four test gases. In order to carry on such a step , we implemented a Matlab program that simulates the PCA result of the virtual arrays to deliver in a quick and efficient way the most promising combination.

PCA plots in the previous sections were always two-dimensional because in all the discussed cases the third principle component almost had no influence on the outcome result. Applying one type of functionalization results in sensors with correlated results in the PCA plot, hence most of the information and the variance within the data is only the first and the second PCs.

Since sensor arrays functionalized with Au, Pd and Cr delivered the most adequate and diverse results in terms of stability as well as gas separation in the PCA plot, we chose these three metals for the different combination in the virtual sensor array. After several simulation iterations and building virtual sensor arrays with only two or three sensors as well, we found that the best combination consists of an array of four sensors: first sensor is bare, the second sensor is functionalized with Au (1.5 nm), the third sensor is functionalized with Pd (0.2 nm) and the fourth sensor is functionalized with Cr (1.0 nm).

The superiority in the normalized response of Au functionalization towards NH_3 and for Pd towards CO_2 with Cr functionalization resulted in CNT sensor array that can isolate NH_3 in one plane, separate between CO, CO_2 and ethanol in the other two planes as shown in fig. 5.12. The data are presented in two different angles to give a better perspective of the 3D results. The simulated sensor array showed a strong influence of the second and the third principle components, which resulted in better distinction between the different gases.

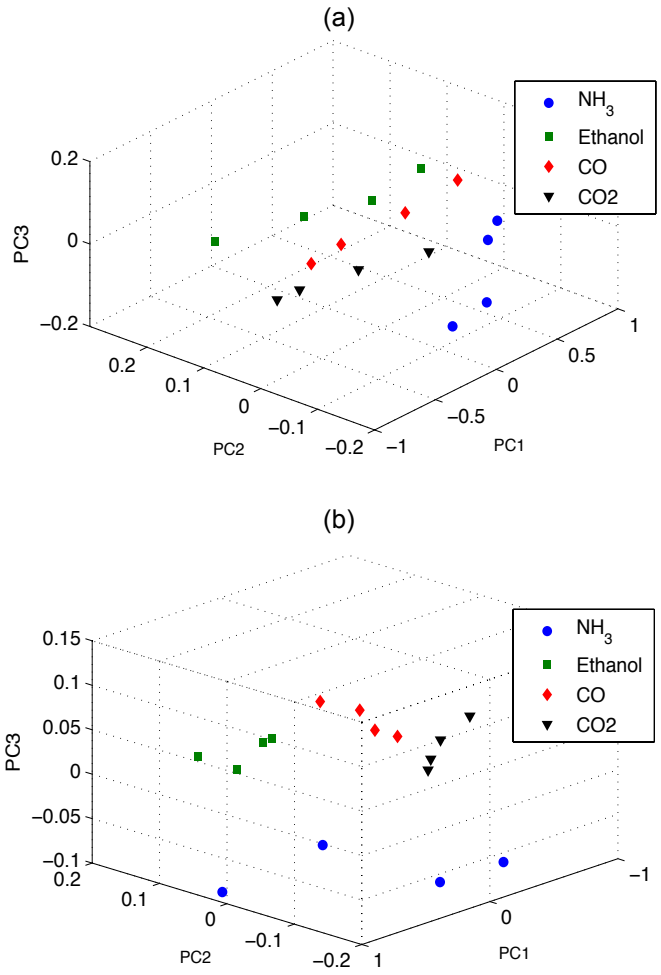

Figure 5.12: PCA plots for the simulated sensor array functionalized with 1.5 nm of Au, 0.2 nm of Pd, 1.0 nm of Cr and the fourth sensor is bare. The data are presented in two different angles to give better perspective of the 3D plot.

5.6 Fabrication of the Optimum Sensor Array

5.6.1 Optimum Sensor Array on Silicon

In this step, we spray deposited CNT solution, which has 90% semiconducting tubes instead of the intrinsic CNT solution (67% semiconducting tubes) that we used in all the previous experiments. Using a semiconducting solution enabled us to deposit significantly thick CNT layers far beyond the percolation threshold and obtaining stable film resistances similar to the values obtained previously (~ 1 kΩ). The higher network density guarantees higher stability in the resistance, thus boost the reproducibility of the sensor. For further confirmation on the stability of the used semiconducting solution, we repeated the common procedure of fabricating one bare sensor array and evaluating its

performance in terms of the resistance stability, normalized response and PCA results. The results presented in fig. 5.13 shows the stability in the resistance during the successive measurements. The normalized response is almost the same for the individual sensors with each test gas and more importantly no clear distinction between the gases can be observed in the PCA plot.

After successfully simulating the most promising combination of metal functionalization, which consists of Au (1.5 nm), Pd (0.2 nm) and Cr (1.0 nm) and a bare sensor, we fabricated and characterized such CNT sensor array. Three sensor arrays were fabricated: Array 1, Array 2 and Array 3. Taking a closer look at the results obtained from characterizing Array 1 in fig. 5.14, we can observe a stable resistance (~ 1 kΩ) for the Au, Pd and bare sensors during the successive measurements. The resistance of the Cr sensor (~ 3.5 kΩ) was almost stable for the first three measurements and then dropped to almost

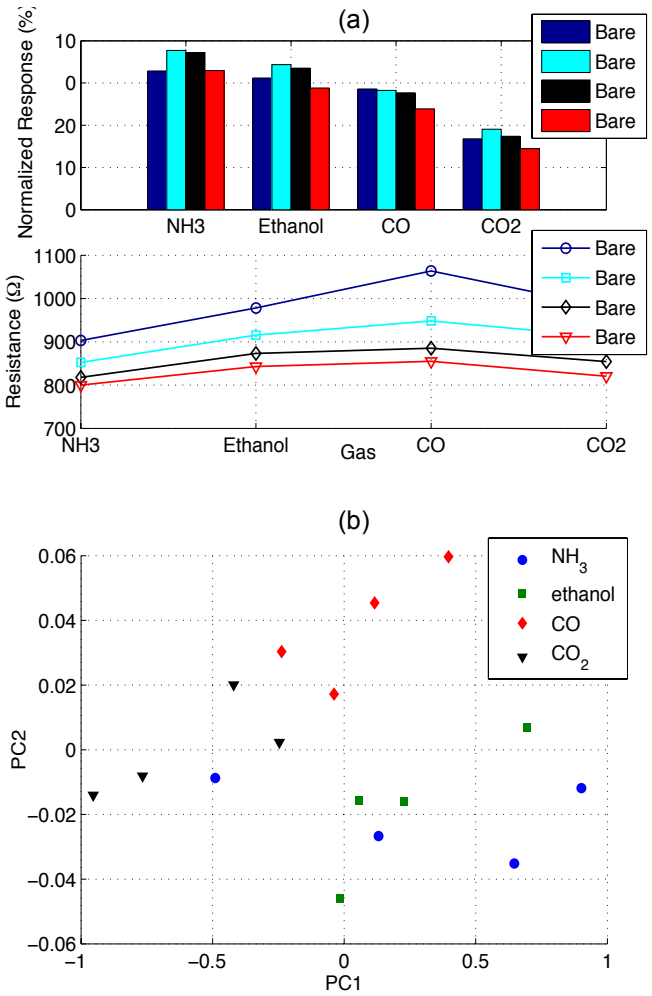

Figure 5.13: Comparison between sensor resistance, normalized response and PCA for a bare sensor array fabricated with 90% semiconducting CNT solution.

half of its value at the last measurement. This behavior is consistent with the result obtained previously for the Cr (1.0 nm) in the Cr sensor array. The PCA plot showed a clear separation of NH_3 data points in one plane, while ethanol, CO and CO_2 remain relatively in another plane. Nevertheless, ethanol is clearly separated from CO and CO_2, which are relatively clustered together. By comparing this result to the results obtained from the simulated sensor array in the last section, we can clearly see the same pattern and the same behavior for the different data points. Such results are remarkable due to the fact that the data points used in the simulated version are extracted from measurements performed in different time periods and at slightly different ambient conditions. This is a strong evidence for the reproducibility of the sensors fabricated at that resistance range.

The results obtained from Array 2 and Array 3 were almost identical to each other but relatively different to the results obtained from Array 1 as shown in fig. 5.15 and fig. 5.16 respectively.

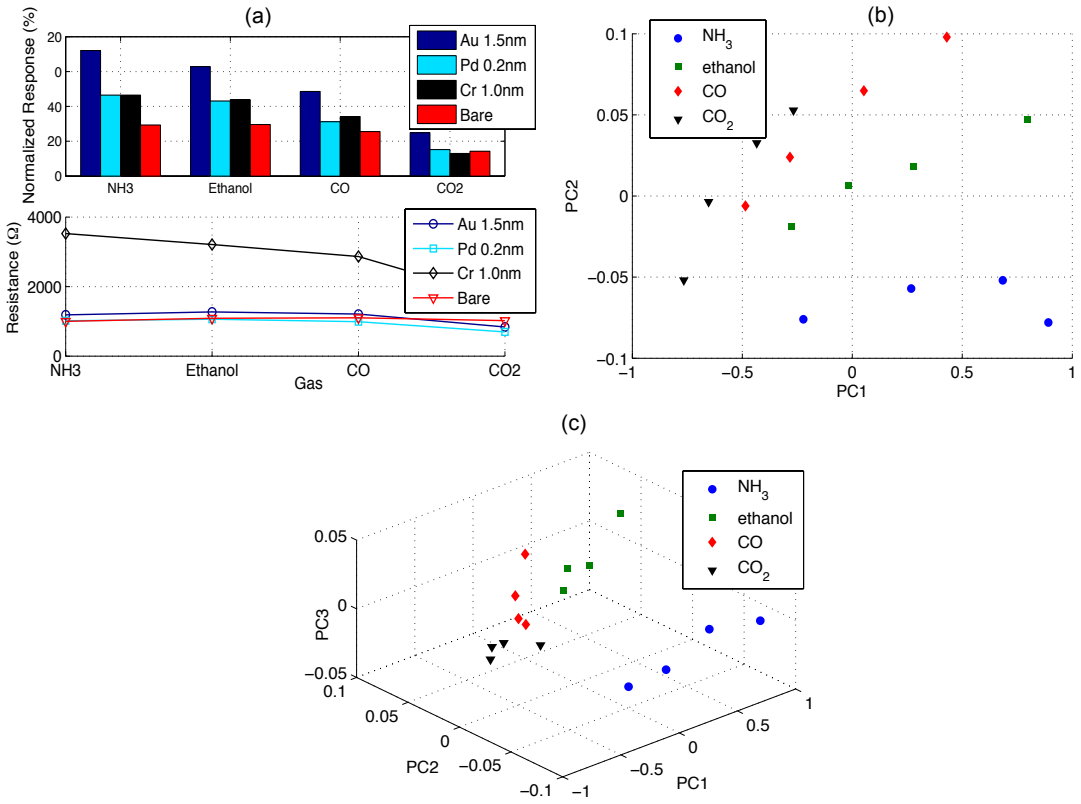

Figure 5.14: (a) The resistances of the individual sensors and their normalized response towards the four test gases (NH_3, ethanol, CO and CO_2) for Array 1 which is functionalized with Au 1.5 nm , Cr 1.0 nm and Pd 0.2 nm. (b) & (c) The PCA plot for such CNT-based gas sensor array in 2D & 3D respectively.

In Array 2 and Array 3, the separation between the gases still exists but is not as clear as it is in the PCA plot of Array 1. The resistances of the individual sensors and its variation behavior in the three arrays were almost the same during the different measurements. Taking a closer look at the normalized response plots, we can point out that for Array 2 and Array 3 sensor functionalized with Cr (1.0 nm) had higher normalized response than Pd (0.2 nm) under the exposure of NH_3 and ethanol, which was not the case in Array 1. Such minor change in the normalized response of one individual sensor affected directly the separation and clustering of the data points in the PCA plots. Note that in the previous discussions, we concentrated mainly on the stability of the resistance as a crucial issue for the outcome of the sensor array. It is important to mention that the outcome result is highly sensitive as well to any minor error in the lithography process, which is the first step in the fabrication process. In general, the result of the sensor array is highly sensitive to any minor changes in the fabrication process, which can be directly reflected in the response of the sensors as well as the PCA plot.

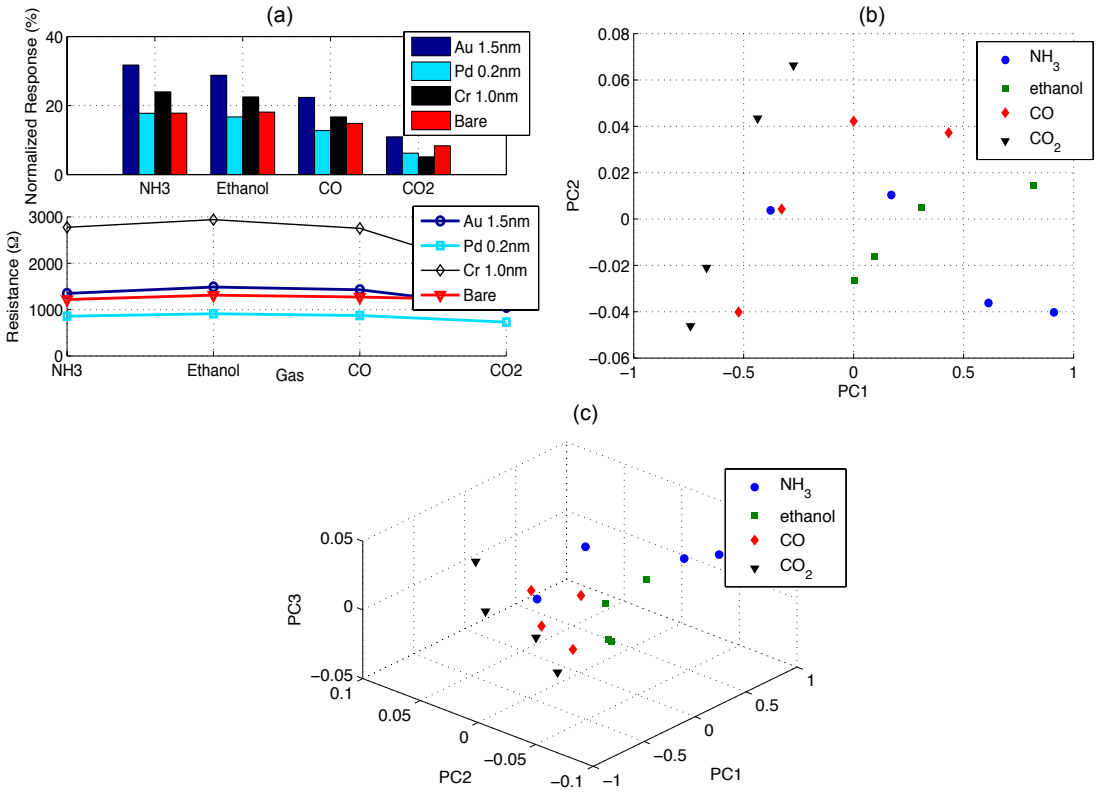

Figure 5.15: (a) The resistances of the individual sensors and their normalized response towards the four test gases (NH_3, ethanol, CO and CO_2) for Array 2 which is functionalized with Au 1.5 nm , Cr 1.0 nm and Pd 0.2 nm. (b) & (c) The PCA plot for such CNT-based gas sensor array in 2D & 3D respectively.

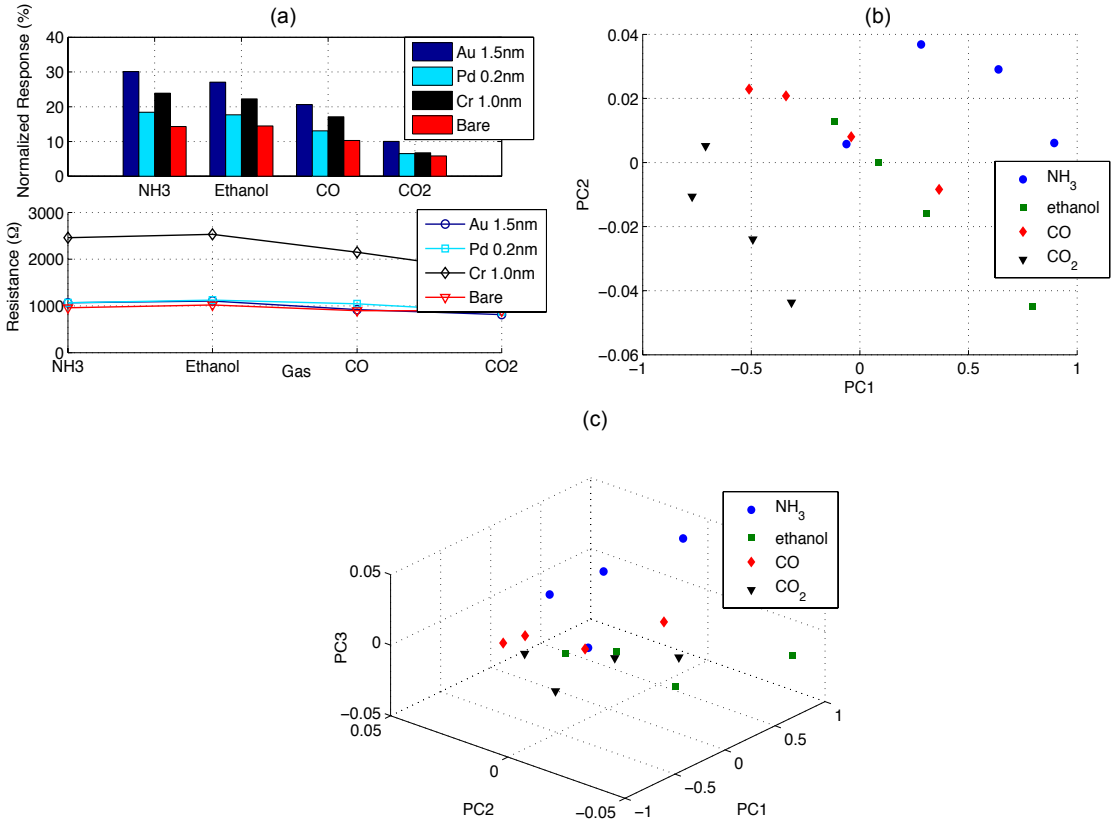

Figure 5.16: (a) The resistances of the individual sensors and their normalized response towards the four test gases (NH_3, ethanol, CO and CO_2) for Array 3 which is functionalized with Au 1.5 nm , Cr 1.0 nm and Pd 0.2 nm. (b) & (c) The PCA plot for such CNT-based gas sensor array in 2D & 3D respectively.

5.6.2 Characterization towards Gas Mixture

Another key aspect for the evaluation of the CNT-based gas sensor array performance is investigating its response towards mixture of two test gases simultaneously. Such a characterization procedure is major step towards realizing CNT-based gas sensor array in wide range of applications where the detected analytes consists of different concentration and of different gases rather than a single pure gas. In order to perform such a step, we examined the response of the optimum CNT-based gas sensor array, described in the last section, towards different mixtures of NH_3 and CO as well as NH_3 and ethanol.

To obtain a systematic and consistent results, we limited this type of characterization only to the three test gases which has pure N_2 as a carrier gas (NH_3, CO and ethanol). Moreover, the total concentrations were always 10 ppm, 25 ppm, 50 ppm and 100 ppm independent from the ratios of the two gases. Before characterizing the sensor array towards the mixture, we measured first its response towards each gas separately.

We chose a ratios of 1:1, 1:2 and 2:1 between the NH_3 and ethanol as well as NH_3 and CO for such characterization procedure. Figure 5.17 shows the PCA plot for the CNT-based gas sensor array towards NH_3 and CO as well as the different mixtures between them. The response towards equal ratios of the two gases lies almost in the middle between the data points for each gas separately. By increasing the ratio of NH_3 w.r.t CO, its data points tends to move towards the NH_3 data points and similarly vice versa. Investigating the response of the sensor array towards different mixtures between NH_3 and ethanol reveals similar results as shown in figure 5.18.

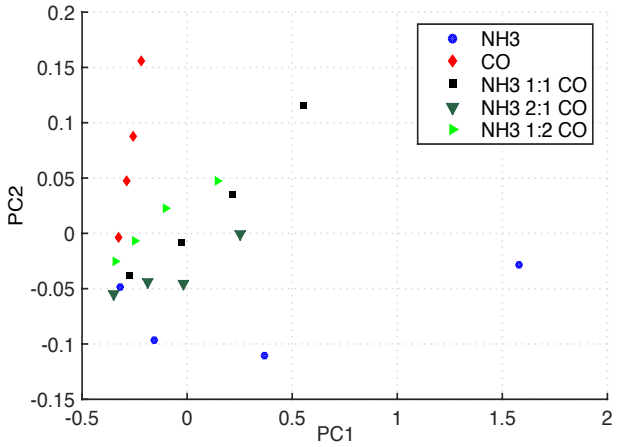

Figure 5.17: PCA plot for the a CNT sensor array functionalized with 1.5 nm of Au, 1.0 nm of Cr, 0.2 nm of Pd and a bare sensor under the exposure of NH_3, CO and three mixture between the two gases of ratios (1:1,1:2 and 2:1).

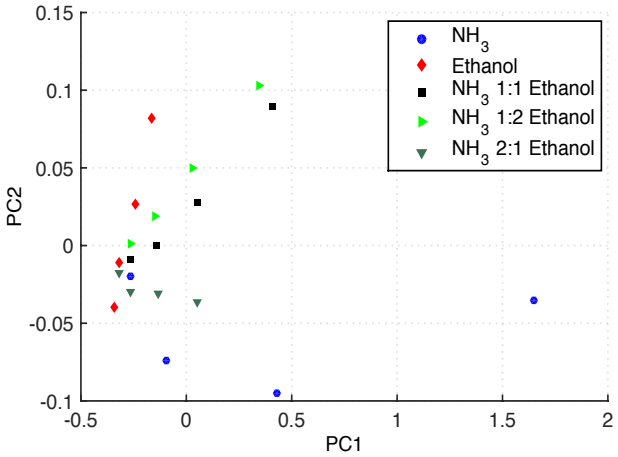

Figure 5.18: PCA plot for the a CNT sensor array functionalized with 1.5 nm of Au, 1.0 nm of Cr, 0.2 nm of Pd and a bare sensor under the exposure of NH_3, ethanol and three mixture between the two gases of ratios (1:1,1:2 and 2:1).

By achieving a separation between any two gases, the response towards a mixture of those two gases should lie in the plane between the data points of each gas separately. Such preliminary results indicate the possibility of identifying not only the type of the different gases in the mixture but their concentrations as well.

5.6.3 Sensor Array on Kapton

Full utilization of the CNT-based gas sensor arrays depends on the capability of fabricating such device on flexible substrates. Such a step is very essential towards realizing CNT-based gas sensor arrays in low cost applications. It is worth mentioning here, that the substrate and the electrodes in CNT-based gas sensor arrays introduced in the previous sections are the most expensive component of the total material cost. In addition to the sensor array fabricated on SiO_2/Si substrates, we fabricated CNT-based gas sensor array on Kapton substrates. As a regular procedure, we fabricated a sensor array, which consists only of bare CNT layers, to re-examine the stability of the resistance of the CNT network on Kapton as well. Taking a look at figure 5.19, we can notice that the PCA plot does not show any separation between the different test gases. The resistances of the different sensors are almost stable from one measurement to the other. The normalized response of the different sensors towards the different gases is rather low when compared to its rigid counterpart on SiO_2/Si. Note that, the overall fabrication process and characterization procedure remained largely unchanged, thereby leaving space for further optimization. We expect that such an optimization process will result in similar responses between the sensor arrays fabricated on the rigid and the flexible substrates.

We chose Au metal for functionalizing the fabricated CNT sensor array on Kapton, due to the fact that Au showed clear distinction between NH_3 and the other test gases in all the previous results. The PCA plot of the Au functionalized CNT-based gas sensor array shows a clear separation of NH_3 as illustrated in figure 5.20. Furthermore, the resistance of the different sensors remains almost the same from one measurement to the other. Such results in principle, shows the possibility of obtaining a selective CNT-based gas sensor array fabricated on flexible substrates. Nevertheless, further systematic investigation and optimization in the fabrication process still needs to be addressed.

5.7 Summary

We reported the complete development of a selective CNT-based gas sensor array fabricated on rigid as well as flexible substrates. We employed the principle component

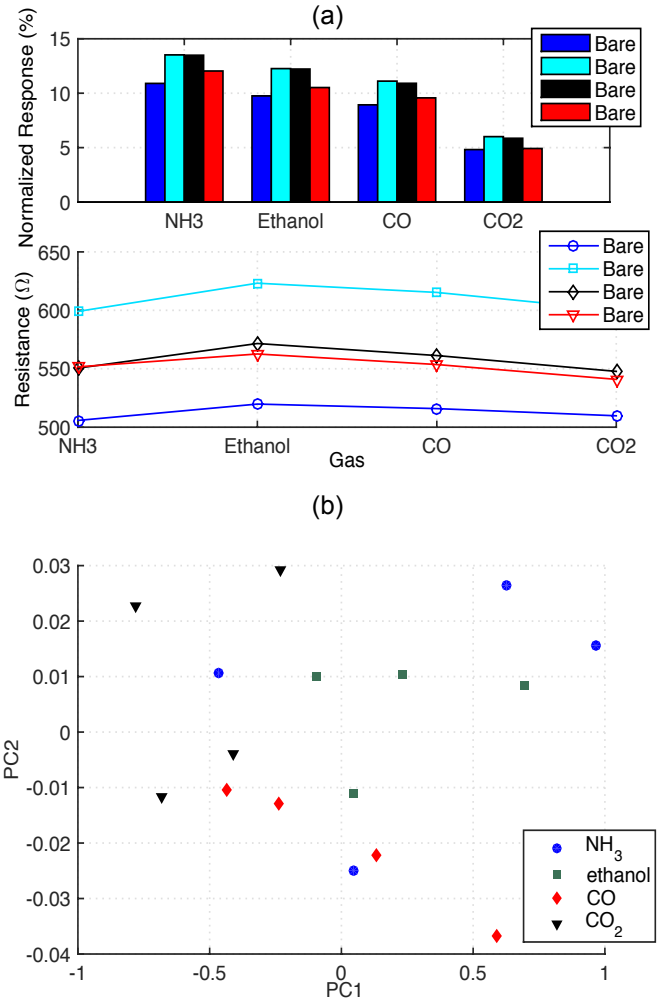

Figure 5.19: (a) The resistances of the individual sensors and their normalized response towards the four test gases (NH_3, ethanol, CO and CO_2) for bare sensor array fabricated on Kapton (b) The PCA plot for such CNT sensor array does not show any distinction between the different test gases.

analysis method for analyzing the response of such sensor array. Reaching the selective CNT-based gas sensor array with optimum combinations of the metallic NPs was done through a developed framework strategy. Such framework took advantage of the knowledge we gained in the last chapter regarding the performance of the CNT network functionalized with different metallic NPs. We adopted the concept of building and simulating CNT virtual sensor arrays depending on the data collected from sensors with different functionalization at different load. Such step played an important role in decreasing the development time.

In order to achieve a selective pattern in the PCA plot, we modified the spraying parameter to obtain a rather thicker layer of the CNT network. Such modification resulted in a

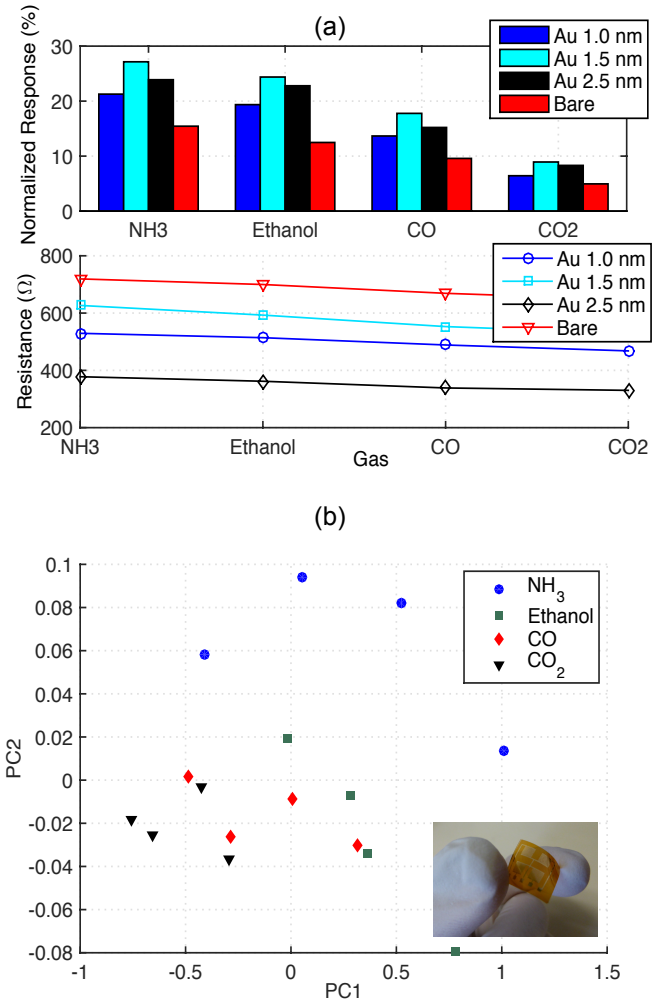

Figure 5.20: (a) The resistances of the individual sensors and their normalized response towards the four test gases (NH_3, ethanol, CO and CO_2) for sensor array fabricated on Kapton functionalized with different loads of Au (1.0 nm, 1.5 nm and 2.5 nm) (b) The PCA plot for such CNT-based gas sensor array.

small sacrifice in the sensitivity of the sensors. Nevertheless, the achieved sensitivity remains among the highest reported in literature. Taking into consideration the short exposure interval used which is only 100 s for all test gases. The best combination of the metallic functionalization was Au at a load of 1.5 nm, Cr at a load of 1.0 nm and Pd at a load of 0.2 nm. The fourth sensor was kept bare. Such combination resulted in a clear distinction between the four test gases (NH_3, ethanol, CO and CO_2) at an acceptable response and a stable film resistance.

We took the characterization of CNT-based sensor array one step further where we investigated its response towards a mixture of two gases simultaneously. The result showed that the data points of the mixture lie on the plane between the data points of the

each gas separately.

Finally, we showed the possibility of fabricating selective CNT sensor arrays on flexible substrates. We used Kapton foil as the substrate to demonstrate such feature. The fabricated CNT sensor array was functionalized with different loads of Au and it showed a clear distinction between NH_3 and the other three gases in the PCA plot.

Chapter 6

Impedance Spectroscopy Measurements

In order to fully exploit the full potential of CNT thin-films based gas sensor, a complete characterization of the performance of the sensor under different conditions is required. One very common characterization technique on gas sensors in general, yet rarely performed on CNT gas sensors, is the complex impedance characterization. In this chapter, we introduce a detailed investigation on the performance of CNT thin films and CNT networks based gas sensors using the complex impedance spectroscopy within a frequency range between 20 Hz and 20 MHz. We show that the frequency response of CNT thin-films is highly dependent on the resistance of the film, thus the film thickness. We characterized four CNT films with different film thicknesses. By modeling the circuit to an equivalent circuit, we can show the change that occur to both components of the impedance (Re(Z) and Im(Z)) with frequency. We investigate the effect of the operating temperature on the CNT thin-film and its effect on the frequency response. Due to the fact that the temperature directly affect the resistance of the film, varying the operating temperature resulted in a shift in the frequency response.

Incorporating such kind of characterization gives more insights and understanding of the CNT thin-films based gas sensors. we exposed the CNT sensors to two test gases (NH_3 and CO) with different concentrations. The equivalent resistance and capacitance of the CNT network under different gas concentration were extracted and fitted to a 1^{st} and 2^{nd} order models. By plotting the nyquist plot of the sensor under different gas concentrations as well as the behavior of the impedance components with frequency, we prove that any change that occurs to the film response is only dependent on the film impedance. The sensitivity of the sensors showed unusual behavior w.r.t the frequency. Such behavior might suggest a change in the sensing mechanism at certain frequencies. Finally, the feasibility of obtaining selective CNT gas sensors based on the sensor recovery characteristics for three different gases (NH_3, CO and ethanol) is demonstrated. We extracted the sensor response and recovery time and fitted the acquired data to the

logistic growth function for the former and to the exponential decaying function for the latter.

6.1 Complex Impedance Characterization Overview

Complex impedance characterization or often called impedance spectroscopy (IS) is a quite common technique used in analyzing and understanding the behavior of electrical systems, where the overall system behavior is determined by a number of strongly coupled processes, each proceeding at a different rates [72]. In devices such as chemical sensors or living cells, the properties of the electrode-material system are assumed to be time-invariant. The purpose of the complex impedance characterization is to determine these properties, their interrelations and their dependencies on other different controllable parameters (temperature, pressure, the applied current or voltage). One common and standard approach to measure the impedance is by applying a single-frequency electrical stimulus (a known voltage or current) at the interface (electrode-material) and measuring the phase shift and amplitude, or real and imaginary parts of the response. Several commercial instruments are available that perform that approach. The range of the frequency can be as low as 1mHz and reaches up to 2 MHz.

Researchers has applied such technique in investigating the properties of disordered solids as well as the dependence of their conductance on the frequency for a long time [122] [123] [124] [125] [126] [127]. The conductivity of such materials shows frequency independent behavior at low frequencies, till the characteristic frequency ω_o, afterwards the conductivity increases to the power of the frequency according to the power law equation shown in 6.1,

$$Re\{\sigma(\omega)\}\ \alpha\ \{\omega^s\} \tag{6.1}$$

Typical value of the exponent s is 0.8 [122]. Power law frequency dependent conductivity has been observed in a wide variety of disordered solids, including amorphous semiconductors, organic solids, and oxide glasses.

In general, complex impedance spectroscopy is a well-established technique always used to characterize gas sensors in different configurations [128]. Labidi et al [129] presented the ac characterization of WO_3 sensors under ethanol vapors. The sensing layer is modeled by a serial association of three parallel RC circuits. Through such model, they showed that grains and the grain boundaries are the main involvement in detecting ethanol vapor for these kind of sensors. Weimar et al [130] performed ac

measurement as well on tin oxide gas sensor. Performing these measurements lead them to detailed understanding of the sensing layer conduction mechanism. They showed as well enhancement in the sensitivity of the sensor and selectivity can be achieved by monitoring ac conductance for different gas components at specific frequencies.

Although the necessity of applying such characterization technique on CNT material and CNT based devices, it is rarely performed. The main focus of the reported literature was on the electrical behavior of the CNT layer at different frequencies, while other few studies investigated the same behavior but for CNT based gas sensors.

Kilbride et al [131] studied the electrical properties of two composite systems formed from a conjugated polymer poly(m-phenylenevinylene-co-2,5dioctyloxy-p-phenylenevinylene) (PmPV and a nonconjugated polymer PVA, both filled with various concentrations of multiwalled nanotubes. They showed a frequency independent conductivity (σ_o) up to a critical frequency ω_o, followed by a region of increasing conductivity. Similarly, Barrau et al [132] showed the same behavior for the conductivity with the frequency for CNTs-polyepoxy composites. Khattari et al [133] investigated the dielectric behavior of polymethyl methacrylate/multi-walled carbon nanocomposites (PMMA/MWCNTs) using IS technique. The study was performed in the frequency range 10-10^5 Hz in a temperature range 30-110 °C at different content of MWCNTs. They showed that the general behavior of the film impedance is similar to the impedance of RC circuit in parallel and this was explained to be due to the presence of charge polarization. The same group reported [134] similar behavior for CNT/ABS nanocomposites as well.

Another few studies focused on the characterization of CNT-based gas sensors. Varghese et al [44] studied the gas sensing behavior of both capacitance and resistance gas sensors employing MWCNTs. The cole-cole plots for both types of sensors showed semicircles, which is the behavior of parallel RC circuit. Hefaiedh et al. [70] presented a MWCNTs based gas sensor for the detection of volatile organic compounds. They performed impedance characterization for the fabricated sensors at a resistance value of the 4192 Ω. The film showed resistive behavior till 100 KHz. They demonstrated as well the possibility of obtaining selective sensors between different organic compounds based on the response time towards each compound.

In this chapter, we employ impedance spectroscopy to characterize CNT thin-films and CNT-based gas sensors with the range 20 Hz-2 MHz. The frequency behavior of CNT thin-films showed high dependence on the initial resistance of the film. We show that any change occur in the resistance of the film due to different operating

temperature or adsorption of gas results immediately in shift in the film cut-off frequency (f_c). Additionally, by analyzing the sensitivity of the CNT-based gas sensors with the frequency upon the exposure to NH_3 and CO, large variation in the response is observed. Finally, we show the possibility of achieving a selective CNT-based gas sensor that partially discriminate between NH_3, ethanol and CO, by extracting the recovery time (τ) for each gas at different frequencies.

6.2 Materials and Methods

6.2.1 Fabrication Process

Spray deposition of CNT films reported in this chapter is performed using an air-atomizing nozzle. For our automated spray system, an industrial air atomizing spray valve (Nordson EFD, USA) is used in combination with an overhead motion platform (Precision Valve and Automation, USA). The calibration of the spray parameters is based on an approach mentioned previously for the fabrication of the CNT thin-films and CNT-based gas sensors. High molecular weight cellulose derivative, sodium carboxymethyl cellulose (CMC), is used to dissolve CNTs in aqueous solution. The solution preparation method is the same as we mentioned in the last chapters. After preparing the solution with CNT and CMC it is sonicated using a probe sonicator for 20 minutes and then centrifuged for 90 minutes afterward it is ready for deposition.

Si wafer with 200 nm of thermally grown SiO_2 are used as substrates. An inter-digitated electrode structure (IDES), with 100 μm spacing, consisting of a 5nm thick Cr layer followed by a 40 nm Au layer is evaporated on top of the SiO_2. The aqueous CNT dispersion is spray deposited to form a transparent conductive film onto the IDES structure. Post-deposition treatment is required to remove the majority of dispersant. For this purpose samples are immersed in 4M HNO_3 solutions for > 12 hours and subsequently dried in air. Note that all steps involved in the CNT film fabrication are performed entirely in ambient conditions.

6.2.2 Characterization Procedure

Agilent E4980A precision LCR meter was used for the complex impedance characterization in the frequency range between 20 Hz and 2 MHz. The measurement procedure works as follow; we apply an input signal (current) at the required frequency and we measure the output voltage, with the help of the developed Labview program we can calculate

the different components of the impedance. Two different measurement protocols were performed for characterizing CNT thin-films and CNT-based gas sensors. The former protocol is performed by changing the frequency every 5 seconds and calculating the resistance and the reactance at each frequency. The latter is performed in four different stages, where at each stage we keep the gas concentration constant and we change the frequency after each exposure cycle. Each gas is measured at four concentration, hence the 4 different stages. Due the fact that one gas exposure cycle takes up to 1000 s, the latter protocol can last for almost 4 h for each gas concentration. Data modeling and data analysis is performed with the aid of an implemented Matlab code.

6.3 Complex Impedance Characterization Framework

We developed a certain framework for proceeding with the impedance characterization of the CNT layers. The working strategy is divided into two main steps as shown in fig. 6.1. The first step is characterizing the behavior of the CNT thin-film without any gas exposure. Such step includes fabricating CNT thin-films with different thicknesses as well as characterizing the performance of the film at different operating temperature as well. The aim from such step is to know in advance the behavior of the CNT network under different frequencies and to separate such behavior from the effect of the test gas, which will be involved in the following step. The second step is investigating the performance of the CNT based gas sensor under the exposure of the test gas within a certain frequency range. Before sweeping the frequency, we characterized CNT gas sensor at a single frequency in order to measure the normalized response due to the change in the reactance. It served also in building the equivalent circuit for the CNT network later on, since such step will show whether CNT sensors have capacitive or inductive response. The frequency is swept between 20 Hz-2 MHz, we monitored the change in Re(Z), Im(Z) as well as the normalized response with the frequency. By measuring such components, we can quantify the behavior of the CNT based gas sensors under different frequencies.

6.4 CNT Thin-Films Resistive Networks

Complex impedance characteristics are highly dependent on the resistance of the film. One main parameter that define the frequency dependence of the film is the fall off frequency (f_c), which is defined as the frequency where Re(Z) drops by 3 dB below the DC value in the log scale and corresponds to the maximum value of Im(Z). Figure 6.2 shows the frequency dependence of Re(Z) of four different films with resistances 100

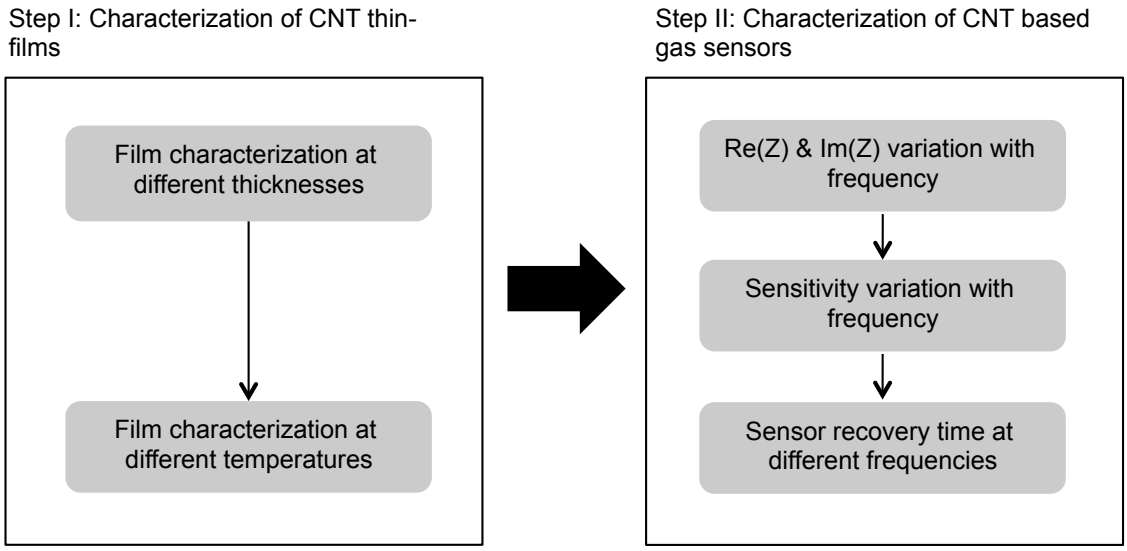

Figure 6.1: A chart shows the two steps for the complex impedance characterization framework

kΩ, 20 kΩ, 3.5 kΩ and 0.7 kΩ. By taking a closer look at the curve, we can notice that fc shifts towards lower values by increasing the resistance of the CNT film. The experimental data are modeled by an equivalent circuit, which consists of a resistor (R) and capacitor (C) in parallel. According to the 1st order model used we can write the Re(Z) and Im(Z) as follows,

$$Re(Z) = \frac{R}{1 + (\omega RC)^2} \tag{6.2}$$

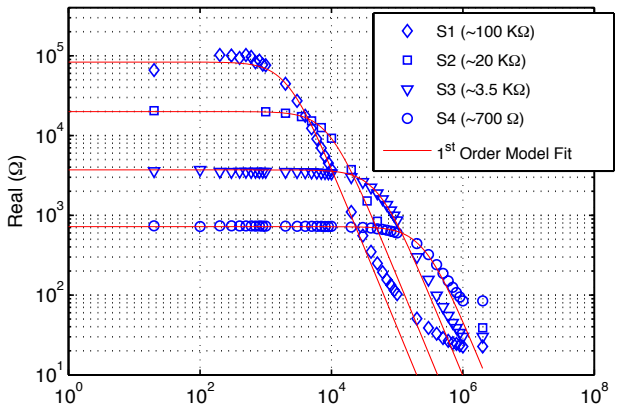

Figure 6.2: The relation between Re(Z) and frequency for different sensors with different resistances.

$$Im(Z) = \frac{R^2 \omega C}{1 + (\omega RC)^2} \tag{6.3}$$

therefore, we can deduct f_c to be,

$$f_c = \frac{1}{2\pi \sqrt{RC}} \tag{6.4}$$

We can notice that f_c is inversely proportional to both the resistance (R) and the capacitance (C) of the network. Using the intrinsic CNT networks, which is two third semiconducting and one third metallic, increasing the film thickness results in more dominance of the metallic nanotubes and increase in the number of junctions as well. The former results in decreasing the total resistance of the film while the latter results in increasing the total capacitance of the film. Taking into consideration the increase that occur to f_c by decreasing the film resistance, implies that the change that occur in the resistance by spraying thicker films is higher than the change that occur in the capacitance. Thus, the effect of the resistance is more dominant on the shifting that occurs to f_c. Furthermore, the dependence of the temperature on the complex impedance characteristics of the CNT network is investigated. Figure6.3 shows the Nyquist plot of a CNT network with an initial resistance $\sim$ 2 kΩ measured at temperatures of 25 °C, 40 °C, 60 °C, 80 °C and 100 °C. The increase in temperature results in semi-circles with smaller radii in the Nyquist plot. It results in a shift in f_c as well. This can be explained due to the effect of the temperature on the resistance of the film. The higher the temperature, the lower the resistance of the film, hence the shift in f_c.

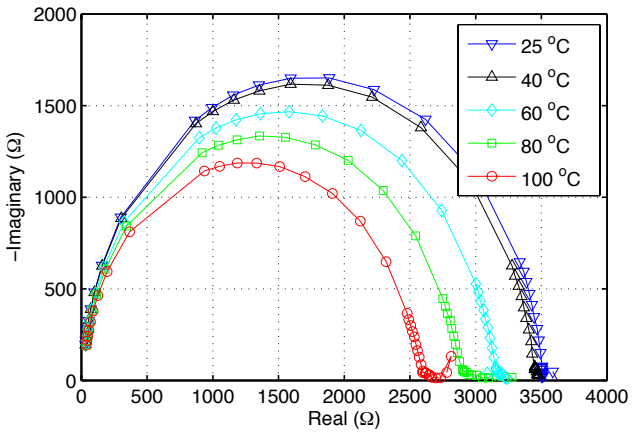

Figure 6.3: Nyquist plot for CNT thin-film at different temperatures in a frequency range between 20 Hz and 2 MHz.

6.5 CNT Thin-Films Based Gas Sensors

As a first step to investigate the behavior of the CNT based gas sensor with a frequency range, we characterized the sensor at single frequency. We choose an excitation signal with a frequency of 1 KHz. By introducing the frequency as a new parameter we can monitor not only the change in the resistance but the change in the reactance as well. Figure shows the result obtained from such characterization in (a), we obtain the normal behavior of the CNT gas sensor when exposed to different concentration of NH_3. In (b), the reactance of the sensor decreases upon gas exposure, this indicates a capacitive behavior of the CNT network. The main figure of merit used to evaluate the sensor performance is the normalized response, defined previously in equation 4.1. By plotting the normalized response due to the change in reactance (circle), we can achieve a sensor sensitivity up to 180% , which we consider as a remarkable value. The sensitivity due to the change in the resistance (square) was up to 50%, which is consistent to the values we reported in the previous chapters for the sensitivity of bare CNT-based gas sensor towards NH_3. After investigating the behavior of the CNT gas sensor at a certain frequency, we then swept the frequency from 20 Hz to 2 MHz and monitored the change in the real and imaginary components of the impedance. Figure 6.5 presents the Nyquist plot of CNT based gas sensors with an initial resistance of ~ 20 kΩ when exposed to different concentrations of NH3 (10 ppm, 25 ppm, 50 ppm, 100 ppm). Each data point corresponds to the final value of the resistance (R_f) at the end of the exposure cycle. The experimental data are modeled with the 1^st order system (red curve) mentioned earlier. Additionally, we modeled the experimental data also with an equivalent circuit, which includes a parallel connection of a resistor (R_1) and a capacitor (C_1) in series with another parallel connection of a resistor (R_2) and a capacitor (C_2). The second order system (black curve), models the resistance and the capacitance of the bundle as well as the junction connection of the CNTs. The value of the resistance is in general directly proportional to the concentration of NH_3 and that explains the increase in the semi circles radii in the Nyquist plot by increasing the concentration of the gas. As mentioned previously, the change in the film resistance corresponds immediately to a shift in the fall off frequency. Figure 6.7 shows the shift that occur to f_c with respect to Im(Z) (a) and Re(Z) (b). The fall off frequency shifts from 9.2 KHz in the case of 0 ppm concentration to 5.3 KHz in the case of 100 ppm concentration. The fall off frequency is equivalent to the maximum point in the Im(Z). This value is shifted by the same amount as Re(Z) by changing the concentration of the NH_3.

By plotting the normalized response, due to the change in the Re(Z) in that case, as

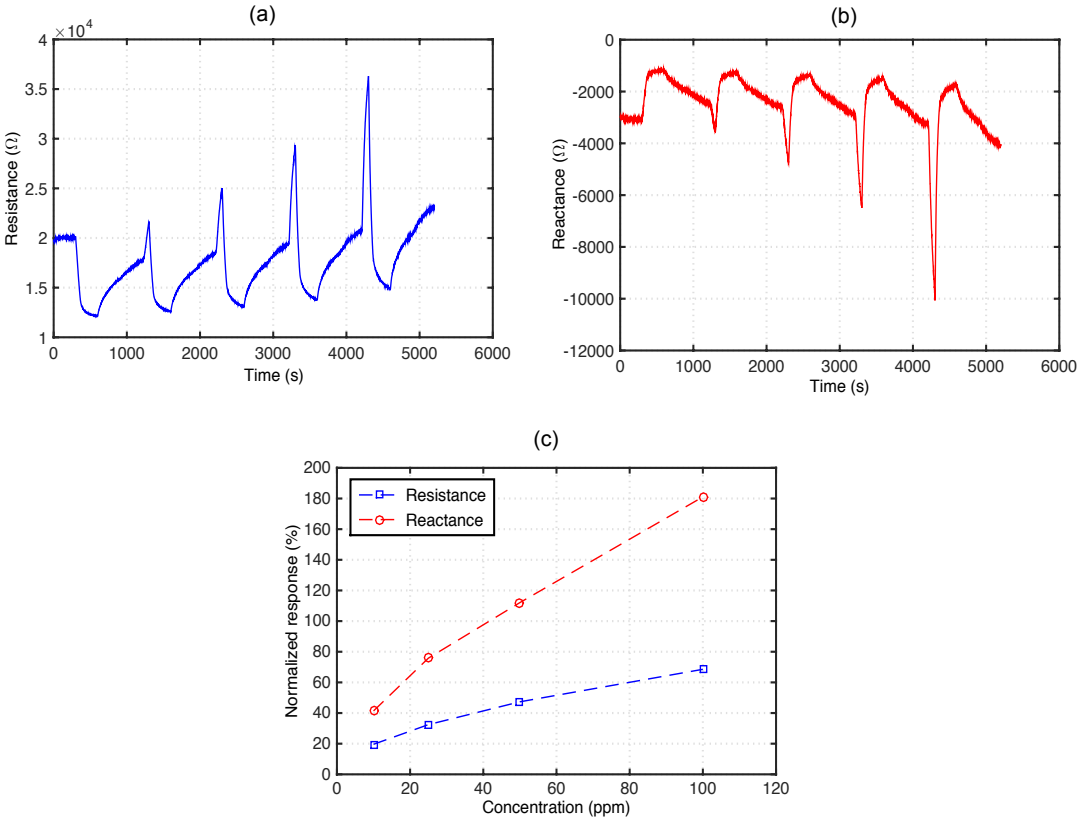

Figure 6.4: Characterization of the CNT gas sensor when exposed to different concentration of NH_3 at 1 KHz. (a) The change of resistance during the different exposure cycles. (b) The change in reactance during the different exposure cycles. (c) The sensitivity due the change in resistance (square) and due to the change in reactance (circle) with different concentrations of NH_3.

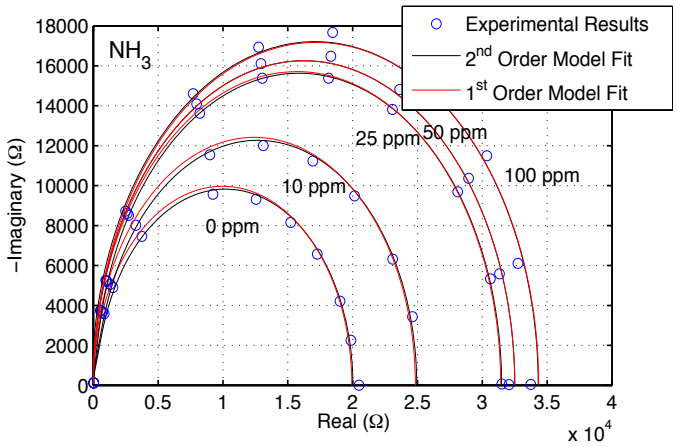

Figure 6.5: The relation between Im(Z) (a) and Re(Z) (b) with the frequency at different concentrations of NH_3.

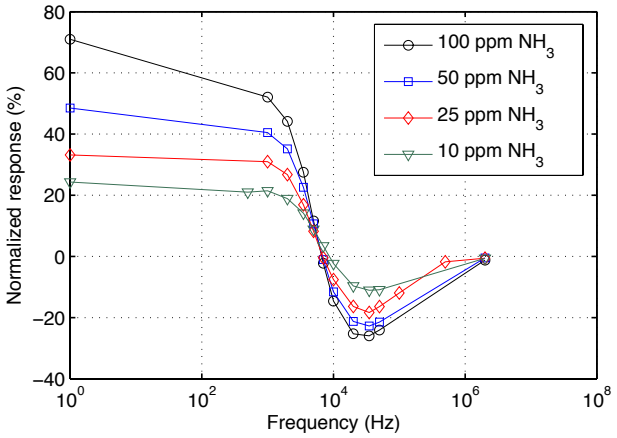

Figure 6.6: The relation between Im(Z) (a) and Re(Z) (b) with the frequency at different concentrations of NH_3.

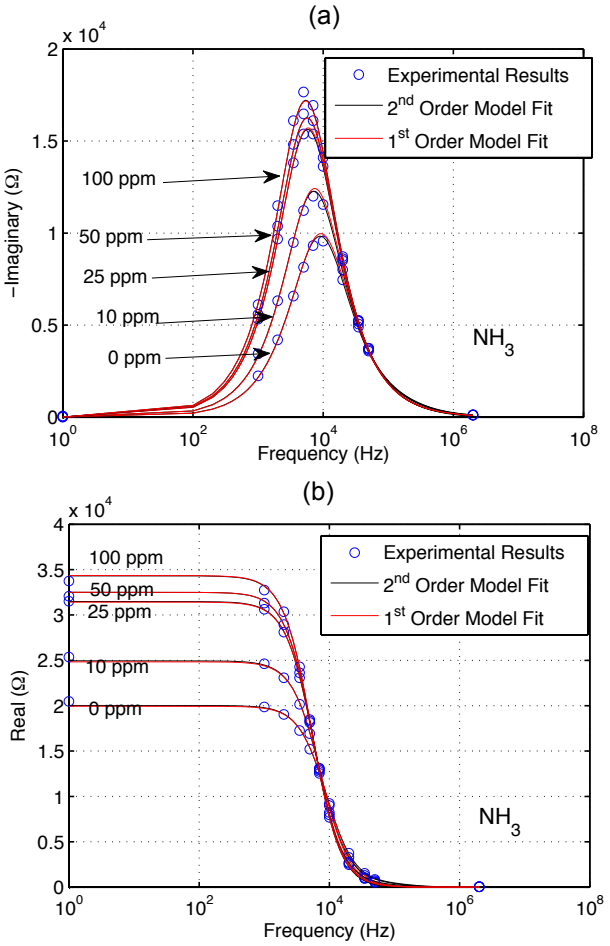

Figure 6.7: The relation between Im(Z) (a) and Re(Z) (b) with the frequency at different concentrations of NH_3.

shown in fig. 6.6 we can identify three critical frequencies which are 20 Hz, 7 KHz and 35 KHz. The first point corresponds to the sensor-normalized response at DC, which does not change till the frequency reaches 1 KHz. This shows the resistive behavior of the film till it reaches f_c. Afterwards the normalized response began to decrease dramatically. The second point when the normalized response is almost zero and this occurs at the same frequency for all concentrations. The third point is when the normalized response reaches its maximum in the negative part. This suggests that at a certain frequency range (7 KHz-35 KHz) the sensing mechanism of the CNT film is reversed towards NH_3. This frequency point is also the same for all gas concentrations. We hypothesize that these points are dependent on the resistance of the CNT network (film thickness) and not dependent on the gas exposure or its concentration. In order to prove this hypothesis, we setup two different experiments. The first one is characterizing the same sensor with a different gas. Thus, we exposed the CNT sensor to CO with concentrations of 5 ppm, 10 ppm , 25 ppm, 50 ppm. By taking a closer look at the results obtained shown in fig. 6.8, we can observe that the critical frequency points occurs again at 20 Hz, 7KHz and 35 KHz as well. It's worth mentioning here that the used equivalent circuit doesn't fit exactly at the high concentrations of CO. This could be due to the fact that the CNT sensitivity towards CO saturates faster than the case towards NH_3. Such saturation behavior is not included in the model used. More complicated equivalent circuit can include such behavior towards CO. The second experiment was exposing another CNT gas sensor, which has lower resistance ($\sim$ 1.5 kΩ), to the same concentrations of NH_3. The result obtained is illustrated in fig. 6.9. Increasing the film thickness results in increasing the number of metallic pathways. This explains the decrease that occurs in the sensitivity at 20 Hz. The critical frequency points are shifted to higher values when compared to the results obtained with the other sensor under the exposure of NH_3 and CO. These results validate our hypothesis that the frequency response of the CNT based gas sensor is not dependent on the concentration or the nature of the test gas but rather on the thickness and the resistance of the film itself. The shift that occurs in the frequency points can be also correlated to the shift that occurs to the f_c due to the change in the film thickness.

6.6 Sensor Response and Recovery Characteristics

Another criterion for characterizing CNT based gas sensors is by extracting the recovery and response times with different gases at different frequencies. This kind of characterization gives more insight on the speed of the sensor as well as its transient behavior [71]. Figure 6.10 shows the characteristic time constant for a CNT sensor, which has an initial resistance $\sim$ 2 kΩ, versus the frequency. The characteristic time constant is calculated by

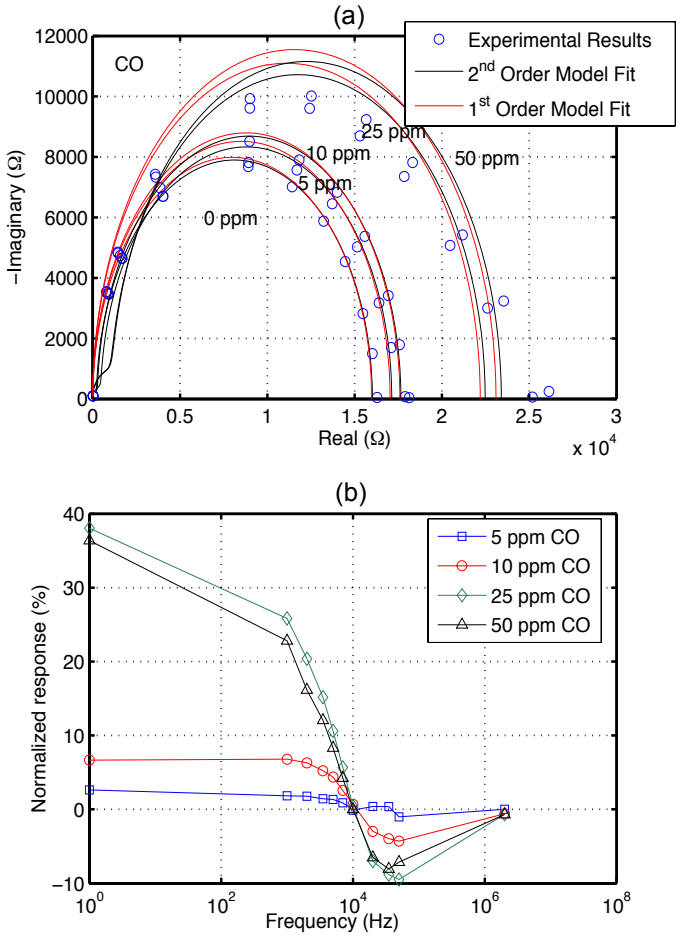

Figure 6.8: The relation between Im(Z) (a) and Re(Z) (b) with the frequency at different concentrations of NH_3.

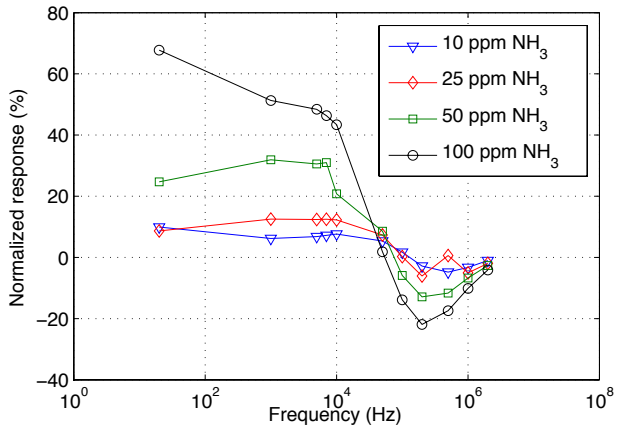

Figure 6.9: Plot of the extracted time constant (τ) with frequency for NH_3 (circle), CO (square) and ethanol (triangle).

fitting the data acquired during the passive recovery to the exponential decay function

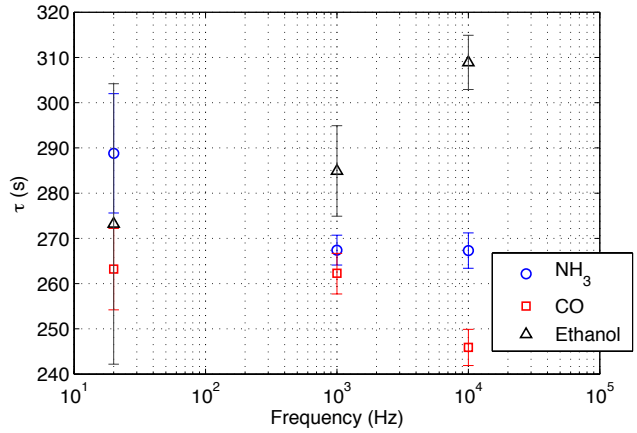

Figure 6.10: Plot of the extracted time constant (τ) with frequency for NH_3 (circle), CO (square) and ethanol (triangle) at three different frequencies 100 Hz, 1 KHz and 10 KHz.

shown below in equation 6.5,

$$f_{recovery}(t) = ae^{\frac{-t}{\tau}} + b \tag{6.5}$$

The concentration of the three test gases was kept at 50 ppm at the different frequencies. At 10 KHz, there is a clear difference in the recovery time of the sensor to the different gases. Although the results obtained show the possibility of gas selectivity at a certain frequency, the results is not reproducible. By repeating this type of characterization on another CNT sensor, which has a similar film resistance and produced with the same fabrication process. The results obtained are illustrated in fig. 6.11. This time at 10

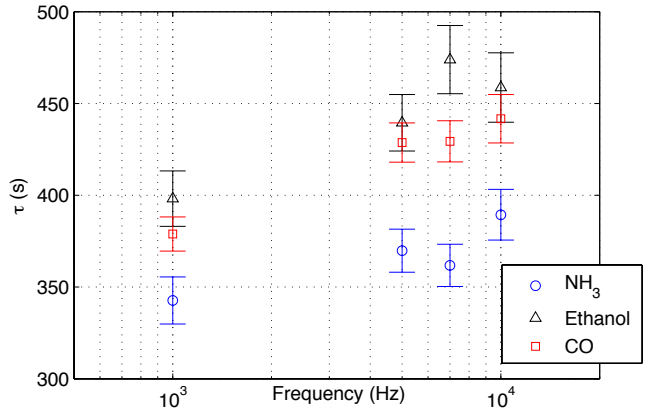

Figure 6.11: Plot of the extracted time constant (τ) with frequency for NH_3 (circle), CO (square) and ethanol (triangle) in a frequency range between 1kHz and 10 KHz.

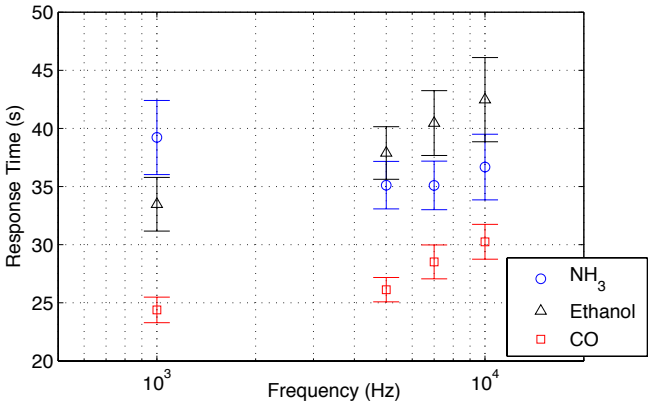

Figure 6.12: Plot of the extracted response time with frequency for NH_3 (circle), CO (square) and ethanol (triangle) in a frequency range between 1 KHz and 10 KHz.

KHz no clear distinction can be observed between the different gases, only NH_3 can be separated from the other two gases. Moreover, in fig 6.10, the recovery time from CO was the shortest while it was the longest with ethanol. In fig. 6.11, recovering from NH_3 was the fastest while the longest time was still needed to recover from ethanol at all frequencies. Such type of characterization is highly sensitive to the environment and the change in the ambient conditions. This could be the main reason for the change in the behavior from one sensor to the other. Similarly, we investigated the response time for CNT gas sensors at different frequencies. The data acquired during the 100 seconds of exposure are fitted to the logistic growth function defined below in equation 6.6,

$$f_{response}(t) = \frac{a}{1 + e^{\frac{-t}{\tau}}} + b \tag{6.6}$$

The results obtained are presented in fig. 6.12. The response time towards CO was the shortest and it was separated from NH_3 and ethanol at all frequencies, which gives the possibility of selecting CO by such type of characterization. By repeating the measurement, it was difficult to obtain the same result due to the same reason mentioned before, which is the high sensitivity of such type of characterization to the change in the environmental condition. Achieving selectivity based on the recovery or response time of the sensor to the different test gases is possible under the condition of guaranteeing the same ambient condition each time the measurement is held.

6.7 Summary

We reported on the full characterization of CNT thin-films and CNT based gas sensor using impedance spectroscopy within the range 20 Hz- 2MHz. The frequency response of CNT thin-films showed clear dependence on the film resistance, hence the film thickness. We presented as well the Nyquist plot for the CNT films under different temperatures, which varied from one temperature to the other due the change introduced in the resistance of the film under different temperatures. Under the exposure of different concentrations of NH_3, the normalized response of the CNT based gas sensor showed large variation with frequency. The same behavior is obtained when the CNT gas sensor is exposed to CO. We reported as well a remarkable change in the normalized response due the change in the reactance that reached 180 % when the sensor exposed to 100 ppm of NH_3. Finally, we showed the possibility of obtaining selective CNT based gas sensors between NH3, CO and ethanol, by extracting the recovery time (τ) for each gas at different frequencies.

Chapter 7

Conclusion and Outlook

In this thesis, we began by giving an overview on the gas sensors technology development in general. In that context, we highlighted the three common technologies employed for manufacturing gas sensors based on electrical variation, metal oxide semiconducting, polymers and carbon nanotubes. We compared between the three technologies based on a certain evaluation criteria, sensitivity, selectivity, response time, energy consumption, reversibility, adsorptive capacity and fabrication cost. We focused further on the CNT technology. We introduced different common techniques for depositing CNT thin-films, vacuum filtration, spin-coating, dip-coating and spray-coating. The comparison between the different techniques was performed according to the criteria, scalability, film-roughness, thickness control, substrate choice and material usage. In order to tackle the selectivity problem, we divided the common approaches for solving such a problem into two categories; fabrication approach and characterization approach. We defined the different methods that can be used in each approach. We compared as well between these different methods according to the criteria, accuracy, total cost, life time and practicality.

We demonstrated the fabrication of high quality CNT thin-films through a reliable, scalable and reproducible spray deposition technique. We investigated the effect of using two dispersive agents, CMC and SDS, in preparing CNT solution on the performance of the deposited layer. The fabricated CNT-thin films were spray deposited on glass as well as plastic substrates. Additionally, we introduced transfer printing process for depositing CNT thin-films on flexible substrates. We compared the performance of the CNT layer before and after he transfer printing process. We achieved similar quality in temrs of raman spectrum, electrical measurement, surface morphology and optical transmission measurements. Independent from the employed substrate or the deposition technique, we were able to report CNT thin-films with quality comparable to the state-of the-art reported in literature.

After optimizing the spray deposition technique for fabricating high performance CNT thin-films, we employed such technique for producing CNT-based gas sensors with exceptional as well as immediate response towards various test gases, NH_3, ethanol, CO and CO_2. We presented as well CNT-based gas sensors functionalized with metallic NPs. Metallic NPs functionalization alter the performance of the gas sensor towards the different gas analytes in a certain degree. This enhance the sensitivity of the gas sensor as well as enabling the differentiation between the different gases. Metallic Nps such as Au, Ag and Pd were deposited by thermal evaporation process where the evaporation rate, the adjusted load and the target substrate plays an important role in the size and the shape of the formed NPs. the We reported a sensitivity as high as 92 % for CNT-based gas sensor functionalized with 1.5 nm of Au under the exposure of 100 ppm of NH_3. Under the exposure of 5000 ppm of CO_2, CNT-based gas sensors functionalized with 0.5 nm of Pd reach sensitivity as high as 17%. We examined as well the interaction between the different types of NPs and the CNT layer. In that context, we investigated the changes occur to the optical properties of the CNT layer after the deposition of the metallic NPs. We showed that Au and Ag functionalization introduces SP on the CNT surface, where the frequency of the SP is dependent on the nominal thickness of the deposited metal as well as the size of the formed NP. Moreover, we showed the change occurs in the work function of the CNT layer upon the deposition of different loads of Au NPs.

The development of selective CNT-based gas sensor array on rigid and flexible substrates was successfully demonstrated. Different metal NPs functionalization was utilized to alter the performance of the different sensing element in the sensor array. The development process was based on a proposed strategy framework which take advantage of the knowledge gained by functionalizing single CNT-based gas sensors. The strategy relies on building and simulating virtual sensor arrays in order to decrease the total development time. The optimized CNT based gas sensor array composed of four sensing elements, where one is kept bare and the other three are functionalized with 1.5 nm of Au, 0.2 nm of Pd and 1.0 nm of Cr respectively. Such a combination was able to discriminate between NH_3, ethanol, CO and CO_2. Moreover, we showed the response of the CNT-based gas sensor array under the exposure of mixture of two gases, NH_3, ethanol and NH_3, CO. The response towards equal ratios of the two test gases lies almost in the middle between data points of each gas separately. Such preliminary results indicate the possibility of identifying not only the concentration of the mixture but also the concentration of the different gases in the mixture. By fabricating CNT-based as sensor array on flexible substrate (Kapton), where the sensing elements were functionalized with different loads of Au, we were able to differentiate between th NH_3 and the other 3 test gases.

Finally, we discussed the possibility of achieving selective behavior from the CNT-based gas sensors by characterizing the response towards different gases at different frequencies. In that context, we introduced complex impedance characterization technique, where we characterized CNT thin-films and CNT-based gas sensors in a frequency range 20Hz-2MHz. We show that the frequency response of CNT thin-films is highly dependent on the resistance of the film, thus the film thickness. Regarding CNT-based gas sensors, sensitivity showed an unusual behavior with frequency. Such behavior suggest a change in the sensing mechanism of the CNT layer at the different frequencies. we prove that any change occur in the sensor response is dependent on the initial impedance of the films rather than the nature of the test gas. Moreover, by extracting the recovery time for the gas sensor towards different test gases at different frequencies, we can categorize the different gases into pre-defined classes.

The performance of CNT thin-films produced in this work is acceptable to be utilized as transparent electrodes but in order to substitute the existing electrodes dominating the marker, ITO, higher performance should be achieved in terms of sheet resistance, optical transmission and surface roughness. Employing thicker plastic substrates that is capable to sustain higher temperatures could result in better performance in the transfer printing process. Additionally, by depending on structured PDMS in the transfer printing process patterned structure of CNT layers could be achieved.

Commercialization of CNT-based gas sensors still requires further development and optimization in the realization of the sensor array. For instance, employing sputtering or e-beam deposition techniques for the functionalization process could result in more stable devices and better control of the NPs sizes can be achieved. We presented CNT-based gas sensor array which consists of four different sensing elements. Nevertheless, realizing sensor arrays based on higher number of sensing elements (8,16,32) will result in better discrimination between the various test gases. Studying the interaction between each kind of metal and the CNT layer is essential to enhance the selectivty of the whole sensor array. Employing other kind of functionalization (polymers) besides metallic NPs could result better discrimination as well.

Complex impedance characterization is an essential step to understand the behavior of the CNT thin-films not only the CNT- based gas sensor. In that context, performing such advanced characterization of different kinds of CNTs could deliver better interpretation for the performance of each kind under different conditions. Further investigation on the behavior of the CNT-based gas sensors under different frequency ranges paves the way for development and evaluation of different approaches for selectivity enhancement. One

possibility is characterizing CNT-based gas sensors at very low frequency range (μHz), such step will give more insights on the transient behavior of the gas sensor. Utilizing more complex equivalent circuits could result as well in better understanding of the sensing mechanism of the CNT layer under different frequencies. Figure 7.1 summarizes our vision for the future outlook of the work presented here.

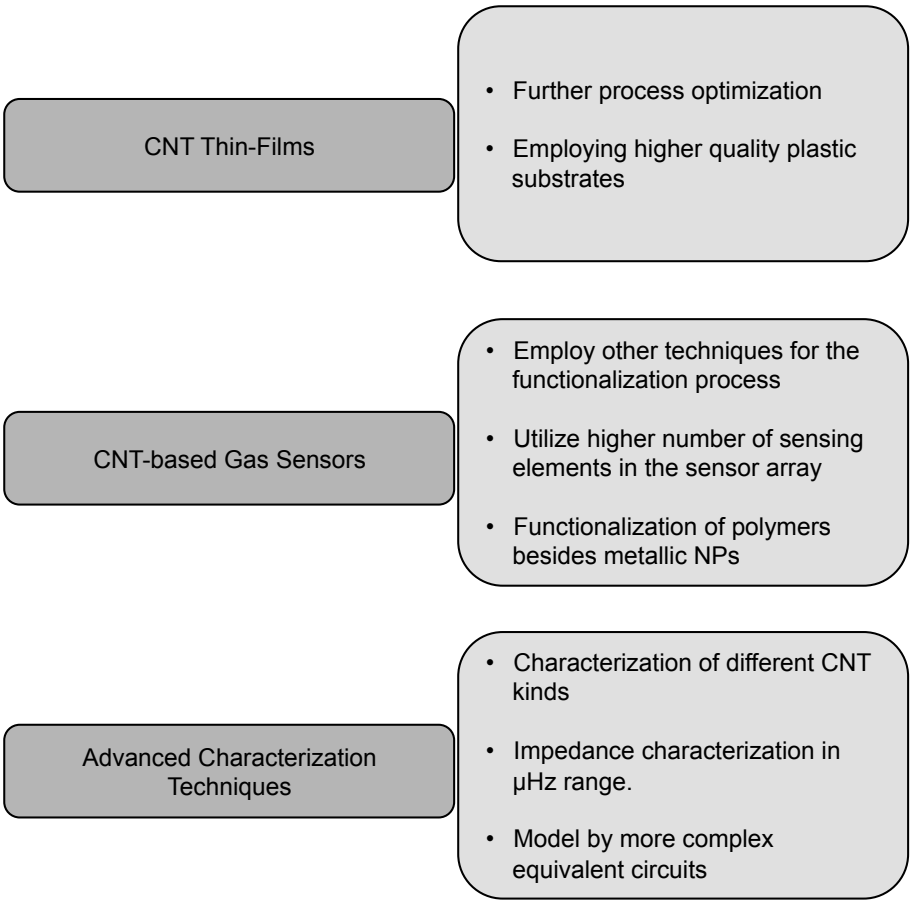

Figure 7.1: Chart summarizes the future outlook for the work presented here.

Appendix A

Transfer Process Recipe

A.1 Materials/Equipments

CNT thin-film deposited on glass (original substrate), plastic substrate (target substrate), Polydimethylsiloxane (PDMS), DI-Water, glass rod, hot Plate

A.2 Substrate Preparation

- 2.5x2.5 cm plastic substrate (e.g. PVC, PET, Kapton).
- Clean substrate with Isopropanol for 10 min in ultrasonic cleaner.
- Substrate is placed in 1wt% 3-Aminopropyltriethoxysilan (APTES) solution in isoprpanol for 15 minutes. APTES solution should be stirred for couple of minutes before placing the substrates.

A.3 Process Steps

- Cut PDMS into pieces of size nearly equal to the plastic substrate
- Stick PDMS piece very carefully over the CNT thin-film deposited on glass. (Glass rod could be gently used to remove any bubble at the interface)
- Place the stack of glass substrate and PDMS in DI-Water for 1 min.
- Take out the sample from water and carefully remove the PDMS layer which now contains the CNT thin-film.
- Slowly blow the PDMS layer with nitrogen to dry it.
- Adjust the hot plate at 65° C

- Carefully stick the PDMS layer on the plastic substrate. Make sure of removing all the bubbles that might occur.
- Place the stack of the PDMS layer and the target substrate on the hot plate, then covered witha small glass baker and leave it on the hot plate for 5 minutes.
- Remove the PDMS layer very carefully from the substrate.
- Film is transferred to plastic and ready for doping or any further processing steps.

Appendix B

Gas Measurement Setup

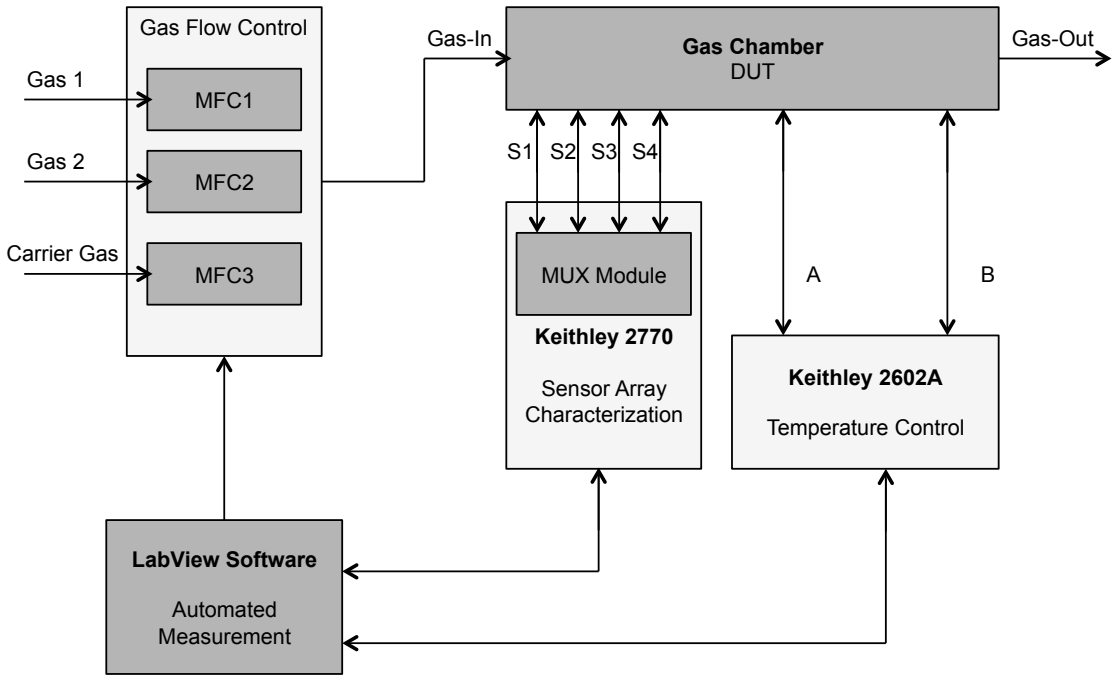

Figure B.1: A chart summarizes the measurement setup utilized to characterize gas sensors developed in this work

Appendix C

Principle Component Analysis

PCA is the expression of the data in a different basis in order to allow representing them graphically. This means searching for a transformation matrix $\mathbf{P}$ which converts the $m \times n$ data matrix $\mathbf{X}$ according to equation C.1

$$\mathbf{Y} = \mathbf{PX} \tag{C.1}$$

$\mathbf{Y}$ is the data matrix $\mathbf{X}$ expressed in the new basis. The new basis are set of orthogonal vectors that represent the data along the dimensions where it is most widely spread. In order to achieve this requirement we have to calculate the $\mathbf{C}$ which is obtained by equation C.2

$$\mathbf{C} = \frac{1}{n}\mathbf{A}\mathbf{A}^T \tag{C.2}$$

For an $m \times n$ matrix A in which m is the number of taken measurements and n is the number of samples (in our case the number of sensors), the covariance matrix is a symmetrical matrix with the dimension n. Its diagonal elements represent the variances of each column of $\mathbf{A}$, which display how wide the values are spread. The non diagonal elements stand for the covariances of the single columns (here sensors) between each other, showing how their values correlate. In order to maximize the variance for each dimension of the new basis and minimize the correlation, the non-diagonal elements of $\mathbf{C}_Y$ should be zero, which means that the covariance matrix $\mathbf{C}_Y$ has to be a diagonal matrix as shown in equation C.3.

$$\mathbf{C}_Y = \mathbf{D} \tag{C.3}$$

We use equation C.2 to relate the conversion matrix $\mathbf{C}_Y$ to the raw data $\mathbf{X}$.

$$\begin{aligned}
\mathbf{C}_Y &= \frac{1}{n}\mathbf{Y}\mathbf{Y}^T \\
&= \frac{1}{n}(\mathbf{P}\mathbf{X})(\mathbf{P}\mathbf{X})^T \\
&= \frac{1}{n}\mathbf{P}\mathbf{X}\mathbf{X}^T\mathbf{P}^T \\
&= \mathbf{P}(\frac{1}{n}\mathbf{X}\mathbf{X}^T\mathbf{P})\mathbf{X}^T \\
\mathbf{C}_Y &= \mathbf{P}\mathbf{C}_X\mathbf{X}^T
\end{aligned} \tag{C.4}$$

In order to have a matrix $\mathbf{P}$ in a way that $\mathbf{C}_Y$ is a diagonal matrix, $\mathbf{C}_X$should be an eigenvector matrix, where the n Eigen vectors are the principle components. The variances of the raw data in the new basis is expressed by the eigenvalues of the matrix $\mathbf{C}_X$, so to select only the principle components with the biggest variance, their eigenvalues have to be arranged in decreasing order. These are the steps to determine the transformation matrix $\mathbf{P}$ and the data can now be transformed in the new basis according to equation C.1. Reduction of dimensions is performed by eliminating the principle components with the least influence (i.e the smallest variance).

Bibliography

[1] J. W. Gardner and P. N. Bartlett, "A brief history of electronic noses," *Sensors and Actuators B: Chemical*, vol. 18, no. 1-3, pp. 210–211, Mar. 1994. [Online]. Available: http://www.sciencedirect.com/science/article/pii/0925400594870853

[2] ——, *Sensors and Sensory Systems for an Electronic Nose*, J. W. Gardner and P. N. Bartlett, Eds. Dordrecht: Springer Netherlands, 1992. [Online]. Available: http://link.springer.com/10.1007/978-94-015-7985-8

[3] T. Aishima, "Aroma discrimination by pattern recognition analysis of responses from semiconductor gas sensor array," *Journal of Agricultural and Food Chemistry*, vol. 39, no. 4, pp. 752–756, Apr. 1991. [Online]. Available: http://dx.doi.org/10.1021/jf00004a027

[4] J. Gardner, H. Shurmer, and T. Tan, "Application of an electronic nose to the discrimination of coffees," *Sensors and Actuators B: Chemical*, vol. 6, no. 1-3, pp. 71–75, Jan. 1992. [Online]. Available: http://www.sciencedirect.com/science/article/pii/092540059280033T

[5] M. Egashira, Y. Shimizu, and Y. Takao, "Trimethylamine sensor based on semiconductive metal oxides for detection of fish freshness," *Sensors and Actuators B: Chemical*, vol. 1, no. 1-6, pp. 108–112, Jan. 1990. [Online]. Available: http://www.sciencedirect.com/science/article/pii/092540059080182Y

[6] F. Winquist, E. G. Hornsten, H. Sundgren, and I. Lundstrom, "Performance of an electronic nose for quality estimation of ground meat," *Measurement Science and Technology*, vol. 4, no. 12, pp. 1493–1500, Dec. 1993. [Online]. Available: http://iopscience.iop.org/0957-0233/4/12/029

[7] W. Tsujita, A. Yoshino, H. Ishida, and T. Moriizumi, "Gas sensor network for air-pollution monitoring," *Sensors and Actuators B: Chemical*, vol. 110, no. 2, pp. 304–311, Oct. 2005. [Online]. Available: http://www.sciencedirect.com/science/article/pii/S0925400505001899

[8] A. Lloyd Spetz, L. Uneus, H. Svenningstorp, P. Tobias, L.-G. Ekedahl, O. Larsson, A. Gï¿½ras, S. Savage, C. Harris, P. Mï¿½rtensson, R. Wigren, P. Salomonsson, B. Hï¿½ggendahl, P. Ljung, M. Mattsson, and I. Lundstrï¿½m, "SiC Based Field Effect Gas Sensors for Industrial Applications," *physica status solidi (a)*, vol. 185, no. 1, pp. 15–25, May 2001. [Online]. Available: http://doi.wiley.com/10.1002/1521-396X%28200105%29185%3A1%3C15%3A%%3AAID-PSSA15%3E3.0.CO%3B2-7

[9] R. A. Potyrailo, C. Surman, S. Go, Y. Lee, T. Sivavec, and W. G. Morris, "Development of radio–frequency identification sensors based on organic electronic sensing materials for selective detection of toxic vapors," *Journal of Applied Physics*, vol. 106, no. 12, p. 124902, Dec. 2009. [Online]. Available: http://scitation.aip.org/content/aip/journal/jap/106/12/10.1063/1.3247069

[10] M. Utriainen, E. Kaerpaenoja, and H. Paakkanen, "Combining miniaturized ion mobility spectrometer and metal oxide gas sensor for the fast detection of toxic chemical vapors," *Sensors and Actuators B: Chemical*, vol. 93, no. 1-3, pp. 17–24, Aug. 2003. [Online]. Available: http://www.sciencedirect.com/science/article/pii/S092540050300337X

[11] L. Marques, U. Nunes, and A. T. de Almeida, "Olfaction–based mobile robot navigation," *Thin Solid Films*, vol. 418, no. 1, pp. 51–58, Oct. 2002. [Online]. Available: http://www.sciencedirect.com/science/article/pii/S004060900200593X

[12] B. Crone, A. Dodabalapur, A. Gelperin, L. Torsi, H. E. Katz, A. J. Lovinger, and Z. Bao, "Electronic sensing of vapors with organic transistors," *Applied Physics Letters*, vol. 78, no. 15, p. 2229, Apr. 2001. [Online]. Available: http://scitation.aip.org/content/aip/journal/apl/78/15/10.1063/1.1360785

[13] D. R. Kauffman and A. Star, "Carbon nanotube gas and vapor sensors." *Angewandte Chemie (International ed. in English)*, vol. 47, no. 35, pp. 6550–70, Jan. 2008. [Online]. Available: http://www.ncbi.nlm.nih.gov/pubmed/18642264

[14] Q. Cao and J. a. Rogers, "Ultrathin Films of Single–Walled Carbon Nanotubes for Electronics and Sensors: A Review of Fundamental and Applied Aspects," *Advanced Materials*, vol. 21, no. 1, pp. 29–53, Jan. 2009. [Online]. Available: http://doi.wiley.com/10.1002/adma.200801995

[15] L. Hu, D. S. Hecht, and G. Gruener, "Carbon nanotube thin films: fabrication, properties, and applications." *Chemical reviews*, vol. 110, no. 10, pp. 5790–844, Oct. 2010. [Online]. Available: http://dx.doi.org/10.1021/cr9002962

[16] S. R. Forrest, "The path to ubiquitous and low–cost organic electronic appliances on plastic." *Nature*, vol. 428, no. 6986, pp. 911–8, Apr. 2004. [Online]. Available: http://dx.doi.org/10.1038/nature02498

[17] S. R. Forrest and M. E. Thompson, "Introduction : Organic Electronics and Optoelectronics," *Chemical Reviews*, vol. 107, no. 4, pp. 1985–1987, 2007.

[18] R. Arsat, M. Breedon, M. Shafiei, P. Spizziri, S. Gilje, R. Kaner, K. Kalantar-zadeh, and W. Wlodarski, "Graphene–like nano–sheets for surface acoustic wave gas sensor applications," *Chemical Physics Letters*, vol. 467, no. 4-6, pp. 344–347, Jan. 2009. [Online]. Available: http://www.sciencedirect.com/science/article/pii/S0009261408015376

[19] G. SCHMERA and L. B. KISH, "FLUCTUATION-ENHANCED GAS SENSING BY SURFACE ACOUSTIC WAVE DEVICES," *Fluctuation and Noise Letters*, vol. 02, no. 02, pp. L117–L123, Jun. 2002. [Online]. Available: http://www.worldscientific.com/doi/abs/10.1142/S0219477502000695?journalCode=fnl

[20] S. Terry, J. Jerman, and J. Angell, "A gas chromatographic air analyzer fabricated on a silicon wafer," *IEEE Transactions on Electron Devices*, vol. 26, no. 12, pp. 1880–1886, Dec. 1979. [Online]. Available: http://ieeexplore.ieee.org/lpdocs/epic03/wrapper.htm?arnumber=1480369

[21] M. C. Bowman and M. Beroza, "Gas chromatographic detector for simultaneous sensing of phosphorus- and sulfur-containing compounds by flame photometry," *Analytical Chemistry*, vol. 40, no. 10, pp. 1448–1452, Aug. 1968. [Online]. Available: http://dx.doi.org/10.1021/ac60266a012

[22] L. Feng, C. J. Musto, and K. S. Suslick, "A simple and highly sensitive colorimetric detection method for gaseous formaldehyde." *Journal of the American Chemical Society*, vol. 132, no. 12, pp. 4046–7, Mar. 2010. [Online]. Available: http://dx.doi.org/10.1021/ja910366p

[23] N. A. Rakow and K. S. Suslick, "A colorimetric sensor array for odour visualization." *Nature*, vol. 406, no. 6797, pp. 710–3, Aug. 2000. [Online]. Available: http://dx.doi.org/10.1038/35021028

[24] G. F. Fine, L. M. Cavanagh, A. Afonja, and R. Binions, "Metal oxide semi–conductor gas sensors in environmental monitoring." *Sensors*

(Basel, Switzerland), vol. 10, no. 6, pp. 5469–502, Jan. 2010. [Online]. Available: http://www.pubmedcentral.nih.gov/articlerender.fcgi?artid=3247717&tool=pmcentrez&rendertype=abstract

[25] N. Barsan, D. Koziej, and U. Weimar, "Metal oxide–based gas sensor research: How to?" *Sensors and Actuators B: Chemical*, vol. 121, no. 1, pp. 18–35, Jan. 2007. [Online]. Available: http://linkinghub.elsevier.com/retrieve/pii/S0925400506006204

[26] G. Korotcenkov, "Metal oxides for solid–state gas sensors: What determines our choice?" *Materials Science and Engineering: B*, vol. 139, no. 1, pp. 1–23, Apr. 2007. [Online]. Available: http://linkinghub.elsevier.com/retrieve/pii/S0921510707000700

[27] T. Seiyama, A. Kato, K. Fujiishi, and M. Nagatani, "A New Detector for Gaseous Components Using Semiconductive Thin Films," *Analytical Chemistry*, vol. 34, no. 11, pp. 1502–1503, 1962.

[28] E. Kanazawa, G. Sakai, K. Shimanoe, Y. Kanmura, Y. Teraoka, N. Miura, and N. Yamazoe, "Metal oxide semiconductor N2O sensor for medical use," *Sensors and Actuators B: Chemical*, vol. 77, no. 1-2, pp. 72–77, Jun. 2001. [Online]. Available: http://www.sciencedirect.com/science/article/pii/S092540050100675X

[29] N. Y. A, G. Sakai, and K. Shimanoe, "Oxide semiconductor gas sensors," *Catalysis Surveys from Asia*, vol. 7, no. 1, pp. 63–75, 2003.

[30] X. Liu, S. Cheng, H. Liu, S. Hu, D. Zhang, and H. Ning, "A survey on gas sensing technology." *Sensors*, vol. 12, no. 7, pp. 9635–65, Jan. 2012. [Online]. Available: http://www.mdpi.com/1424-8220/12/7/9635/htm

[31] W. J. Moon, J. I. H. Yu, and G. M. Choi, "Selective Gas Detection of SnO 2 –TiO 2 Gas Sensors," *Journal of Electroceramics*, vol. 13, pp. 707–713, 2004.

[32] S. M. Kanan, O. M. El-Kadri, I. A. Abu-Yousef, and M. C. Kanan, "Semiconducting metal oxide based sensors for selective gas pollutant detection." *Sensors (Basel, Switzerland)*, vol. 9, no. 10, pp. 8158–96, Jan. 2009. [Online]. Available: http://www.mdpi.com/1424-8220/9/10/8158/htm

[33] B. M and U. Diebold, "The surface and materials science of tin oxide," *Progress in Surface Science*, vol. 79, no. 2-4, pp. 47–154, 2005. [Online]. Available: http://www.sciencedirect.com/science/article/pii/S007968160500050X

[34] Dong Hyun Yun, Chul Han Kwon, Hyung–Ki Hong, Seung-Ryeol Kim, Kyuchung Lee, Ho Geun Song, and Ji Eon Kim, "Highly sensitive and selective ammonia gas sensor," in *Proceedings of International Solid State Sensors and Actuators Conference (Transducers '97)*, vol. 2. IEEE, 1997, pp. 959–962. [Online]. Available: http://ieeexplore.ieee.org/lpdocs/epic03/wrapper.htm?arnumber=635262

[35] K. T. Ng, F. Boussaid, and A. Bermak, "A CMOS Single–Chip Gas Recognition Circuit for Metal Oxide Gas Sensor Arrays," *IEEE Transactions on Circuits and Systems I: Regular Papers*, vol. 58, no. 7, pp. 1569–1580, Jul. 2011. [Online]. Available: http://ieeexplore.ieee.org/lpdocs/epic03/wrapper.htm?arnumber=5766791

[36] H. Bai and G. Shi, "Gas Sensors Based on Conducting Polymers," *Sensors*, vol. 7, pp. 267–307, 2007.

[37] T. Zhang, S. Mubeen, N. V. Myung, and M. a. Deshusses, "Recent progress in carbon nanotube-based gas sensors." *Nanotechnology*, vol. 19, no. 33, p. 332001, Aug. 2008. [Online]. Available: http://www.ncbi.nlm.nih.gov/pubmed/21730614

[38] Y. Liu, M. Chen, M. Mohebbi, M. Wang, and M. R. Dokmeci, "The effect of sequence length on DNA decorated CNT gas sensors," in *2011 16th International Solid-State Sensors, Actuators and Microsystems Conference*. IEEE, Jun. 2011, pp. 2156–2159. [Online]. Available: http://ieeexplore.ieee.org/lpdocs/epic03/wrapper.htm?arnumber=5969345

[39] F. Schedin, A. K. Geim, S. V. Morozov, E. W. Hill, P. Blake, M. I. Katsnelson, and K. S. Novoselov, "Detection of individual gas molecules adsorbed on graphene." *Nature materials*, vol. 6, no. 9, pp. 652–5, Sep. 2007. [Online]. Available: http://dx.doi.org/10.1038/nmat1967

[40] S. IIjima, "Helical microtubules of graphitic carbon," *Nature*, vol. 354, pp. 56–58, 1991.

[41] D. Zhang, K. Ryu, X. Liu, E. Polikarpov, J. Ly, M. E. Tompson, and C. Zhou, "Transparent, conductive, and flexible carbon nanotube films and their application in organic light–emitting diodes." *Nano letters*, vol. 6, no. 9, pp. 1880–6, Sep. 2006. [Online]. Available: http://www.ncbi.nlm.nih.gov/pubmed/16967995

[42] J. Kong, "Nanotube Molecular Wires as Chemical Sensors," *Science*, vol. 287, no. 5453, pp. 622–625, Jan. 2000. [Online]. Available: http://www.sciencemag.org/content/287/5453/622.abstract

[43] Y. Wang, Z. Zhou, Z. Yang, X. Chen, D. Xu, and Y. Zhang, "Gas sensors based on deposited single-walled carbon nanotube networks for DMMP detection." *Nanotechnology*, vol. 20, no. 34, p. 345502, Aug. 2009. [Online]. Available: http://stacks.iop.org/0957-4484/20/i=34/a=345502

[44] O. Varghese, P. Kichambre, D. Gong, K. Ong, E. Dickey, and C. Grimes, "Gas sensing characteristics of multi–wall carbon nanotubes," *Sensors and Actuators B: Chemical*, vol. 81, no. 1, pp. 32–41, Dec. 2001. [Online]. Available: http://linkinghub.elsevier.com/retrieve/pii/S0925400501009236

[45] Y. Wang, N. Hu, Z. Zhou, D. Xu, Z. Wang, Z. Yang, H. Wei, E. S.-W. Kong, and Y. Zhang, "Single-walled carbon nanotube/cobalt phthalocyanine derivative hybrid material: preparation, characterization and its gas sensing properties," *Journal of Materials Chemistry*, vol. 21, no. 11, p. 3779, Mar. 2011. [Online]. Available: http://pubs.rsc.org/en/content/articlehtml/2011/jm/c0jm03567j

[46] Y.-T. Jang, S.-I. Moon, J.-H. Ahn, Y.-H. Lee, and B.-K. Ju, "A simple approach in fabricating chemical sensor using laterally grown multi-walled carbon nanotubes," *Sensors and Actuators B: Chemical*, vol. 99, no. 1, pp. 118–122, Apr. 2004. [Online]. Available: http://www.sciencedirect.com/science/article/pii/S0925400503008293

[47] M. Arab, F. Berger, F. Picaud, C. Ramseyer, J. Glory, and M. Mayne-L'Hermite, "Direct growth of the multi-walled carbon nanotubes as a tool to detect ammonia at room temperature," *Chemical Physics Letters*, vol. 433, no. 1-3, pp. 175–181, Dec. 2006. [Online]. Available: http://www.sciencedirect.com/science/article/pii/S0009261406015338

[48] R. Martel, T. Schmidt, H. R. Shea, T. Hertel, and P. Avouris, "Single- and multi-wall carbon nanotube field-effect transistors," *Applied Physics Letters*, vol. 73, no. 17, p. 2447, 1998. [Online]. Available: http://link.aip.org/link/APPLAB/v73/i17/p2447/s1&Agg=doi

[49] J. Li, Y. Lu, Q. Ye, M. Cinke, J. Han, and M. Meyyappan, "Carbon Nanotube Sensors for Gas and Organic Vapor Detection," *Nano Letters*, vol. 3, no. 7, pp. 929–933, Jul. 2003. [Online]. Available: http://pubs.acs.org/doi/abs/10.1021/nl034220x

[50] J. K. Abraham, B. Philip, A. Witchurch, V. K. Varadan, and C. C. Reddy, "A compact wireless gas sensor using a carbon nanotube/PMMA thin film chemiresistor," *Smart Materials and Structures*, vol. 13, no. 5, pp. 1045–1049, Oct. 2004. [Online]. Available: http://stacks.iop.org/0964-1726/13/i=5/a=010

[51] M. Penza, G. Cassano, R. Rossi, M. Alvisi, a. Rizzo, M. a. Signore, T. Dikonimos, E. Serra, and R. Giorgi, "Enhancement of sensitivity in gas chemiresistors based on carbon nanotube surface functionalized with noble metal (Au, Pt) nanoclusters," *Applied Physics Letters*, vol. 90, no. 17, p. 173123, 2007. [Online]. Available: http://link.aip.org/link/APPLAB/v90/i17/p173123/s1&Agg=doi

[52] J. Mäklin, T. Mustonen, N. Halonen, G. Tóth, K. Kordás, J. Vähäkangas, H. Moilanen, A. Kukovecz, Z. Kónya, H. Haspel, Z. Gingl, P. Heszler, R. Vajtai, and P. M. Ajayan, "Inkjet printed resistive and chemical–FET carbon nanotube gas sensors," *physica status solidi (b)*, vol. 245, no. 10, pp. 2335–2338, Oct. 2008. [Online]. Available: http://doi.wiley.com/10.1002/pssb.200879580

[53] T. Helbling, C. Hierold, L. Durrer, C. Roman, R. Pohle, and M. Fleischer, "Suspended and non-suspended carbon nanotube transistors for NO2 sensing – A qualitative comparison," *physica status solidi (b)*, vol. 245, no. 10, pp. 2326–2330, Oct. 2008. [Online]. Available: http://doi.wiley.com/10.1002/pssb.200879599

[54] Y. Zhou, L. Hu, and G. Gruener, "A method of printing carbon nanotube thin films," *Applied Physics Letters*, vol. 88, no. 12, p. 123109, Mar. 2006. [Online]. Available: http://scitation.aip.org/content/aip/journal/apl/88/12/10.1063/1.2187945

[55] ——, "A method of printing carbon nanotube thin films," *Applied Physics Letters*, vol. 88, no. 12, p. 123109, 2006. [Online]. Available: http://link.aip.org/link/APPLAB/v88/i12/p123109/s1&Agg=doi

[56] E. Y. Jang, T. J. Kang, H. W. Im, D. W. Kim, and Y. H. Kim, "Single–walled carbon-nanotube networks on large-area glass substrate by the dip–coating method." *Small (Weinheim an der Bergstrasse, Germany)*, vol. 4, no. 12, pp. 2255–61, Dec. 2008. [Online]. Available: http://www.ncbi.nlm.nih.gov/pubmed/19016494

[57] Y. Song, G. Kim, H. Choi, H. Jeong, K. Kim, C.-M. Yang, S. Lim, K. An, K. Jung, and Y. Lee, "Fabrication of Carbon Nanotube Field Emitters Using a Dip-Coating Method," *Chemical Vapor Deposition*, vol. 12, no. 6, pp. 375–379, Jun. 2006. [Online]. Available: http://doi.wiley.com/10.1002/cvde.200506442

[58] M. A. Meitl, Y. Zhou, A. Gaur, S. Jeon, M. L. Usrey, M. S. Strano, and J. A. Rogers, "Solution Casting and Transfer Printing Single–Walled Carbon Nanotube Films," *Nano Letters*, vol. 4, no. 9, pp. 1643–1647, Sep. 2004. [Online]. Available: http://dx.doi.org/10.1021/nl0491935

[59] R. C. Tenent, T. M. Barnes, J. D. Bergeson, A. J. Ferguson, B. To, L. M. Gedvilas, M. J. Heben, and J. L. Blackburn, "Ultrasmooth, Large-Area, High-Uniformity, Conductive Transparent Single–Walled–Carbon–Nanotube Films for Photovoltaics Produced by Ultrasonic Spraying," *Advanced Materials*, vol. 21, no. 31, pp. 3210–3216, Aug. 2009. [Online]. Available: http://doi.wiley.com/10.1002/adma.200803551

[60] A. Abdellah, K. S. Virdi, R. Meier, M. Döblinger, P. Müller-Buschbaum, C. Scheu, P. Lugli, and G. Scarpa, "Successive Spray Deposition of P3HT/PCBM Organic Photoactive Layers: Material Composition and Device Characteristics," *Advanced Functional Materials*, pp. n/a–n/a, Jun. 2012. [Online]. Available: http://doi.wiley.com/10.1002/adfm.201200548

[61] A. Abdellah, B. Fabel, P. Lugli, and G. Scarpa, "Spray deposition of organic semiconducting thin–films: Towards the fabrication of arbitrary shaped organic electronic devices," *Organic Electronics*, vol. 11, no. 6, pp. 1031–1038, Jun. 2010. [Online]. Available: http://linkinghub.elsevier.com/retrieve/pii/S1566119910000844

[62] M. Penza, R. Rossi, M. Alvisi, G. Cassano, M. Signore, E. Serra, and R. Giorgi, "Pt- and Pd–nanoclusters functionalized carbon nanotubes networked films for sub-ppm gas sensors," *Sensors and Actuators B: Chemical*, vol. 135, no. 1, pp. 289–297, Dec. 2008. [Online]. Available: http://linkinghub.elsevier.com/retrieve/pii/S0925400508005820

[63] M. Penza, R. Rossi, M. Alvisi, G. Cassano, and E. Serra, "Functional characterization of carbon nanotube networked films functionalized with tuned loading of Au nanoclusters for gas sensing applications," *Sensors and Actuators B: Chemical*, vol. 140, no. 1, pp. 176–184, Jun. 2009. [Online]. Available: http://linkinghub.elsevier.com/retrieve/pii/S0925400509003293

[64] M. Penza, R. Rossi, M. Alvisi, D. Suriano, and E. Serra, "Pt–modified carbon nanotube networked layers for enhanced gas microsensors," *Thin Solid Films*, vol. 520, no. 3, pp. 959–965, Nov. 2011. [Online]. Available: http://linkinghub.elsevier.com/retrieve/pii/S0040609011010194

[65] M. Penza, R. Rossi, M. Alvisi, M. Signore, G. Cassano, D. Dimaio, R. Pentassuglia, E. Piscopiello, E. Serra, and M. Falconieri, "Characterization of metal-modified and vertically–aligned carbon nanotube films for functionally enhanced gas sensor applications," *Thin Solid Films*, vol. 517, no. 22, pp. 6211–6216, Sep. 2009. [Online]. Available: http://linkinghub.elsevier.com/retrieve/pii/S0040609009007329

[66] M. Scarselli, L. Camilli, P. Castrucci, F. Nanni, S. Del Gobbo, E. Gautron, S. Lefrant, and M. De Crescenzi, "In situ formation of noble metal nanoparticles on multiwalled carbon nanotubes and its implication in metal–nanotube interactions," *Carbon*, vol. 50, no. 3, pp. 875–884, Mar. 2012. [Online]. Available: http://linkinghub.elsevier.com/retrieve/pii/S0008622311008037

[67] D. Gingery and P. Bühlmann, "Formation of gold nanoparticles on multiwalled carbon nanotubes by thermal evaporation," *Carbon*, vol. 46, no. 14, pp. 1966–1972, Nov. 2008. [Online]. Available: http://linkinghub.elsevier.com/retrieve/pii/S0008622308004144

[68] S. Mubeen, J.-H. Lim, A. Srirangarajan, A. Mulchandani, M. a. Deshusses, and N. V. Myung, "Gas Sensing Mechanism of Gold Nanoparticles Decorated Single–Walled Carbon Nanotubes," *Electroanalysis*, vol. 23, no. 11, pp. 2687–2692, Nov. 2011. [Online]. Available: http://doi.wiley.com/10.1002/elan.201100299

[69] P. Qi, O. Vermesh, M. Grecu, A. Javey, Q. Wang, H. Dai, S. Peng, and K. J. Cho, "Toward Large Arrays of Multiplex Functionalized Carbon Nanotube Sensors for Highly Sensitive and Selective Molecular Detection," *Nano Letters*, vol. 3, no. 3, pp. 347–351, Mar. 2003. [Online]. Available: http://dx.doi.org/10.1021/nl034010k

[70] I. Hafaiedh, W. Elleuch, P. Clement, E. Llobet, and A. Abdelghani, "Multi–walled carbon nanotubes for volatile organic compound detection," *Sensors and Actuators B: Chemical*, vol. 182, pp. 344–350, Jun. 2013. [Online]. Available: http://linkinghub.elsevier.com/retrieve/pii/S0925400513003018

[71] A. Abdellah, A. Abdelhalim, M. Horn, G. Scarpa, and P. Lugli, "Scalable Spray Deposition Process for High-Performance Carbon Nanotube Gas Sensors," *IEEE Transactions On Nanotechnology*, vol. 12, no. 2, pp. 174–181, 2013.

[72] J. R. M. Evgenij Barsoukov, *Wiley: Impedance Spectroscopy: Theory, Experiment, and Applications, 2nd Edition*, 2005. [Online]. Available: http://eu.wiley.com/WileyCDA/WileyTitle/productCd-0471647497.html

[73] J. a. Misewich, R. Martel, P. Avouris, J. C. Tsang, S. Heinze, and J. Tersoff, "Electrically induced optical emission from a carbon nanotube FET." *Science (New York, N.Y.)*, vol. 300, no. 5620, pp. 783–6, May 2003. [Online]. Available: http://www.ncbi.nlm.nih.gov/pubmed/12730598

[74] P. Bondavalli, P. Legagneux, and D. Pribat, "Sensors and Actuators B : Chemical Carbon nanotubes based transistors as gas sensors : State of the art and critical review," *Sensors And Actuators*, vol. 140, pp. 304–318, 2009.

[75] E. S. Snow, P. M. Campbell, M. G. Ancona, and J. P. Novak, "High-mobility carbon–nanotube thin-film transistors on a polymeric substrate," *Applied Physics Letters*, vol. 86, no. 3, p. 033105, 2005. [Online]. Available: http://link.aip.org/link/APPLAB/v86/i3/p033105/s1&Agg=doi

[76] A. Javey, J. Guo, D. B. Farmer, Q. Wang, D. Wang, R. G. Gordon, M. Lundstrom, and H. Dai, "Carbon Nanotube Field-Effect Transistors with Integrated Ohmic Contacts and High–κ Gate Dielectrics," *Nano Letters*, vol. 4, no. 3, pp. 447–450, Mar. 2004. [Online]. Available: http://pubs.acs.org/doi/abs/10.1021/nl035185x

[77] Y.-M. Chien, F. Lefevre, I. Shih, and R. Izquierdo, "A solution processed top emission OLED with transparent carbon nanotube electrodes." *Nanotechnology*, vol. 21, no. 13, p. 134020, Apr. 2010. [Online]. Available: http://www.ncbi.nlm.nih.gov/pubmed/20208120

[78] V. Scardaci, R. Coull, and J. N. Coleman, "Very thin transparent, conductive carbon nanotube films on flexible substrates," *Applied Physics Letters*, vol. 97, no. 2, p. 023114, 2010. [Online]. Available: http://link.aip.org/link/APPLAB/v97/i2/p023114/s1&Agg=doi

[79] S. Kim, J. Yim, X. Wang, D. D. Bradley, S. Lee, and J. C. DeMello, "Spin– and Spray–Deposited Single–Walled Carbon-Nanotube Electrodes for Organic Solar Cells," *Advanced Functional Materials*, vol. 3, pp. n/a–n/a, Jun. 2010. [Online]. Available: http://doi.wiley.com/10.1002/adfm.200902369

[80] B. Chandra, H. Park, A. Maarouf, G. J. Martyna, and G. S. Tulevski, "Carbon nanotube thin film transistors on flexible substrates," *Applied Physics Letters*, vol. 99, no. 7, p. 072110, 2011. [Online]. Available: http://link.aip.org/link/APPLAB/v99/i7/p072110/s1&Agg=doi

[81] Q. Cao, H.-s. Kim, N. Pimparkar, J. P. Kulkarni, C. Wang, M. Shim, K. Roy, M. a. Alam, and J. a. Rogers, "Medium–scale carbon nanotube thin-film integrated

circuits on flexible plastic substrates." *Nature*, vol. 454, no. 7203, pp. 495–500, Jul. 2008. [Online]. Available: http://www.ncbi.nlm.nih.gov/pubmed/18650920

[82] Q. Liu, T. Fujigaya, H.-M. Cheng, and N. Nakashima, "Free–standing highly conductive transparent ultrathin single–walled carbon nanotube films." *Journal of the American Chemical Society*, vol. 132, no. 46, pp. 16 581–6, Nov. 2010. [Online]. Available: http://www.ncbi.nlm.nih.gov/pubmed/21028804

[83] K. Yurekli, C. A. Mitchell, and R. Krishnamoorti, "Small-angle neutron scattering from surfactant-assisted aqueous dispersions of carbon nanotubes." *Journal of the American Chemical Society*, vol. 126, no. 32, pp. 9902–3, Aug. 2004. [Online]. Available: http://dx.doi.org/10.1021/ja047451u

[84] H.-C. Su, C.-H. Chen, Y.-C. Chen, D.-J. Yao, H. Chen, Y.-C. Chang, and T.-R. Yew, "Improving the adhesion of carbon nanotubes to a substrate using microwave treatment," *Carbon*, vol. 48, no. 3, pp. 805–812, Mar. 2010. [Online]. Available: http://linkinghub.elsevier.com/retrieve/pii/S0008622309007052

[85] H. Liu, D. Takagi, S. Chiashi, and Y. Homma, "Transfer and alignment of random single-walled carbon nanotube films by contact printing." *ACS nano*, vol. 4, no. 2, pp. 933–8, Feb. 2010. [Online]. Available: http://www.ncbi.nlm.nih.gov/pubmed/20104866

[86] A. Mata, A. J. Fleischman, and S. Roy, "Characterization of polydimethylsiloxane (PDMS) properties for biomedical micro/nanosystems." *Biomedical microdevices*, vol. 7, no. 4, pp. 281–93, Dec. 2005. [Online]. Available: http://www.ncbi.nlm.nih.gov/pubmed/16404506

[87] L. Hu, D. S. Hecht, and G. Gruener, "Percolation in Transparent and Conducting Carbon Nanotube Networks," *Nano Letters*, vol. 4, no. 12, pp. 2513–2517, Dec. 2004. [Online]. Available: http://dx.doi.org/10.1021/nl048435y

[88] a. C. Ferrari, J. C. Meyer, V. Scardaci, C. Casiraghi, M. Lazzeri, F. Mauri, S. Piscanec, D. Jiang, K. S. Novoselov, S. Roth, and a. K. Geim, "Raman Spectrum of Graphene and Graphene Layers," *Physical Review Letters*, vol. 97, no. 18, p. 187401, Oct. 2006. [Online]. Available: http://link.aps.org/doi/10.1103/PhysRevLett.97.187401

[89] Z. H. Ni, T. Yu, Y. H. Lu, Y. Y. Wang, Y. P. Feng, and Z. X. Shen, "Uniaxial Strain on Graphene : Raman Spectroscopy Study and Band–Gap Opening," *ACS nano*, vol. 2, no. 11, pp. 2301–2305, 2008.

[90] S. De, P. J. King, M. Lotya, A. O'Neill, E. M. Doherty, Y. Hernandez, G. S. Duesberg, and J. N. Coleman, "Flexible, transparent, conducting films of randomly stacked graphene from surfactant–stabilized, oxide-free graphene dispersions." *Small (Weinheim an der Bergstrasse, Germany)*, vol. 6, no. 3, pp. 458–64, Feb. 2010. [Online]. Available: http://www.ncbi.nlm.nih.gov/pubmed/19859943

[91] S. Hyun, Y.-b. Park, and K. H. Yoon, "Rheological and mechanical properties of surface modified multi–walled carbon nanotube–filled PET composite," *Composites Science and Technology*, vol. 67, pp. 3434–3441, 2007.

[92] J. P. Novak, E. S. Snow, E. J. Houser, D. Park, J. L. Stepnowski, and R. A. McGill, "Nerve agent detection using networks of single-walled carbon nanotubes," *Applied Physics Letters*, vol. 83, no. 19, p. 4026, Nov. 2003. [Online]. Available: http://scitation.aip.org/content/aip/journal/apl/83/19/10.1063/1.1626265

[93] L. Valentini, I. Armentano, J. M. Kenny, C. Cantalini, L. Lozzi, and S. Santucci, "Sensors for sub–ppm NO[sub 2] gas detection based on carbon nanotube thin films," *Applied Physics Letters*, vol. 82, no. 6, p. 961, Feb. 2003. [Online]. Available: http://scitation.aip.org/content/aip/journal/apl/82/6/10.1063/1.1545166

[94] Q. Zhao, M. Buongiorno Nardelli, W. Lu, and J. Bernholc, "Carbon nanotube–metal cluster composites: a new road to chemical sensors?" *Nano letters*, vol. 5, no. 5, pp. 847–51, May 2005. [Online]. Available: http://www.ncbi.nlm.nih.gov/pubmed/15884882

[95] K. H. An, S. Y. Jeong, H. R. Hwang, and Y. H. Lee, "Enhanced Sensitivity of a Gas Sensor Incorporating Single-Walled Carbon Nanotube–Polypyrrole Nanocomposites," *Advanced Materials*, vol. 16, no. 12, pp. 1005–1009, Jun. 2004. [Online]. Available: http://doi.wiley.com/10.1002/adma.200306176

[96] Z. Zanolli, R. Leghrib, A. Felten, J.-J. Pireaux, E. Llobet, and J.-C. Charlier, "Gas sensing with Au–decorated carbon nanotubes." *ACS nano*, vol. 5, no. 6, pp. 4592–9, Jun. 2011. [Online]. Available: http://www.ncbi.nlm.nih.gov/pubmed/21553864

[97] B.-K. Kim, N. Park, P. S. Na, H.-M. So, J.-J. Kim, H. Kim, K.-J. Kong, H. Chang, B.-H. Ryu, Y. Choi, and J.-O. Lee, "The effect of metal cluster coatings on carbon nanotubes," *Nanotechnology*, vol. 17, no. 2, pp. 496–500, Jan. 2006. [Online]. Available: http://stacks.iop.org/0957-4484/17/i=2/a=025?key=crossref.c37f9b1d328658fc80cd40a13dc29f12

[98] D. R. Kauffman, D. C. Sorescu, D. P. Schofield, B. L. Allen, K. D. Jordan, and A. Star, "Understanding the Sensor Response of Metal–decorated Carbon Nanotubes," *Nano*, pp. 958–963, 2010.

[99] D. R. Kauffman and A. Star, "Chemically Induced Potential Barriers at the Carbon Nanotube Metal Nanoparticle Interface," *Nano letters*, vol. 7, 2007.

[100] A. Serrano, O. Rodriguez de la Fuente, and M. a. Garcia, "Extended and localized surface plasmons in annealed Au films on glass substrates," *Journal of Applied Physics*, vol. 108, no. 7, p. 074303, 2010. [Online]. Available: http://link.aip.org/link/JAPIAU/v108/i7/p074303/s1&Agg=doi

[101] H. Sun, M. Yu, G. Wang, X. Sun, and J. Lian, "Temperature–Dependent Morphology Evolution and Surface Plasmon Absorption of Ultrathin Gold Island Films," *The Journal of Physical Chemistry C*, vol. 116, no. 16, pp. 9000–9008, Apr. 2012. [Online]. Available: http://pubs.acs.org/doi/abs/10.1021/jp300260h

[102] T. Takahashi, K. Tsunoda, H. Yajima, and T. Ishii, "Dispersion and Purification of Single–Wall Carbon Nanotubes Using Carboxymethylcellulose," *Japanese Journal of Applied Physics*, vol. 43, no. 6A, pp. 3636–3639, Jun. 2004. [Online]. Available: http://jjap.jsap.jp/link?JJAP/43/3636/

[103] S. K. Sharma and S. J., "Hillock Formation, Hole Growth and Agglomeration in Thin Silver Films," *Thin Solid Films*, vol. 65, pp. 339–350, 1980.

[104] S.-J. Hwang, J.-H. Lee, C.-O. Jeong, and Y.-C. Joo, "Effect of film thickness and annealing temperature on hillock distributions in pure Al films," *Scripta Materialia*, vol. 56, no. 1, pp. 17–20, Jan. 2007. [Online]. Available: http://linkinghub.elsevier.com/retrieve/pii/S135964620600666X

[105] V. Robbiano, A. Abdellah, L. Santarelli, A. Falco, S. El-Molla, L. V. Titova, D. N. Purschke, F. A. Hegmann, F. Cacialli, and P. Lugli, "Analysis of sprayed Carbon nanotube films on rigid and flexible substrates," in *IEEE Nanotechnology*, 2014, pp. 650–654. [Online]. Available: http://ieeexplore.ieee.org/xpls/icp.jsp?arnumber=6968021&tag=1

[106] A. Abdellah, S. Member, A. Yaqub, C. Ferrari, B. Fabel, P. Lugli, and G. Scarpa, "Spray Deposition of Highly Uniform CNT Films and Their Application in Gas Sensing," *IEEE NANO*, pp. 1118–1123, 2011.

[107] N. Peng, Q. Zhang, C. L. Chow, O. K. Tan, and N. Marzari, "Sensing mechanisms for carbon nanotube based NH3 gas detection." *Nano letters*, vol. 9, no. 4, pp. 1626–30, Apr. 2009. [Online]. Available: http://dx.doi.org/10.1021/nl803930w

[108] V. Lordi, N. Yao, and J. Wei, "Method for Supporting Platinum on Single–Walled Carbon Nanotubes for a Selective Hydrogenation Catalyst," *Chemistry of Materials*, vol. 13, no. 3, pp. 733–737, Mar. 2001. [Online]. Available: http://pubs.acs.org/doi/abs/10.1021/cm000210a

[109] A. Bilic, J. R. Reimers, N. S. Hush, and J. Hafner, "Adsorption of ammonia on the gold (111) surface," *The Journal of Chemical Physics*, vol. 116, no. 20, p. 8981, 2002. [Online]. Available: http://link.aip.org/link/JCPSA6/v116/i20/p8981/s1&Agg=doi

[110] A. Corma and H. Garcia, "Supported gold nanoparticles as catalysts for organic reactions." *Chemical Society reviews*, vol. 37, no. 9, pp. 2096–126, Sep. 2008. [Online]. Available: http://www.ncbi.nlm.nih.gov/pubmed/18762848

[111] A. A. Tomchenko, G. P. Harmer, B. T. Marquis, and J. W. Allen, "Semiconducting metal oxide sensor array for the selective detection of combustion gases," *Sensors and Actuators B: Chemical*, vol. 93, no. 1-3, pp. 126–134, Aug. 2003. [Online]. Available: http://www.sciencedirect.com/science/article/pii/S0925400503002405

[112] B. T. Marquis and J. F. Vetelino, "A semiconducting metal oxide sensor array for the detection of NOx and NH3," *Sensors and Actuators B: Chemical*, vol. 77, no. 1-2, pp. 100–110, Jun. 2001. [Online]. Available: http://www.sciencedirect.com/science/article/pii/S0925400501006803

[113] F. Zee and J. W. Judy, "Micromachined polymer–based chemical gas sensor array," *Sensors and Actuators B: Chemical*, vol. 72, no. 2, pp. 120–128, Jan. 2001. [Online]. Available: http://www.sciencedirect.com/science/article/pii/S0925400500006389

[114] T. C. Pearce, J. W. Gardner, S. Friel, P. N. Bartlett, and N. Blair, "Electronic nose for monitoring the flavour of beers," *The Analyst*, vol. 118, no. 4, p. 371, Jan. 1993. [Online]. Available: http://pubs.rsc.org/en/content/articlehtml/1993/an/an9931800371

[115] G. Peng, E. Trock, and H. Haick, "Detecting simulated patterns of lung cancer biomarkers by random network of single-walled carbon nanotubes coated with

nonpolymeric organic materials." *Nano letters*, vol. 8, no. 11, pp. 3631–5, Nov. 2008. [Online]. Available: http://www.ncbi.nlm.nih.gov/pubmed/18839997

[116] H. Abe, T. Yoshimura, S. Kanaya, Y. Takahashi, Y. Miyashita, and S.-I. Sasaki, "Automated odor–sensing system based on plural semiconductor gas sensors and computerized pattern recognition techniques," *Analytica Chimica Acta*, vol. 194, pp. 1–9, Jan. 1987. [Online]. Available: http://www.sciencedirect.com/science/article/pii/S0003267000847558

[117] T. Nakamoto, A. Fukuda, and T. Moriizumi, "Perfume and flavour identification by odour-sensing system using quartz–resonator sensor array and neural-network pattern recognition," *Sensors and Actuators B: Chemical*, vol. 10, no. 2, pp. 85–90, Jan. 1993. [Online]. Available: http://www.sciencedirect.com/science/article/pii/092540059380030F

[118] J. W. Gardner, "Detection of vapours and odours from a multisensor array using pattern recognition Part 1. Principal component and cluster analysis," *Sensors and Actuators B: Chemical*, vol. 4, no. 1-2, pp. 109–115, May 1991. [Online]. Available: http://www.sciencedirect.com/science/article/pii/092540059180185M

[119] A. Star, V. Joshi, S. Skarupo, D. Thomas, and J.-C. P. Gabriel, "Gas sensor array based on metal-decorated carbon nanotubes." *The journal of physical chemistry. B*, vol. 110, no. 42, pp. 21 014–20, Oct. 2006. [Online]. Available: http://www.ncbi.nlm.nih.gov/pubmed/17048920

[120] Y. Lu, C. Partridge, M. Meyyappan, and J. Li, "A carbon nanotube sensor array for sensitive gas discrimination using principal component analysis," *Journal of Electroanalytical Chemistry*, vol. 593, no. 1-2, pp. 105–110, Aug. 2006. [Online]. Available: http://www.sciencedirect.com/science/article/pii/S0022072806001756

[121] P. C. Jurs, G. A. Bakken, and H. E. Mcclelland, "Computational Methods for the Analysis of Chemical Sensor Array Data from Volatile Analytes," *Chemical review*, vol. 100, no. July, pp. 2649–2678, 2000.

[122] J. C. Dyre, "A simple model of ac hopping conductivity in disordered solids," *Physics Letters A*, vol. 108, no. 9, pp. 457–461, Apr. 1985. [Online]. Available: http://linkinghub.elsevier.com/retrieve/pii/0375960185900398

[123] ——, "The random free–energy barrier model for ac conduction in disordered solids," *Journal of Applied Physics*, vol. 64, no. 5, p. 2456, Sep. 1988. [Online]. Available: http://scitation.aip.org/content/aip/journal/jap/64/5/10.1063/1.341681

[124] S. Elliott, "A.c. conduction in amorphous chalcogenide and pnictide semiconductors," *Advances in Physics*, vol. 36, no. 2, pp. 135–217, Jan. 1987. [Online]. Available: http://www.tandfonline.com/doi/abs/10.1080/00018738700101971

[125] J. Dyre and T. Schrø der, "Universality of ac conduction in disordered solids," *Reviews of Modern Physics*, vol. 72, no. 3, pp. 873–892, Jul. 2000. [Online]. Available: http://link.aps.org/doi/10.1103/RevModPhys.72.873

[126] T. B. Schroder and J. C. Dyre, "Scaling and Universality of ac Conduction in Disordered Solids," *Physical Review Letters*, pp. 2–5, 2000.

[127] J. C. Dyre, P. Maass, B. Roling, and D. L. Sidebottom, "Fundamental questions relating to ion conduction in disordered solids," *Reports on Progress in Physics*, vol. 72, no. 4, p. 046501, Apr. 2009. [Online]. Available: http://stacks.iop.org/0034-4885/72/i=4/a=046501

[128] G. Faglia, P. Nelli, and G. Sberveglieri, "Frequency effect on highly sensitive NO2 sensors based on RGTO SnO2(Al) thin films," *Sensors and Actuators B*, vol. 19, pp. 497–499, 1994.

[129] a. Labidi, C. Lambert-Mauriat, C. Jacolin, M. Bendahan, M. Maaref, and K. Aguir, "Dc and Ac characterizations of WO3 sensors under ethanol vapors," *Sensors and Actuators B: Chemical*, vol. 119, no. 2, pp. 374–379, Dec. 2006. [Online]. Available: http://linkinghub.elsevier.com/retrieve/pii/S0925400505009949

[130] U. Weimar and W. Göpel, "A.c. measurements on tin oxide sensors to improve selectivities and sensitivities," *Sensors and Actuators B*, pp. 13–18, 1995.

[131] B. E. Kilbride, J. N. Coleman, J. Fraysse, P. Fournet, M. Cadek, A. Drury, S. Hutzler, S. Roth, and W. J. Blau, "Experimental observation of scaling laws for alternating current and direct current conductivity in polymer-carbon nanotube composite thin films," *Journal of Applied Physics*, vol. 92, no. 7, p. 4024, Sep. 2002. [Online]. Available: http://scitation.aip.org/content/aip/journal/jap/92/7/10.1063/1.1506397

[132] S. Barrau, P. Demont, A. Peigney, C. Laurent, and C. Lacabanne, "DC and AC Conductivity of Carbon Nanotubes – Polyepoxy Composites," *Macromolecules*, pp. 5187–5194, 2003.

[133] Z. Khattari, M. Maghrabi, T. McNally, and S. Abdul Jawad, "Impedance study of polymethyl methacrylate composites/multi-walled carbon nanotubes

(PMMA/MWCNTs)," *Physica B: Condensed Matter*, vol. 407, no. 4, pp. 759–764, Feb. 2012. [Online]. Available: http://linkinghub.elsevier.com/retrieve/pii/S0921452611012129

[134] M. H. Al-Saleh, H. K. Al-Anid, Y. A. Husain, H. M. El-Ghanem, and S. A. Jawad, "Impedance characteristics and conductivity of CNT/ABS nanocomposites," *Journal of Physics D: Applied Physics*, vol. 46, no. 38, p. 385305, Sep. 2013. [Online]. Available: http://stacks.iop.org/0022-3727/46/i=38/a=385305

List of Publications

Peer Reviewed Journals

1. Abdelhalim, A., Winkler, M., Loghin, F., Zeiser, C., Lugli, P., & Abdellah, A. (2015). Highly sensitive and selective carbon nanotube-based gas sensor arrays functionalized with different metallic nanoparticles. Sensor and Actuators B: Chemical, 220, 1288-1296.

2. Abdelhalim, A., Abdellah, A., Scarpa, G., & Lugli, P. (2014). Metallic nanoparticles functionalizing carbon nanotube networks for gas sensing applications. Nanotechnology, 25(5), 055208.

3. Abdelhalim, A., Abdellah, A., Scarpa, G., & Lugli, P. (2013). Fabrication of carbon nanotube thin films on flexible substrates by spray deposition and transfer printing. Carbon, 61, 72-79.

4. Abdellah, A., Abdelhalim, A., Horn, M., Scarpa, G., & Lugli, P. (2013). Scalable Spray Deposition Process for High-Performance Carbon Nanotube Gas Sensors. IEEE Transactions On Nanotechnology, 12(2), 174-181.

5. Abdellah, A., Abdelhalim, A., Loghin, F., Koehler, P., Ahmad, Z., Scarpa, G., & Lugli, P. (2013). Flexible Carbon Nanotube Based Gas Sensors Fabricated by Large-Scale Spray Deposition. IEEE Sensors Journal, 13(10), 4014-4021.

Conference Proceedings

1. Abdelhalim, A., Abdellah, A., & Lugli, P. (2014). Complex impedance characterization of highly sensitive carbon nanotube gas sensors. In IEEE SENSORS 2014 Proceedings (pp. 47-50). IEEE.

Acknowledgment

The possibility and success of this work would not have been likely without the trust, patience and support of several individuals. I hereby thank all those who contributed to this work in any way.

First and foremost, I would like to thank my supervisor Prof. Paolo Lugli for giving me the chance to realize a lifelong dream of pursuing a Doctor in engineering while simultaneously taking part in state-of-the-art research topics. His continuous guidance, friendly attitude and the level of trust he granted me made the ph.D journey more exciting and joyful.

I would like to thank as well my former supervisor Giuseppe Scarpa for his support. His guidance and advise had a great impact on the quality of work presented in this thesis.

A big words of thanks goes to my friend and my brother Alaa Abdellah for his guidance throughout my work at the institute. The discussion we had on the work and the personal level were always a source of motivation for me.

The research conducted during my 3 years at the institute wouldn't have been possible without the enormous support of the following colleagues and friends: Aniello Falco, Simone Colasanti, Katharina Melzer, Vijay Bhatt, Alina Lyuleeva, Ahmed Mahmoud, Morten Schmidt, Florin Loghin, Engin Cagatay, Anandi Yadav, Atyab Imtaar, Arsany Basta, Sherif Zaidan, Mohamed Montasser, Mohamed Fahmy, Amr Khairy and Ahmed Ghoniem.

Moreover, I am honored to have supervised students throughout their B.Sc./M.Sc. theses, I am thankful to those among them who contributed and added value to my work, Maximilian Winkler, Lorenzo de Santis and Christopher Zeiser.

I am also bound to my childhood friend Mina Hanna for his continuous encouragement, relentless support and his faith in me even when i doubted myself.

Words fail to express the gratitude I owe to my mother, my father and my lovely sister, their unwavering support and their belief that I can reach my goals whatever they may

be, instilling in me the confidence I needed to see this endeavor through. Thank you for all you have done for me, I am forever grateful.